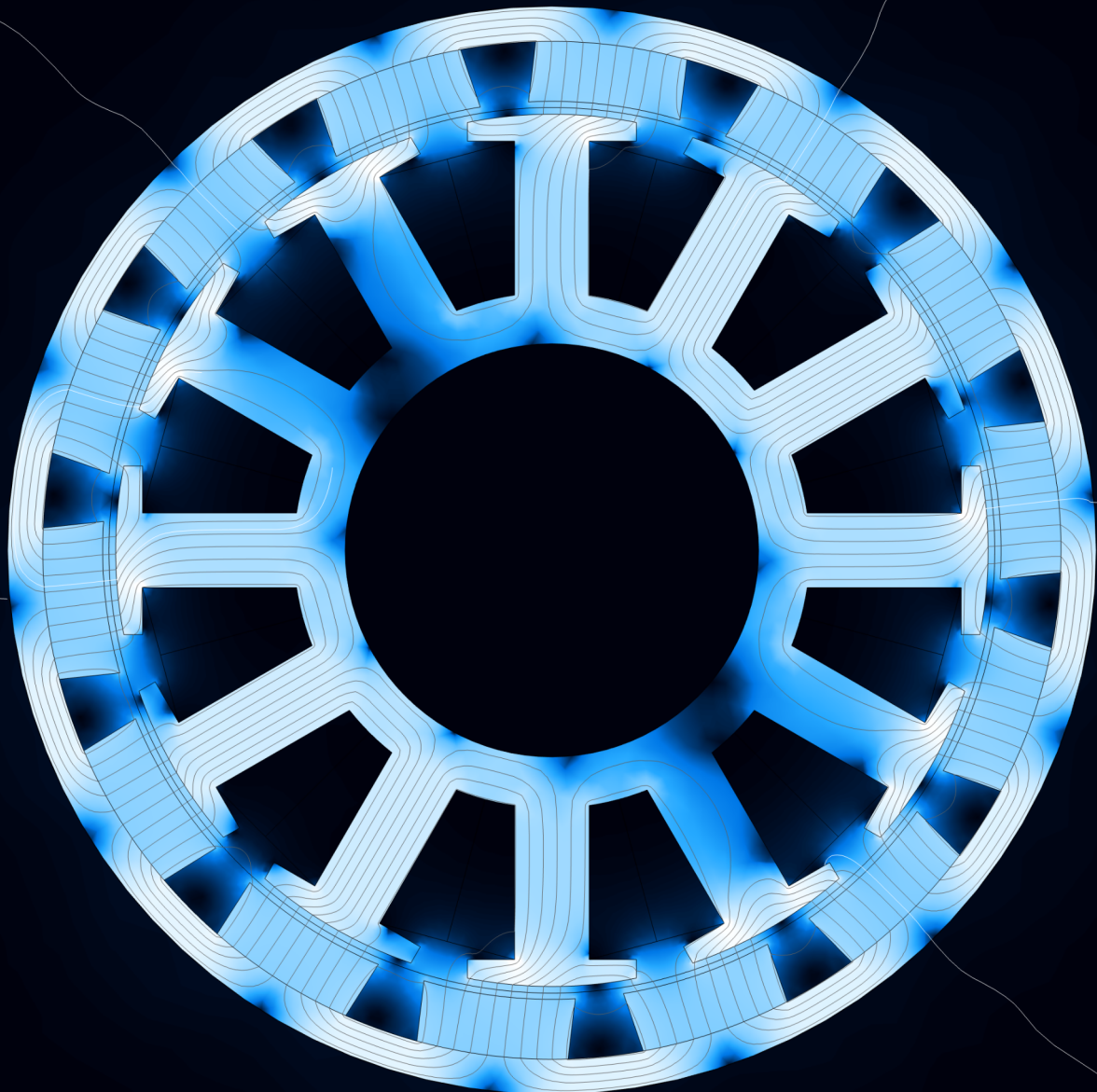


# Acoustic Noise Analysis and Reduction of Electric Motors

Using Numerical Electromagnetic, Mechanic and Acoustic Finite Element Method Noise Modelling

F.C.B. Pacilly



# Acoustic Noise Analysis and Reduction of Electric Motors

Using Numerical Electromagnetic, Mechanic and  
Acoustic Finite Element Method Noise Modelling

by

F.C.B. Pacilly

To obtain the degree of Master of Science in Electrical Engineering,  
at the Delft University of Technology,

to be defended publicly on Thursday July 20 2023, at 10:00 AM.

Project duration: November 14<sup>th</sup>, 2022 – July 6<sup>th</sup>, 2023  
Thesis committee: Dr.ir. P. Bauer, TU Delft, Thesis advisor  
Dr. Jianning Dong, TU Delft, Daily supervisor  
Dr. D.J.P. Lahaye, TU Delft

An electronic version of this thesis is available at <http://repository.tudelft.nl/>.

# Preface

*This thesis is the result of my final work in obtaining my master's degree in electrical engineering. The past five years of studying at the Delft University of Technology, have learned me a lot about the technical aspects in the field of electrical engineering, and also about how to critically look at information and tackle difficult problems. Over these years, my interest in electronics, and especially the development of mechanical (power) electronic systems, has grown. This also led me to choosing a mechatronics based topic for my master thesis, which you are reading right now. The research performed for this thesis did not always progress as smoothly as planned, but in the end I am proud of the result. I would like to thank my daily supervisor, Jianning Dong, for making time to meet with me every week to discuss the progress of the research and help me with difficult problems when I got stuck. Furthermore, I would like to thank Pavol Bauer and Domenico Lahaye, for being part of my thesis defense committee. Finally, last but not least, I would like to thank my friends and family for their continued support, not only during my final thesis project but for the entire duration of my study.*

*F.C.B. Pacilly  
Delft, July 2023*

# Abstract

*In this thesis, the acoustic noise emitted by a small electric outrunner motor, such as the ones commonly used in unmanned aerial vehicles, is analyzed using a multiphysics simulation based on the finite element method. The simulation covers the electromagnetic, mechanical and acoustic domain. The electromagnetic simulation is performed in the 2D time domain, the mechanical simulation in the 3D time domain and frequency domain and the acoustic simulation in the 3D frequency domain. The difference between results of the time and frequency domain mechanical study is investigated, as well as the difference between the obtained results and those obtained in other available literature. Furthermore, the results are compared to acoustic noise measurements performed in the laboratory. Based on the obtained results, noise reduction methods, specifically focussed on small electric outrunner PMSMs, are proposed and verified using the developed simulation.*

# Contents

<b>Preface</b>	<b>i</b>
<b>Abstract</b>	<b>ii</b>
<b>Nomenclature</b>	<b>v</b>
<b>1 Introduction</b>	<b>1</b>
1.1 Background of Acoustic Noise in Electric Motors	1
1.2 Goal of the Research and the Research Questions	2
1.3 Case Study	2
1.4 Challenges	3
1.5 Methodology	4
1.5.1 Coupling Between the Sub-simulations	4
1.5.2 Stationary, Time and Frequency Domain	4
1.6 Thesis Structure	5
<b>2 Sources of Acoustic Noise in Electric Motors</b>	<b>6</b>
2.1 Acoustic Noise Basics	6
2.2 Acoustic Noise Sources in Electric Motors	7
2.3 Propagation of Acoustic Noise in Electric Motors	7
2.3.1 Airborne Acoustic Noise Transmission for Outrunner Motors	7
2.4 Perception of Acoustic Noise	8
2.4.1 Noise Reduction	9
<b>3 Electromagnetic Analysis</b>	<b>10</b>
3.1 Motor Structure (2D)	10
3.2 Magnetic Simulation	11
3.2.1 Implementation of the B-H Relationship	11
3.2.2 Moving Mesh of the Rotor	12
3.2.3 Winding Configuration	12
3.2.4 The Electromagnetic Force Acting on the Rotor	13
3.2.5 Magnetic Simulation Length	13
3.3 Spatial and Temporal Harmonics Analysis	14
3.3.1 2-Dimensional Fast Fourier Transform	14
3.3.2 Rotor Field and Stator Saliency	15
<b>4 Mechanical Analysis</b>	<b>18</b>
4.1 Motor Structure (3D)	18
4.2 Mechanical Simulation	19
4.2.1 Motor Geometry, Materials and Constraints	19
4.2.2 Mechanical Mechanics	19
4.2.3 Time Domain Study	19
4.2.4 Frequency Domain Study	20
4.2.5 Conversion From Rotor Domain to Stator Domain	21
<b>5 Acoustic Analysis</b>	<b>22</b>
5.1 Acoustic Domain and Boundary Conditions	22
5.2 Acoustic Mechanics	23
5.3 Meshing of the Acoustic Domain	24
<b>6 Investigation and Results of the Numerical Model</b>	<b>25</b>
6.1 Magnetic Simulation	25
6.1.1 Magnetic Flux Density	25

6.1.2	Radial Air Gap Flux . . . . .	26
6.1.3	Magnetic Force . . . . .	26
6.1.4	Spatial and Temporal Force Harmonics . . . . .	27
6.2	Mechanical Simulation . . . . .	28
6.2.1	Time Domain Results . . . . .	29
6.2.2	Frequency Domain Results . . . . .	30
6.2.3	Eigenfrequency Analysis . . . . .	31
6.3	Acoustic Simulation . . . . .	32
6.3.1	Total Acoustic Radiated Power . . . . .	32
6.3.2	Acoustic Pressure Isosurfaces . . . . .	34
<b>7</b>	<b>Comparison and Reflection of the Results</b>	<b>36</b>
7.1	Computation Duration of Simulation Steps . . . . .	36
7.2	Comparison of the Results with Measured Noise . . . . .	37
7.2.1	Current Measurements . . . . .	39
7.3	Comparison of the Results with Available Research . . . . .	40
7.3.1	Implementation of the Simulation . . . . .	40
7.3.2	Vibrational Modes of the Motor . . . . .	40
7.4	Reflection of the Simulation Results . . . . .	41
7.4.1	Mode 1 Oscillations . . . . .	41
7.4.2	Comparison of the Results with the Measurements . . . . .	42
7.4.3	Difference Between Time and Frequency Domain Mechanical Study . . . . .	42
<b>8</b>	<b>Noise Reduction Recommendations</b>	<b>44</b>
8.1	Rotor Balancing . . . . .	44
8.2	Improving the End Cap Design . . . . .	45
8.3	Two Side Rotor Support . . . . .	46
<b>9</b>	<b>Conclusion</b>	<b>49</b>
9.1	The Simulation . . . . .	49
9.2	Results of the Simulation . . . . .	50
9.3	Noise Reduction Methods . . . . .	50
9.4	Future Work . . . . .	51
	<b>References</b>	<b>52</b>
<b>A</b>	<b>More Simulation, Analysis and Measurement Results</b>	<b>54</b>
A.1	Rotor Reference Frame Force Harmonics . . . . .	54
A.2	Full Measurement Results . . . . .	54
A.2.1	Acoustic Emitted Noise Waterfall Plot . . . . .	55
A.2.2	Measured Alpha-Beta Current Waterfall Plot . . . . .	56
A.3	Acoustic Isosurfaces with Proposed Front Cap . . . . .	57
<b>B</b>	<b>MATLAB Code Used for Analysis and Processing of the Data</b>	<b>58</b>
B.1	Plotting of Analytical Force Harmonics . . . . .	58
B.2	Processing of the Rotor Force . . . . .	59
B.2.1	Exporting the Rotor Force from COMSOL . . . . .	59
B.2.2	Rotor Force Harmonic Analysis (2D FFT) . . . . .	60
B.2.3	Conversion from Time Domain to Frequency Domain . . . . .	62
B.3	Processing the Mechanical Simulation Results . . . . .	63
B.3.1	Rotor Deformation Harmonic Analysis (2D FFT) - Time Domain Study . . . . .	63
B.3.2	Rotor Deformation Harmonic Analysis (2D FFT) - Frequency Domain Study . . . . .	64
B.3.3	Rotor to Stator Reference Frame Conversion . . . . .	66
B.4	Eigenshape Oscillation Animation Export . . . . .	67
B.5	Acoustic Isosurfaces Animation Export . . . . .	68
B.6	Processing of Laboratory Measurements . . . . .	69
B.6.1	Acoustic Noise Analysis . . . . .	69
B.6.2	Measured Current Analysis . . . . .	70

# Nomenclature

## Abbreviations

Abbreviation	Definition
2D	2 Dimensional
3D	3 Dimensional
BLDC (motor)	BrushLess Direct Current (motor)
FEM	Finite Element Method
FFT	Fast Fourier Transform
IFFT	Inverse Fast Fourier Transform
MMF	Magnetomotive Force
NGO	Non-Grain Oriented
PMSM	Permanent Magnet Synchronous Machine
RMS	Root Mean Square

## Symbols

Symbol	Definition	Unit
$B$	Magnetic flux density	[T]
$B_{ag}$	Air gap magnetic flux density	[T]
$B_r$	Remanent magnetic flux density	[T]
$c$	Propagation velocity	[m/s]
$F_r$	Radial rotor force distribution	[N/m]
$\mathcal{F}_r$	Rotor magnetomotive force	[At]
$h$	Harmonic of mechanical angular velocity	[-]
$H$	Magnetic field strength	[A/m]
$i$	Sound intensity	[W/m <sup>2</sup> ]
$I$	RMS sound intensity	[W/m <sup>2</sup> ]
$I_{eff}$	Effective RMS sound intensity	[W/m <sup>2</sup> ]
$I_0$	Threshold of hearing, Effective sound intensity	[W/m <sup>2</sup> ]
$L$	Sound level	[dB]
$L_s$	Loudness	[phon]
$N_{ph}$	Number of phases	[-]
$N_s$	Number of stator slots	[-]
$m$	Spatial vibration mode	[(2 $\pi$ rad) <sup>-1</sup> ]
$p$	Number of pole pairs	[-]
$p_s$	Sound pressure	[Pa]
$p_0$	Threshold of hearing, Sound pressure	[Pa]
$P$	RMS sound pressure	[Pa]
$q$	Slots per pole per phase	[-]
$\hat{r}$	Radial unit vector	[-]
$R$	The radial position	[m]
$S$	Perceived loudness	[sone]
$T_{mech}$	Mechanical period	[s]
$v_s$	Sound velocity	[m/s]
$V$	RMS sound velocity	[m/s]
$x, y, z$	The coordinates used in a rectangular system	[m]

---

Symbol	Definition	Unit
$\varphi$	The angular position	[rad]
$\Lambda_s$	Stator reluctance	[1/H]
$\mu_0$	Permeability of vacuum	[N/A <sup>2</sup> ]
$\mu_r$	Relative permeability	[-]
$\mu_{rec}$	Relative recoil permeability	[-]
$\omega_m$	Angular velocity corresponding to mode $m$	[rad/s]
$\omega_{mech}$	Mechanical angular velocity	[rad/s]

---

# 1

## Introduction

*As a society, we are constantly searching for ways to automate more and more of our every day or labor-intensive tasks. Combined with a growing accessibility of electricity due to the energy transition, electric motors are increasingly more important and frequently used as crucial components in products like electric appliances, drones and robots. Due to the increasing number of products that are operated in closed space areas or in the vicinity of humans, the acoustic performance and vibrations caused by such electric motors are of increasing importance. Although research about vibrations and acoustic noise caused by electric motors has already been performed, research specifically focussed on the simulation of small electric permanent magnet synchronous motors is hard to find. In this thesis, it is investigated how to simulate a small electric outrunner permanent magnet synchronous machine, such as the ones used in unmanned aerial vehicles or other small electronic equipment where a motor with a high power density is required. The simulation will be used to obtain the acoustically radiated power emitted by the motor used as a case study, and should be usable to investigate ways to reduce the noise emitted by such a motor. Furthermore, the radiation spectrum will be compared to that of larger electric motors from other literature and to the results of actual measurements done in the laboratory on a similar motor.*

### 1.1. Background of Acoustic Noise in Electric Motors

As long as electric motors have existed, the vibrations and acoustic noise that they generate have been important factors in their performance, as they can have a severe impact on the rest of the system or the people working with the system. When focussing on the acoustic noise emitted by electric motors, it can be subdivided into separate categories based on the source of the vibration, namely noise with electromagnetic origin, mechanical origin and aerodynamic origin [1]. Noise with an electromagnetic origin is caused by forces acting on the structure of the motor due to the electromagnetic field, noise with a mechanical origin is for example caused by the bearings of the motor and noise with an aerodynamic origin is for example caused by the disturbance of the air as a result of surface friction. Of these categories, electromagnetic and mechanical noise are indirectly transmitted to the air, they first need to make the structure of the motor vibrate, which in turn causes a vibration in the air. Noise with an aerodynamic source, however, is directly created in the air surrounding the motor [2]. Small synchronous motors, that are commonly used for aerial applications, are known to emit a significant amount of acoustic noise. Although a large part of this noise is often for example caused by the aerodynamic fluctuations of the propellers driven by the motor, there is also noise generated by the motor with an electromagnetic source. It has been shown that in certain frequency bands, electromagnetic effects can even be the dominating source of the acoustic noise emitted by such motors [3]. This has to do with the fact that these motors are often outrunners, which means that the outer shell of the motor

is part of the rotor and rotating. This allows vibrations in the rotor of the motor to directly be radiated into the surrounded air [3].

Manufacturing a newly designed motor, only to find out during testing that it has a poor acoustic performance, can be very costly. This makes optimizing the acoustic behavior of electric motors a complicated process. Therefore, it is no surprise that previous efforts to simulate the acoustic noise emitted by electric motors have already been performed. However, research about the simulation of electric motors seems to have started with a focus on relatively large induction motors [4]. Over time, research about permanent magnet synchronous machines has also been performed [2], [4], [5], but they are still mostly focussed on large automotive or industrial applications. Little to non research can be found about the modelling of small outrunning motors, such as the one studied in this thesis.

## 1.2. Goal of the Research and the Research Questions

The goal of this thesis is to develop and verify a simulation procedure that provides accurate results about the acoustic noise radiated by a small electric motor, which can be used to investigate ways to reduce that noise. The scope of the simulation should cover the electromagnetic forces generated during the rotation of the motor, the mechanical deformations that occur as a result of these forces and the acoustic pressure waves that are emitted due to these deformations, so only acoustically radiated noise with an electromagnetic source. This means that the mounting of the motor, the vibrations induced by the bearings, nor the noise caused by the load that is driven by the motor, are considered. Each step of the simulation that will be developed should be verified, either by theoretical analysis or actual laboratory measurements of the motor in the lab.

Running an elaborate multiphysics simulation, may easily become very computational expensive. To make the simulation useful for testing whether small changes to the motor cause improved acoustic performance, it should be possible to run the simulation multiple times in a short timespan without requiring a large computational investment. Therefore, extra effort will be taken to make the simulation computational efficient. Also, in future studies, it might be desirable to extend the simulation to include modelling of the motor's drive in the electrical domain or extend the simulation to incorporate noise generated with a mechanical or aerodynamic source. To make such an addition possible, the multiphysics simulation will be divided into separate sub simulations with clearly defined in- and outputs.

Based on these goals, the research questions that are going to be answered in this thesis are:

- “How to model the acoustic noise, with an electromagnetic origin, emitted by a small permanent magnet synchronous outrunner motor?”
- “How do the results of the multiphysics finite element method (FEM) simulation compare to real world measurements?”
- “What are the difference between the noise emission mechanisms of a small permanent magnet outrunner motor, compared to the noise emitted by motors already investigated in other literature?”
- “How can the noise emitted by a small permanent magnet outrunner motor be reduced?”

## 1.3. Case Study

A case study on a specific motor is performed, to test the simulation that is developed and to verify the results of this simulation. The simulation developed in this thesis is therefore based on this motor, however the used methods and derivations are valid for different but similar motors. Physical testing of the motor is outside the scope of this thesis, however, another project is performed in parallel to this project based on the same motor model. Therefore, physical measurements of the acoustic noise emitted by this motor are available and can be used to verify the results of the numerical simulation.

### The Motor Used as Case Study

The motor used as a case study in this thesis is a small, 35 mm in diameter, permanent magnet synchronous machine (PMSM). In this motor, the outside shell of the motor is rotating, and thus considered the rotor. Motors such as these are commonly used in drones or other unmanned aerial vehicles, and called outrunners. Sometimes motors like these are also referred to as brushless direct current (BLDC) motors. The permanent magnets are fixed to the rotor, which is thus the outer part of the motor. This rotor is at one side mounted to the axle, which runs through the stator. A load is typically connected to the other side of the axle. This is also the side where the stator extends a bit further than the rotor and can therefore be used to mount the motor. Figure 1.1 shows an image of the motor.



**Figure 1.1:** A photo of the motor that will be studied as a case study in this thesis.

The motor that is used has 14 magnets that are alternately aligned, so a total of 7 pole pairs. The stator consists of 12 slots and has a 3-phase winding. This means that the machine has a fractional slot winding, with a q-factor of  $\frac{2}{7}$  slots per pole per phase. A large advantage of a fractional slot machine is that due to the fact that the magnetic poles and stator slots are never aligned all at once, there is a significantly lower torque ripple (cogging torque), compared to machines using an integer slot winding [6].

## 1.4. Challenges

There are several factors that distinguish the research done in this thesis from the aforementioned and already available literature, such as the focus on a relatively small motor and that the studied motor is an outrunner. These also bring with them challenges that need to be tackled to bring this research to a successful conclusion. Although the size of the motor does not directly pose any challenges, the outrunner design of the motor does complicate the simulation. In electric motors, the radiated noise is almost entirely dependent on the vibrations in the outer shell of the motor. This means that usually only the outer shell of the electric motor needs to be simulated in the mechanical and acoustic domain. Since in an outrunner motor, the shell is rotating, the mechanical simulation will have to be done in a rotating reference frame. This means that the results of the simulations will have to be converted back and forth between these reference frames in time and in frequency domain. Also, some methods or simplifications made in other literature are not valid for small or outrunner motors.

Another challenge that has to be tackled is to keep the computational cost of the simulation low. A simulation, that spans multiple physical domains and dimensions, has to deal with a lot of data. Especially if processing of the data has to be done in different programs, the methods used to read, process and store data can have a significant impact on the overall length of the simulation. Also, since the simulation itself will likely span multiple minutes or even hours, the testing and debugging of a simulation can become a time-consuming process. A possible way to overcome this challenge might be to subdivide the development of the simulation into multiple parts that can be tested and verified independently.

The last challenge is the time available for the research. Developing, testing, running and verifying a multiphysics simulation can take a lot of time. Although some processes are simple enough to come up with, getting used to the software and actually implementing or coding the process in the software can be complicated and require a lot of debugging. The goal to keep the simulation inputs simple and well-defined helps in the long-term as it keeps the various steps in simulation versatile, but increases the time required to implement a simulation in the short term.

## 1.5. Methodology

The acoustic noise generated by an electric motor has to propagate through the electromagnetic, mechanical and acoustic physical domains before it is radiated into the air. Therefore, the simulation procedure will span multiple physics domains, making it a multiphysics simulation. For each type of physics in a multiphysics simulation, a separate simulation is used, which is referred to as a sub-simulation. The sub-simulations and their in-/outputs that are used for the simulation of an electric motor in this thesis are shown in figure 1.2.

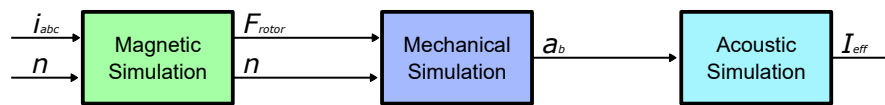


**Figure 1.2:** The numerical simulation procedure, consisting of four separate one-way coupled simulations.

The input of the simulation will be the current,  $I_{abc}$ , and the angular velocity,  $n$ , of the motor. The electromagnetic simulation will use these inputs to determine the magnetic force acting on the rotor of the motor,  $F_{rotor}$ . In the mechanical simulation, this force will be used to determine the deformation of the rotor's structure. The acoustic model is used to determine the pressure and acoustic intensity  $I_{eff}$  in the air around the motor, based on the acceleration of the outer boundary of the rotor,  $a_b$ . Based on the acoustic intensity, the total acoustically transmitted power at each frequency is determined.

### 1.5.1. Coupling Between the Sub-simulations

An important factor in a multiphysics simulation is the coupling between the sub-simulations. In this thesis, the coupling between the sub-simulations is direct, i.e. the sub-simulations are performed sequentially and are not back-coupled. This means that there is no feedback from the subsequent sub-simulations to the previous sub-simulations. In the case of an electric motor such as the one simulated in this thesis, direct coupling is a reasonable approximation of the real world scenario, since the effect of mechanical deformation of the rotor on the magnetic model is very small. The same is true for the effect of acoustic pressure on the mechanical deformation.

### 1.5.2. Stationary, Time and Frequency Domain

Each sub-simulation can either be performed in the stationary, time or frequency domain. Performing the simulations in each of these domains has its own requirements, assumptions, advantages and disadvantages. Generally, performing a simulation in the stationary domain is the simplest to implement but for a dynamic system such as an electric motor also the least accurate. The time domain is more suitable to simulate dynamic effects, and usually the closest to the real world scenario and most straight forward to interpret. However, the quality of a time domain simulation is often severely limited by the available computational power. To obtain meaningful results from a time domain simulation, the duration for which the model is simulated needs to be of sufficient length. Performing a simulation in the frequency domain, is generally the fastest option. A frequency domain simulation, however, can only produce valid results if the physics behave linearly, so the principle of superposition applies. Also, the results that a frequency simulation produces are generally less intuitive and harder to comprehend. The domain(s) chosen for each sub-simulation are elaborated on in the subsequent sections.

### Magnetic Simulation

Since the magnetic model will be highly non-linear due to saturation in the steel of the motor, a frequency domain simulation for the magnetic model is not possible. Computing a stationary solution for each rotor position would ignore dynamic effects that occur due to the rotation of the rotor, and therefore produce unreliable results. However, such a solution would still be useful, for example to find the maximum load in a short circuit or blocked rotor situation. Therefore, the magnetic simulation will first be implemented to compute stationary results for each rotor position to get used to the software, but the final magnetic simulation will be performed in time domain.

### Mechanical Simulation

In the mechanical simulation, a stationary solution has no use, since static deformation of the motor's structure does not cause vibrations in the surrounding air. The mechanical simulation can however be performed in both the time and frequency domain. The advantage of a simulation in the time domain is that the results from the magnetic simulation, which is also in time domain, can directly be mapped to the mechanical simulation. However, the disadvantage is that when the results of the mechanical simulation are converted to frequency domain, to be used in the acoustic simulation, leakage will occur in the frequency spectrum based on the length of the mechanical simulation. Therefore, to achieve results of high quality, the mechanical simulation has to be performed for a sufficient duration, which will significantly increase the computational cost of the simulation in general. That is why performing the mechanical simulation in frequency domain may be more desirable. However, this complicates the coupling between the sub-simulations and may therefore result in larger numerical errors. In this thesis, the mechanical simulation is performed in both the time and frequency domain. This way the implementation, results and computational cost of both implementations can be compared.

### Acoustic Simulation

Acoustics behave linearly and are by nature periodic, since the concept of acoustics is waves traveling through a medium. Therefore, the acoustic simulation is performed in the frequency domain. Performing the acoustic simulation in time domain, would be extremely computationally expensive and is unnecessary to obtain reliable results.

## 1.6. Thesis Structure

In the next chapter, chapter 2, a more detailed introduction is given into the concept of noise in electric motors. It covers the basics of acoustic noise, as well as where noise is originated and how it propagates through electric motors. Following up, chapter 3, 4 and 5 discuss the electromagnetic, mechanic and acoustic simulation and analysis, respectively. After this, in chapter 6, the results of the simulation are analyzed and visualized. These results are then in chapter 7 compared to the results of other available literature and real world measurements. Furthermore, in chapter 8, recommendations to reduce the noise emitted by small electric motors are provided, explained and tested. Finally, chapter 9 is the conclusion of this thesis.

# 2

## Sources of Acoustic Noise in Electric Motors

Since this thesis is working towards the simulating of the acoustic noise emitted by electric motors, it is important to first clarify what acoustic noise is, how it is defined and how it is parameterized. Section 2.1 elaborates on this. Furthermore, the source of acoustic noise in electric motors and how it propagates through electric motors and the surrounding air is explained in section 2.2 and section 2.3. Both are important to understand and to interpret the results provided by this thesis correctly, and also, to understand how the acoustic noise can be reduced based on these results. How acoustic noise is perceived by humans and what factors play a role in this is discussed in section 2.4.

### 2.1. Acoustic Noise Basics

Electric motors are designed to convert power between the electrical and the mechanical domain. In most cases, mechanical vibrations emitted in this process are unintentional and preferably as low as possible. Vibrations in a medium, which can be a solid, a liquid or a gas, are the definition of sound [7]. In this thesis, '*acoustic noise*' refers to unintentional sound generated by an electric motor.

For sound to exist, energy has to be stored in different mechanisms alternatingly [8]. Therefore, an (elastic) medium is required which serves this function. When a sound occurs in a solid, it is referred to as structure borne and when a sound is present in air it is referred to as airborne. In structure borne vibrations, the energy is stored by means of the elastic and kinetic energy in the material, while for airborne vibrations the energy is stored by means of compression and movement of the air. For electrical motors, the vibrations usually originate in the motor as structure borne vibrations and are then, via the surface of the motor, transferred to the air as airborne vibrations, i.e., sound.

To describe vibrations in a medium, three parameters are key. The frequency of the oscillations, the amplitude of the vibrations and the speed at which the wave propagates through the medium. The frequency describes how often the energy is stored and released per unit of time at a specific point in space. The amplitude describes the maximum amount of energy that is stored. And the speed at which the wave propagates through the medium, also known as the speed of sound, depends on the elasticity or compressibility of the medium and is constant in a homogeneous medium. The speed of sound is higher in a medium with a lower elasticity or compressibility [9].

## 2.2. Acoustic Noise Sources in Electric Motors

In electric motors, acoustic noise is generated due to forces acting on the structure of the motor. These forces can be caused by electromagnetic interactions, torque variations, imbalance and backlash or play in the structure of the motor [9]. For this thesis, only acoustic noise with an electromagnetic source is considered. Acoustic noise with a mechanical source would require a more detailed and complicated mechanical model. And acoustic noise generated by load-torque variations is largely dependent on the specific use case of the motor.

During normal operation of an electric motor, various electromagnetic forces act on the structure of the motor. Some of these are intentional and some of these are parasitic. The structure borne vibrations caused by these forces are transmitted as airborne vibrations on the outer surface of the motor. Therefore, only the deformation of the outer surface and thus only the forces acting on the outer body are of relevance for the transmitted airborne acoustic noise [2]. These forces depend on the shape and magnetic properties of the motor structure, the winding currents and the rotational velocity of the rotor.

## 2.3. Propagation of Acoustic Noise in Electric Motors

Once a vibration has established in the structure of the motor, due to the aforementioned forces, it will propagate and cause the entire structure to vibrate. The frequency of this vibration and the corresponding shape in which it vibrates is largely inherent to the structure of the motor and the mechanical properties of the materials. The frequencies at which the structure tends to vibrate, and the corresponding shapes, are called the eigenfrequencies and the eigenshapes. An eigenshape can also be referred to as a vibration mode. In this case, the order of the vibration mode depicts how many displacement periods occur. Figure 2.1 shows an example of some vibrational modes with different orders and their eigenshapes for a rotationally symmetric shape.

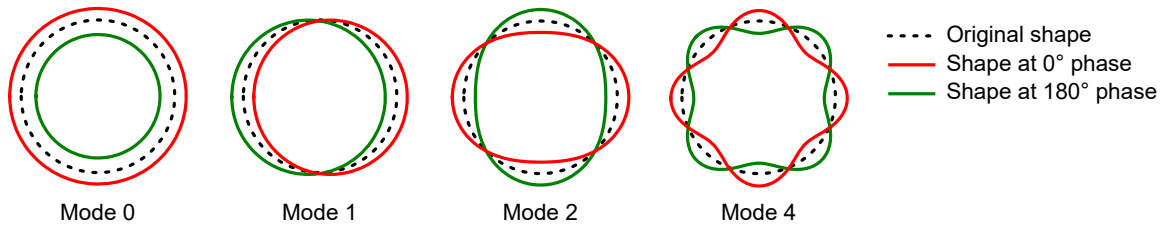


**Figure 2.1:** An example of various mode orders and their corresponding vibration shapes.

The vibration of the motor's outer surface in turn causes pressure variations in the surrounding air and therefore airborne acoustic noise. The amplitude of the pressure differences, and therefore the sound level, is dependent on the normal surface acceleration of the rotor's shell [2].

### 2.3.1. Airborne Acoustic Noise Transmission for Outrunner Motors

Since the motor that is used as a case study in this thesis is an outrunner, the transmission from the structure borne vibrations to the airborne vibrations is more complicated. The frequencies that are transmitted are shifted to a higher frequency by the rotational frequency of the rotor. Furthermore, additional aerodynamic effects will occur at the surface of the rotor due to skin friction. To simulate these effects, a skin friction coefficient has to be defined, and the acoustic simulation has to be done in time domain. This would take too much time to implement and too much computational power, and is out of the scope of this project.

## 2.4. Perception of Acoustic Noise

Humans can perceive both structure borne and airborne vibrations caused by electric motors. Structure borne vibrations are perceived via the sense of touch, while airborne vibrations are perceived via the sense of hearing. Most of the time, the sensation of vibrations is undesirable. Therefore, often, a requirement is set up to minimize or optimize the acoustic noise level that can be perceived.

Acoustic vibrations are described by energy which is alternatingly stored as pressure in and the motion of the medium. The effective value of the pressure occurring in the medium is called the sound pressure,  $p_s$ . The effective value of the velocity of the medium is called the sound (vibrational) velocity,  $v_s$ , (not to be mistaken for the velocity of sound, which refers to the propagation velocity). The sound intensity,  $i$ , is defined as the product between the sound pressure and the sound velocity, as in equation 2.1 [9].

$$i = p_s \cdot v_s \quad [\text{W/m}^2] \quad (2.1)$$

Since humans can perceive sound across approximately 6 powers of 10, the sound intensity is usually described in a logarithmic scale, according to equation 2.2, using the threshold of hearing,  $I_0$ , as a reference.  $I$  is the RMS value of the sound intensity  $i$ . In this equation,  $L$  is called the sound level [9].

$$L = 10 \cdot \log \left( \frac{I}{I_0} \right) \quad [\text{dB}] \quad (2.2)$$

How a human perceives a fixed sound intensity is different for different frequencies. Figure 2.2 shows curves that depict what sound levels are perceived as equally loud over the frequency range from 20 Hz to 20 kHz. To account for how well humans perceive sound at different frequencies, the loudness level,  $L_s$ , is introduced. The loudness level is scaled such that, a value with a fixed loudness is perceived as equally loud across all frequencies, and that the loudness is equal to the sound level at 1 kHz [9].

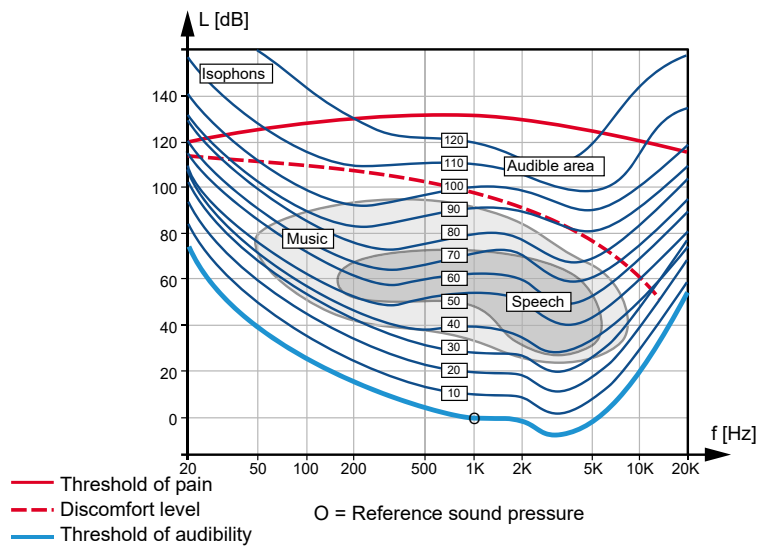


**Figure 2.2:** Curves showing sound levels that are perceived to be of equal loudness [9].

To compare different loudness levels with each other, the perceived loudness,  $S$  is used. This is defined such that it is proportional to how loud a sound is perceived, and is determined as in equation 2.3 [9].

$$S = 2^{\frac{(L_s - 40)}{10}} \quad [\text{sone}] \quad (2.3)$$

### 2.4.1. Noise Reduction

The reduction of emitted acoustic noise can have two different meanings. Since it concerns the very core of what this thesis is about, it is important to distinguish between the two. The most obvious way to reduce the noise level is to reduce the overall noise power that is emitted. To do this, the amplitude of vibrations generated by the motor has to be reduced, which reduces the power transferred from the motor's surface into the surrounding air. This way, the total power, regardless of frequency, which is transmitted is reduced. The second, slightly less obvious, way of reducing noise is by changing the frequency distribution of the emitted noise, such that the negative sensation that is caused by the noise is reduced. For example, frequencies that cause such a sensation can be changed to less "*irritating*" frequencies, or shifted to higher frequencies to which humans are less sensitive, without actually reducing the power. Although this method is generally easier to achieve, the perception of noise is subjective, and therefore the effectiveness of such methods is hard to verify.

# 3

## Electromagnetic Analysis

This chapter will discuss the electromagnetic analysis of the motor. A magnetic simulation is developed to determine the electromagnetic forces acting on the rotor of the motor, based on the rotational speed and phase currents. Furthermore, the spatial and temporal harmonics that are expected to be present in the air gap flux density and electromagnetic force are analytically determined. The result of this analysis will be used in chapter 6 to verify the results of the electromagnetic simulation. First, in section 3.1, the structure that is used for the simulation and analysis is defined. Then, section 3.2 elaborates on the details of the developed electromagnetic simulation. And finally, in section 3.3, the harmonic analysis on the air gap flux density and electromagnetic force is performed.

### 3.1. Motor Structure (2D)

For the magnetic simulation, the 2-dimensional (2D) structure of the motor has to be defined. Therefore, the physical dimensions of the motor have been measured. The measurements have been performed by hand, so some inaccuracy may be present, but the crucial dimensions have been measured accurately enough to obtain valid simulation results. Also, small motors such as these are usually not produced to meet extremely high standards, which means it is not guaranteed that a different motor of the same type would have exactly the same dimensions. This does however also mean that the tolerances in the design of such motors are generally larger, and thus the effects of inaccuracies in the measurements are relatively smaller. Figure 3.1 shows the measured dimensions.

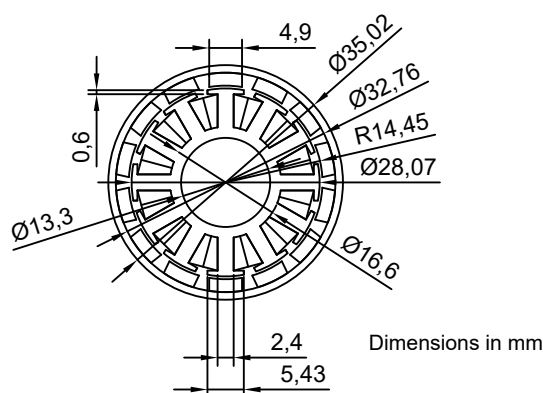


**Figure 3.1:** A cross-section of the motor studied in this thesis, showing the dimensions measured and used for the analysis in the simulation. All dimensions are measured by hand and depicted in millimeters.

## 3.2. Magnetic Simulation

The magnetic simulation is a FEM based simulation, implemented in COMSOL Multiphysics. The magnetic simulation is 2D and performed in the time domain. A 3-dimensional (3D) simulation would increase the accuracy as fringing and other 3D effects would be taken into account, however this would take too much computational time to be feasible. Simulating the model in frequency domain would require it to be a linear problem, which is not the case. Figure 3.2 shows the structure of the motor, which is used for the magnetic model, and the materials designated to each part of the structure.

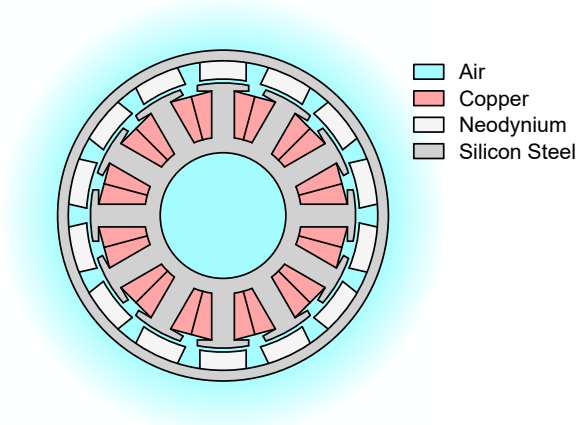


**Figure 3.2:** The 2-dimensional structure used for the magnetic simulation of the motor. The colors indicate what materials are designated to the domains.

The magnetic model is implemented using the rotating machinery physics module of COMSOL. This is a derivation from the Magnetic Fields physics and uses Ampère's Law to solve for the magnetic field [10]. Once the magnetic field is determined, Maxwell's Surface Stress Tensor is applied to the boundary of the rotor, to determine the forces acting on the rotor. The load on the rotor of the motor and the angular rotational position of the rotor, both as a function of time, are the output of the magnetic model.

### 3.2.1. Implementation of the B-H Relationship

For the air and the copper, the B-H relationship between the magnetic flux density  $B$  and magnetic field strength,  $H$ , is implemented according to equation 3.1. Herein,  $\mu_0$  is the permeability of free space and  $\mu_r$  is the relative permeability of the material to which the relation is applied.

$$\mathbf{B} = \mu_0 \mu_r \mathbf{H} \quad (3.1)$$

For the neodymium permanent magnets, the remanent magnetic flux density,  $B_r$ , of the permanent magnets is added to the total magnetic flux density and the recoil permeability,  $\mu_{rec}$ , is used, according to equation 3.2. Since the remanent flux density in the material is given as a scalar, it is multiplied with the radial unit vector  $\hat{r}$ . This unit vector is alternately defined outwards and inwards to account for the orientation of the permanent magnets. A recoil permeability of 1.05 and remanent flux density of 11.1 T has been used for the magnets.

$$\mathbf{B} = \mu_0 \mu_{rec} \mathbf{H} + B_r \hat{r} \quad (3.2)$$

Because silicon steel has a non-linear magnetic behavior, the B-H relationship of the silicon steel is defined using an interpolated B-H curve. Since the exact properties of the silicon steel are not known,

the BH-curve of a similar non-grain oriented (NGO) laminated silicon steel with a similar lamination thickness was used [11]. Figure 3.3 shows a plot of the used B-H curve.

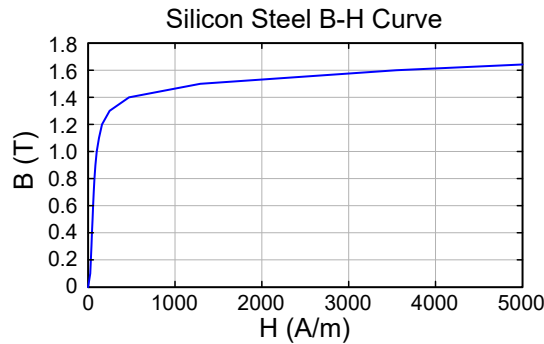


**Figure 3.3:** The B-H curve used for the silicon steel in the magnetic simulation.

### 3.2.2. Moving Mesh of the Rotor

The domains of the motor structure that are part of the rotor are rotating around the center over time. This is implemented in the FEM model using a moving mesh. The mesh of the rotor domains are rotated, and continuity conditions are applied to the boundaries between the rotating and stationary domains. There are two continuity boundaries, one in the center of the air gap and one at the outer boundary of the rotor. Figure 3.4 shows the domains that are stationary, the domain that is rotating and the boundaries where a continuity condition is applied. As the name suggests, the continuity condition forces the magnetic flux at both sides of the boundary to be continue, so no jump in magnetic flux can occur at the boundary.

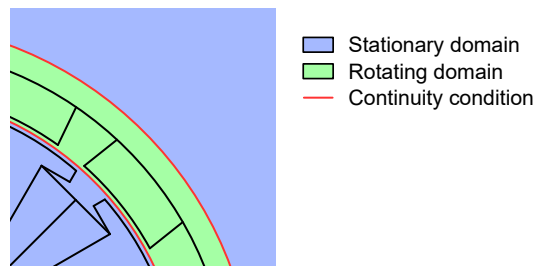


**Figure 3.4:** The domains where the moving mesh is (rotating domain) and is not (stationary domain) applied. On the boundary between the two, a continuity condition is applied. This is shown as a red line.

### 3.2.3. Winding Configuration

The motor has 12 stator slots and 14 magnetic poles on the rotor. There are multiple possible winding configurations for such a motor, but the configuration that is used most is the dLRK configuration [12]. For this reason and since it can be seen from visual inspection of the motor, the motor is assumed to have this configuration. Figure 3.5 shows this configuration in the structure of the motor and how it is applied in the magnetic model. Note that each letter in figure 3.5 represents a half turn, therefore when writing out the winding configuration in full coils, it becomes **AaBbCcAaBbCc**. Herein, lower case and upper case letters represent coils that are wound in opposite direction.

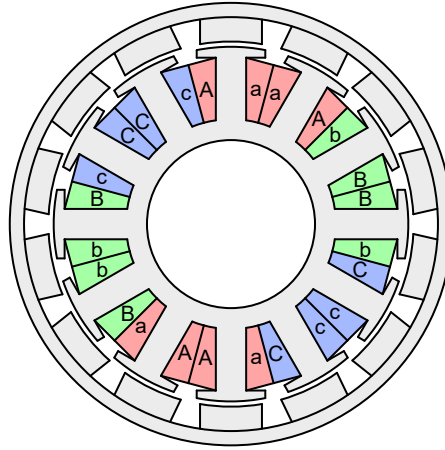


**Figure 3.5:** The order and directions of the motor's winding. The letters and colors indicate the phase. Lower case and upper case letters represent half-turns in opposite direction.

### 3.2.4. The Electromagnetic Force Acting on the Rotor

The power that is transmitted into the air by a vibrating surface can be estimated using equation 3.3, in which  $P_0$  is the radiated power,  $Z_0$  the free-field impedance,  $S$  the surface area and  $v_n$  the normal velocity of the surface [2]. The acoustic noise emitted by a motor is almost entirely determined by the deformation of the outer shell of the motor, since this is that part that will experience most vibrations and can directly transmit these vibrations into the surrounding air. Therefore, only the outer shell of the motor will be simulated in the mechanical model, and only the forces acting on the outer part of the motor have to be determined. For an outrunner motor, this means the force acting on the rotor. To determine the forces acting on the rotor, Maxwell's Surface Stress Tensor is applied to the boundary of the solid domains that are part of the rotor.

$$P_0 = Z_0 \cdot S \cdot |v_n^2| \quad (3.3)$$

### 3.2.5. Magnetic Simulation Length

During one physical rotation of the motor, multiple symmetries in time and in space can be observed. To save computation time, it is desired to prevent having to compute anything when it is not absolutely necessary. Therefore, the duration of the magnetic simulation has to be carefully considered.

Since the rotor magnets are alternately north and south aligned, when the rotor has rotated for  $4\pi/p$  rad (two times the angular distance between the rotor poles), the same magnetic situation and results will be repeated. Therefore, simulating from  $t = 0$  to  $t = 2 \cdot T_{mech}/p$ , in which  $T_{mech}$  is the mechanical period, will be sufficient. If a longer duration is desired, for example for increased FFT resolution, the result can simply be repeated multiple times. Furthermore, the force is proportional to the flux density squared, and therefore the direction of the magnetic field (positive or negative) is not important for the force acting on the rotor. This means that, from a force perspective, the passing of a north-pole aligned magnet is equal to the passing of a south-aligned magnet. Therefore, when only the force is desired, simulating half of the previously mentioned duration is sufficient, i.e. simulating until  $t = T_{mech}/p$ .

Next to the temporal symmetries just mentioned, a spatial symmetry can be observed. When a magnet is exactly aligned with a stator slot, the rotor has to rotate for  $\pi / (pN_s)$  rad (the angular distance between the rotor poles, divided by the number of stator slots, times the number of poles that are simultaneously aligned), until the adjacent magnet in the direction of movement is aligned. After this duration, the situation and therefore the results are the same, but rotated in space by  $2\pi/N_s$  rad in the opposite direction of the rotation of the rotor. Using this knowledge, the simulation only has to be simulated until

$t = 2 \cdot T_{mech} / (pN_s)$ . However, to obtain the results of a full mechanical rotation, the results at different positions on the rotor have to be appended in time. This means that the mesh nodes on the rotor need to be rotational symmetric with order  $p$ . Figure 3.6 shows an example of how the force at one specific node is constructed out of segments from different locations. The code in which this is implemented is added in appendix B.2.3

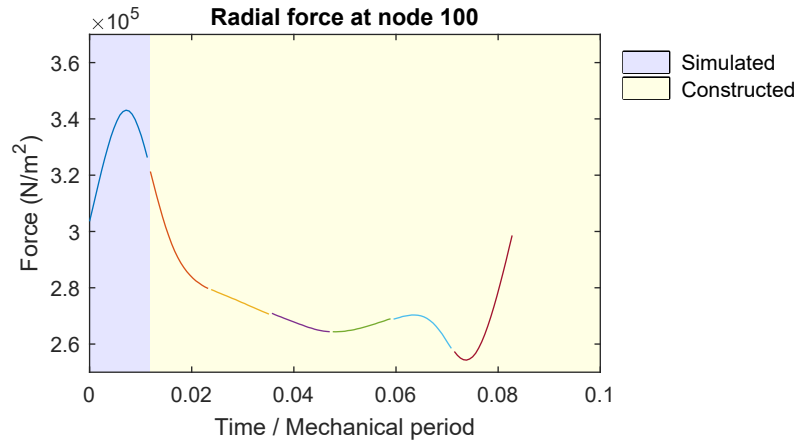


**Figure 3.6:** A visual representation of how the force during a full electrical cycle is constructed based on segments of a shorter result evaluated at different positions. Each line color represents a different location. The x-axis shows time, normalized to the time required for one mechanical rotation.

### 3.3. Spatial and Temporal Harmonics Analysis

The air gap flux density and electromagnetic force in a PMSM consists of spatial and temporal harmonics. The force harmonics that are present in an electric motor can be predicted based on the structure of the motor. The spatial harmonics that are present in the rotor force indicate what vibration modes will be excited in the shell of the motor. The temporal harmonics, together with the rotational speed of the motor, determine the frequencies at which this excitation occurs. The closer the frequencies in the rotor force are to the eigenfrequencies of the corresponding vibrational modes, the more prominent the vibration of this mode will be. And therefore, the more acoustic noise will be transmitted at this eigenfrequency.

Section 3.3.1 clarifies how a 2D FFT is used to decompose the results of the electromagnetic simulation into spatial and temporal harmonics. This will be used to verify the rotor force obtained from the FEM simulations. In section 3.3.2 the harmonics that should be present in the rotor force based on the interaction between the rotor and stator are determined.

#### 3.3.1. 2-Dimensional Fast Fourier Transform

To compare the rotor force resulting from the simulation with analytical predictions, it is characterized by its spatial and temporal harmonics. The radial rotor force distribution,  $F_r$ , can be described using a 2-dimensional Fourier series, as in equation 3.4. Herein,  $m$  is the harmonic over space, also commonly called the mode, and  $h$  is the harmonic in the temporal domain.  $\varphi$  is the angular position and  $\omega$  is the base frequency.  $A_{mh}$  and  $\theta_{mh}$  are the amplitude and the phase of the complex-valued Fourier coefficient, corresponding to each spatial and temporal harmonic.

$$F_r = \sum_m \sum_h A_{mh} \cos(m\varphi + h\omega + \theta_{mh}) \quad (3.4)$$

To obtain the Fourier coefficients present in the magnetic force, which will result from the magnetic model, two consecutive fast Fourier transforms (FFTs) are executed. The FFT of a real value signal will always result in a symmetric spectrum. Since the magnetic force is real-valued, the result of the first FFT will be symmetric. However, since the result of the first FFT will be complex-valued, the result of the second FFT will be non-symmetric.

In this report, the first FFT will be performed over the spatial domain and the second FFT will be performed over the temporal domain. Therefore, when the result of the 2D FFT is plotted, only the positive spatial harmonics will be plotted, while both the negative and positive temporal harmonics will be plotted.

### 3.3.2. Rotor Field and Stator Saliency

In permanent magnet electric machines with stator saliency, such as the one investigated in this thesis, the interaction between the magnetic field created by the permanent magnets and the saliency of the stator will cause large variations in the air gap flux density and therefore also in the force. The harmonics caused by this interaction are expected to be most prominent in the result of the magnetic simulation, as this is usually the case in permanent magnet machines [6]. Figure 3.7 shows the structure of the rotor and the stator and the corresponding distribution of the rotors magnetomotive force (MMF) over the angular position,  $\varphi$ , due to the rotors permanent magnets, as well as the stator reluctance distribution over  $\varphi$  as a result of the stator slots.

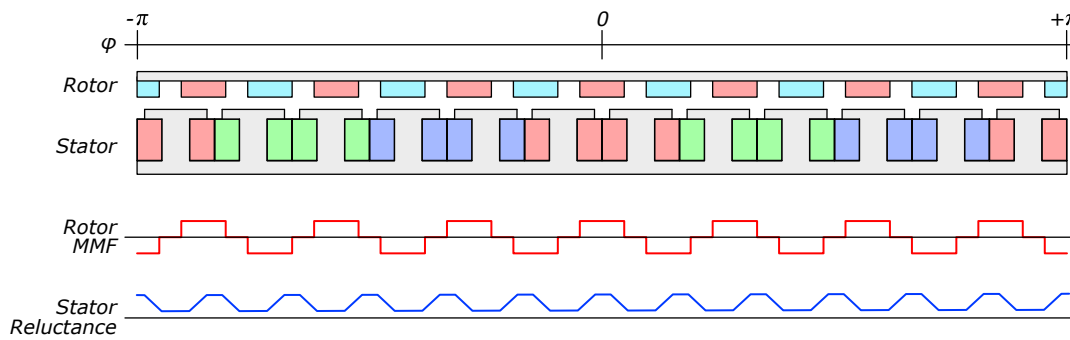


**Figure 3.7:** The rotor and stator structure and the corresponding distribution of the rotor magnetomotive force and the stator reluctance.

The rotor MMF and stator reluctance distributions will be expressed with infinite Fourier series. The rotor MMF is a 3-level square wave, which can be seen as two shifted rectangular waves, with a duty cycle of  $\frac{1}{2}$ , added to each other. This means that the Fourier representation of the rotor MMF will consist of only odd harmonics, i.e.  $v = 1, 3, 5, \dots$ . Since the rotor will be rotating, and therefore moving over time, the Fourier representation also has an  $\omega t$  part, in which the angular frequency  $\omega$  is the mechanical angular velocity multiplied by the mode order,  $v$ , and the number of pole pairs,  $p$ , resulting in  $\omega_v = vp\omega_{mech}$ . There might be a phase shift between the rotor poles and stator slots, which is denoted by  $\theta$ , however this phase shift has no effect on the harmonics. Based on these statements, the Fourier representation of the rotor MMF is given by equation 3.5.

$$\mathcal{F}_r = \sum_v^{\infty} A_v \cos(vp\varphi - \omega_v t + \theta) \quad (3.5)$$

The stator reluctance is represented by a rectangular wave with a duty cycle not equal to  $\frac{1}{2}$ . Therefore, the Fourier representation of the stator reluctance will include all harmonics, i.e.  $\mu = 0, 1, 2, \dots$ . The stator slots will not be moving in time, so there is no  $\omega t$  part. The phase shift between the rotor MMF and stator reluctance is already accounted for in equation 3.5, so the Fourier coefficients will be purely

real valued. Based on this, equation 3.6 is the Fourier representation of the stator reluctance, in which  $N_s$  is the number of stator slots.

$$\Lambda_s = \sum_{\mu}^{\infty} A_{\mu} \cos(\mu N_s \varphi) \quad (3.6)$$

To determine the harmonics present in the rotor force, it is not necessary to derive the amplitude of the coefficients of the Fourier representation. The rotor has no saliency and under no-load conditions the stator will not generate any MMF, therefore the magnetic flux density in the air gap will be proportional to the product of the rotor MMF and the stator saliency, as in equation 3.7.

$$B_{ag} \propto \mathcal{F}_r \cdot \Lambda_s \\ \propto \sum_v^{\infty} \sum_{\mu}^{\infty} A_v A_{\mu} \cos((vp \pm kN_s) \varphi - \omega_v t + \theta) \quad (3.7)$$

According to Maxwell's stress tensor, the force acting on the rotor is proportional to the magnetic flux density squared. By squaring the summation in equation 3.7, the infinite sum in equation 3.8 is obtained. Herein,  $v_1$  and  $v_2$  as well as  $\mu_1$  and  $\mu_2$  are independently counted versions of  $v$  and  $\mu$ , respectively.

$$F_r \propto B_{ag}^2 \\ \propto \sum_{v_1}^{\infty} \sum_{v_2}^{\infty} \sum_{\mu_1}^{\infty} \sum_{\mu_2}^{\infty} A_{v_1} A_{v_2} A_{\mu_1} A_{\mu_2} \cos(((v_1 \pm v_2)p \pm (\mu_1 \pm \mu_2)N_s) \varphi - (\omega_{v_1} \pm \omega_{v_2})t + \theta) \quad (3.8)$$

Based on equation 3.8, the spatial and temporal harmonics present in the rotor force are given by equation 3.9 and 3.10 respectively. In which  $v_1$  and  $v_2$  are sets of all positive odd numbers and  $\mu_1$  and  $\mu_2$  are sets of all non-negative integers.

$$m = (v_1 \pm v_2)p \pm (\mu_1 \pm \mu_2)N_s \quad (3.9)$$

$$\omega_m = \omega_{v_1} \mp \omega_{v_2} = (v_1 \mp v_2)p \omega_{mech} \quad (3.10)$$

Since the sum or difference of two odd numbers will always result in an even number,  $(v_1 \pm v_2)$  will result in a set of all (positive and negative) even numbers,  $k_1$ . Since the sum or difference between integers will always result in another integer, the plus-minus sum of two sets of positive integers  $(\mu_1 \pm \mu_2)$  can be replaced with a set of all (positive and negative) integers,  $k_2$ . Using this reasoning, the equations for the spatial harmonics and temporal harmonics are rewritten into equation 3.11 and equation 3.12, respectively. In which  $k_1$  and  $k_2$  are given by 3.13.

$$m = k_1 p \pm k_2 N_s \quad (3.11)$$

$$\omega_m = -k_1 p \omega_{mech} \quad (3.12)$$

$$\begin{cases} k_1 \in \{\dots, -4, -2, 0, 2, 4, \dots\} \\ k_2 \in \{\dots, -2, -1, 0, 1, 2, \dots\} \end{cases} \tag{3.13}$$

Based on equation 3.11 - 3.13, the harmonics that are expected to be present are calculated and plotted, resulting in figure 3.8. This figure will be compared to the results of the magnetic simulation.

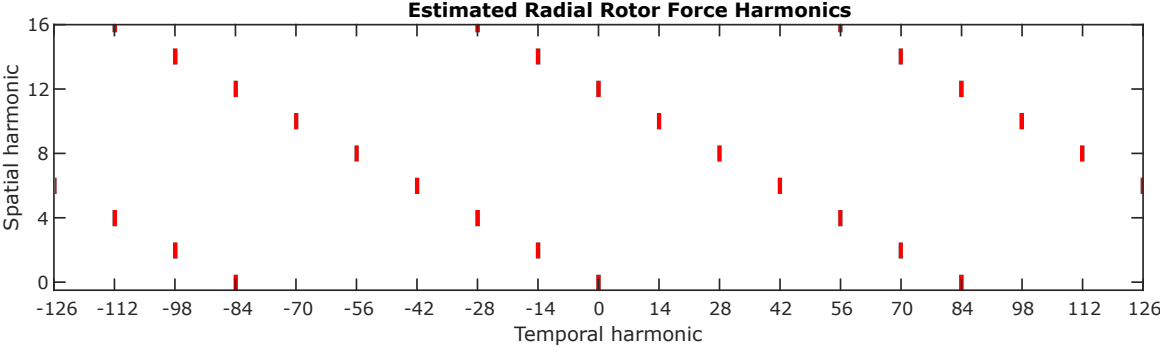


**Figure 3.8:** The spatial and temporal harmonics,  $m$  and  $h$  respectively, that should be present in the rotor force due to the interaction between the rotor magnetomotive force and the stator saliency.

# 4

## Mechanical Analysis

This chapter focuses on the implementation of the mechanical sub-simulation. This simulation computes the deformation of the rotor, based on the electromagnetic forces resulting from the magnetic sub-simulation and the rotational velocity of the rotor. The mechanical study is performed in 3D and in both the time and frequency domain. This way, the results in time and frequency domain can be compared, and the advantages and disadvantages of both implementations can be investigated. First in section 4.1 the 3D structure that is used for the mechanical study is defined. Next, in section 4.2 the implementation of the mechanical model is explained. Section 4.2.3 and 4.2.4 elaborate on the specifics for the time and frequency domain study, respectively. Finally, section 4.2.5 explains how the results of the mechanical simulation are converted from the rotor to the stator reference frame.

### 4.1. Motor Structure (3D)

For the magnetic model, the 2D cross-section defined in section 3.1 could directly be imported into COMSOL and used for the magnetic simulation. The mechanical simulation, however, requires a 3D model. Since no CAD model of the motor is available and no CAD files can be imported into COMSOL without the CAD module, the 3D structures have to be implemented directly in COMSOL using the build in primitive shapes and boolean operations. For mechanical simulation, only the structure of the rotor is of relevance, which means no 3D model of the stator is necessary. The 3D model of the rotor that is developed for the mechanical model is based on an extrusion of the 2D cross-section. The dimensions of the silicon steel ring and aluminum end cap are measured by hand. In figure 4.1, the structure used for the mechanical simulation can be seen.

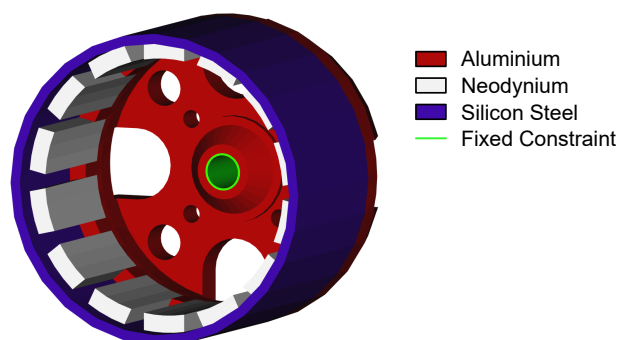


**Figure 4.1:** The geometry implemented in COMSOL, representing the structure of the rotor from the motor that is studied. The constraint prevents the rotor from moving, where it is fixed to the axle. The different colors represent different materials.

## 4.2. Mechanical Simulation

The mechanical simulation is also based on the Finite Element Method and implemented in COMSOL Multiphysics. Since the acoustic noise generated by the motor almost entirely depends on the vibration of the outer surface [2], only the outer part of the motor is mechanically simulated. Since the motor that is analyzed in this thesis is an outrunner, the rotor part of the motor is simulated. For small outrunner motors, the outer rotor is often only supported on one side. This allows to reach the winding of the stator via the other side. Due to this asymmetry, it is crucial that the mechanical simulation is performed in 3D. Although a 3D simulation is crucial for accurate results, this does come at the cost of increased computational costs. Therefore, the mechanical study is implemented in both the time domain and the frequency domain. This makes it possible to compare a time and frequency domain simulation in terms of complexity, accuracy and computational efficiency. The specifics of the time domain study are discussed in 4.2.3 and those of the frequency domain are discussed in 4.2.4.

### 4.2.1. Motor Geometry, Materials and Constraints

For the mechanical simulation, three materials are used, neodymium for the magnets, silicon steel for the flux ring and aluminum for the end cap. To fix the rotor in place, a constraint is applied to the slot where the axle is located. Although the axle is normally able to rotate, for vibrational analysis at the relevant frequencies, the inertia of the load connected to the axle will prevent it from oscillating together with the rotor. Therefore, both radial and angular motion is fixed by the constraint. Figure 4.1 shows the materials used for the mechanical motor, as implemented in COMSOL. The different colors represent the materials used for the structure. The green surface is where the constraint is applied.

### 4.2.2. Mechanical Mechanics

The solid mechanics physics node of COMSOL is used to implement the mechanical model. This module determines the deformation of, and stresses in, the geometry based on the equations of motion and a constitutive model for linear elastic material [13]. In this model, the material is defined by its density, Young's modulus and Poisson's ratio. The parameters used for the materials are shown in Table 4.1.

MATERIAL	YOUNG'S MODULUS	POISSONS RATIO	DENSITY
Aluminum	71.7 GPa	0.33	2810 kg/m <sup>3</sup>
Neodymium	160 Gpa	0.24	7850 kg/m <sup>3</sup>
Silicon Steel	200 GPa	0.30	7650 kg/m <sup>3</sup>

**Table 4.1:** The material properties used for the materials in the mechanical simulation.

#### Material Dampening

The damping in the rotor material is largely dependent on the amplitude of the deformation [14] and properties of the material. Since the deformation of the rotor structure will be very low and because metals have a relatively low damping ratio, the damping within the motor structure will be low. To prevent oscillations due to transient forces and to prevent singularities in the frequency analysis, viscous damping is still considered. Both the bulk- and shear viscosity are therefore set to  $0.01 \text{ Pa} \cdot \text{s}$ .

### 4.2.3. Time Domain Study

The first study implemented is the time domain study, since it requires the least amount of effort to implement. For the time domain study, the model is first simulated with coarse dynamically determined time steps, until it reaches a steady state oscillation. From this point on, the model is solved for fixed

time steps. The time increment for each time step is chosen to be 10 times lower than the period corresponding to the maximum frequency of interest. The total number of output times is chosen, such as to obtain a sufficiently high frequency resolution after the FFT will be performed, while keeping the simulation time reasonable. However, since the total number of times for which the model can be solved is limited, spectral leakage in the result of the FFT will be inevitable. The effect of this will be further investigated by comparing the results of the time-domain and frequency domain studies.

### Magnetic Forces

The forces resulting from the 2D magnetic simulation have to be applied to the rotor structure in the 3D mechanical simulation. The magnetic simulation has to be mapped to the mechanical simulation in space and in time. In space, the result is extruded in the axle direction, and applied to the surface of the rotor. In time, the result has to be interpolated, since the output times of the magnetic model do not match the times at which the mechanical model is computed. Since the mechanical simulation will span more time than one electrical period, the result of the magnetic model has to be repeated. This is implemented by using the modulo function, inside the reference from the mechanical simulation back to the magnetic simulation. Furthermore, every time one electrical period has passed, the spatial mapping is shifted one pole. This is implemented using a rotating reference frame, that again uses the modulo function and the simulation time.

### Rotating Domain

Naturally, the rotor of the motor is rotating. Making the structure rotate in the simulations, would require the structure to be re-meshed for every time step, making the simulation unnecessarily complex. Therefore, the simulation is performed in a rotating reference frame, meaning that the structure (and mesh) are kept stationary. The forces that result from the rotation of the motor are applied to the structure, which makes the simulation representable for the real world situation. Since the axle of the rotor is assumed to be rotating at a constant angular speed, the Euler force is not implemented. Furthermore, since the displacement of the rotor will be very small, it is not necessary to account for Coriolis force.

## 4.2.4. Frequency Domain Study

The mechanical study has also been implemented in the frequency domain. Since the deformation of the rotor due to the magnetic force is very small, it is valid to assume that the deformation of the structure is linearly proportional to the force acting on the structure [2]. Since this is the case, the principle of superposition applies, and a frequency domain simulation is a valid approximation of the real world situation. Performing the mechanical simulation in the frequency domain makes it less computationally intensive and allows the sampling time of the electromagnetic simulation to be changed without consequences for the mechanical simulation. Performing the mechanical simulation in frequency domain does however make the coupling from the electromagnetic simulation and to the acoustic simulation more complex and more prone to numerical calculation errors.

The frequencies present in the magnetic force have been analyzed in section 3.3, and are therefore known beforehand. Since there will be no force excitation at other frequencies than those, there will also be no deformation. Therefore, the mechanical simulation only has to be performed at frequencies that are present in the rotor force. In the rotor reference frame, this means all multiples of the mechanical frequency multiplied by the number of poles on the rotor, i.e., equation 4.1.

$$f = 2\pi n p \omega_{mech} \text{ for } n \in \{1, 2, 3, \dots\}. \quad (4.1)$$

### Magnetic Forces

The forces resulting from the 2D magnetic simulation have to be converted to the frequency domain and have to be mapped to the 3D mechanical simulation. The conversion from time domain

to frequency domain is implemented in MATLAB. Since this means that the results have to be interchanged between COMSOL and MATLAB anyway, the remapping introduced in section 3.2.5 has been implemented, which is now a viable optimization since this can only be implemented in MATLAB. This reduces the duration for which the magnetic simulation has to be computed by 7 times.

Once the forces acting on the rotor are exported from COMSOL, imported into MATLAB and reconstructed, the FFT is performed for each position and the result is stored in spreadsheet format. In this format, the data consists of 7 columns. The first 3 indicate the position in 3D space, and the next 4 store the real and imaginary part of the force in both the radial and angular direction. In this format, the results can directly be imported by COMSOL using an interpolation node. The code in which the reconstruction and conversion to frequency domain is implemented can be found in appendix B.2.3.

#### Rotational Forces in the Frequency Domain

The forces that act on the rotor due to the rotation of the rotor, are not changing over time, as long as the rotational velocity remains constant. Since this is the case, the forces acting on the rotor due to the rotation do not have to be accounted for in the frequency domain study.

### 4.2.5. Conversion From Rotor Domain to Stator Domain

Both the time domain and frequency domain studies are performed in the rotor reference frame, to reduce the temporal and computational cost of the simulation. This does mean, however, that before the results of the mechanical study can be used in the acoustic simulation, they have to be converted from the rotor domain to the stator domain.

For the time domain study, switching between both reference frames can be done by shifting the  $\varphi$ -coordinate of the results with a time dependent quantity. This means that the actual results are not changed, only the position where the result is applied is changing. This is implemented in COMSOL using a rotating coordinate system, which is rotating together with the rotor reference frame. Using the transformation matrix of this coordinate system, the results are converted to the global coordinate system, which is stationary and therefore the same as the stator reference frame.

In the frequency domain study, switching between both reference frames is more complicated. The results of the mechanical simulation are defined for every point on the outer surface of the rotor for each  $\varphi$ -coordinate, Z-coordinates and for each frequency. Since no direct equation could be found to shift such results with a value that is changing at a constant rate in time, a workaround has been used. The results of the frequency domain mechanical simulation are first converted from the frequency domain to the time domain using an inverse fast Fourier transform (IFFT), next they are rotated in time using a circular shift operator. After the rotation has been performed, the results are converted back to the frequency domain using a normal FFT. The code in which this process has been implemented can be found in appendix B.3.3. Figure 4.2 shows a schematic representation of this process.

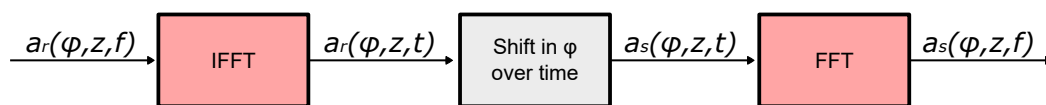


**Figure 4.2:** The process used to convert the frequency domain results of the mechanical simulation from the rotor reference frame to the stationary reference frame.

# 5

## Acoustic Analysis

The last domain in the simulation is the acoustic domain. In this chapter, the implementation of the acoustic sub-simulation is discussed. In the acoustic simulation, the pressure variations in the air around the motor are determined. Since the acoustic simulation is performed in the frequency domain, this is computed for each frequency. The input of the acoustic simulation is the acceleration of the outer surface of the motor. The output of the acoustic simulation is the pressure at each node in the domain, for each frequency. The first section, section 5.1, focuses on the geometry, domain and boundary conditions used for the acoustic simulation. Next, section 5.2 describes how the mechanics used for the acoustic simulation are implemented.

### 5.1. Acoustic Domain and Boundary Conditions

The acoustic noise emitted by an electric motor depends almost entirely on the normal surface acceleration of the outer surface of the motor [2]. This means that for the structure, only the outer shell of the motor has to be implemented, which is a cylinder. The size of the cylinder is based on the size of the structures used in the previous simulations, namely  $R = 17.51$  mm and  $L = 17.4$  mm.

The domain of the acoustic simulation is the air surrounding the motor. This thesis only focuses on the sound emitted by the motor, and not on sound effects caused by the surrounding of the motor. Therefore, no reflections from the boundary should be present in the area of interest. To achieve this, a spherically radiated wave boundary condition has been applied. This boundary condition makes sure that outgoing spherical waves, coming from the center of the domain, can leave the domain with minimal reflections occurring. This means that the domain for which the model has to be solved can be small, while still providing results as if the motor is spinning in an infinitely large domain. Therefore, when the sound power within the domain is analyzed, all of this power is guaranteed to directly come from the motor.

Still, a tradeoff has to be made when deciding on the size of the domain for the acoustic simulation. The size of the domain has to be large enough to make sure that the waves coming from the motor have been merged into spherical waves when they arrive at the domain's boundary. This depends on the lowest frequency of interest, since this will produce the waves with the longest wavelength. At the same time, the larger the domain, the more periods are covered within the domain. This increases the computational cost of the simulation and especially of visualizing the results. Therefore, the domain has to be small enough that the time required for solving the model and visualizing the result is reasonable, even at the highest frequencies, since they have the shortest wavelengths. Based on this tradeoff, a domain with size  $R = 100$  mm has been chosen.

Figure 5.1 shows the geometry used in the acoustic simulation, based on the previously mentioned dimensions.

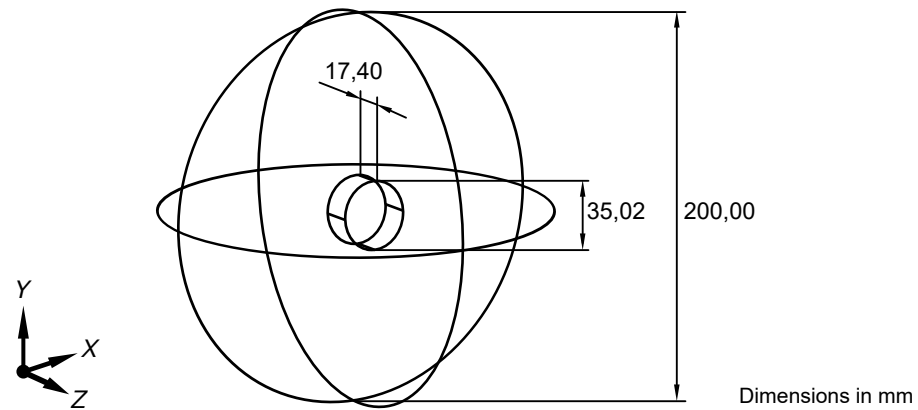


**Figure 5.1:** The geometry and dimensions used in the acoustic sub-simulation.

### Dynamic Domain Size

A possible way to prevent, or at least narrow down, the previously explained tradeoff that has to be made to choose a domain size, could be to implement a dynamic domain size. In such a simulation, the size of the domain could be changed for simulating different frequency bands. Although this does require the geometry to be remeshed every time the domain is updated, the overall time saved due to the higher computational efficiency at higher frequencies while maintaining the accuracy at lower frequencies, might make such an implementation a feasible method to reduce the overall computational effort required. In this thesis, however, this has not been implemented, and a fixed domain size is chosen instead.

## 5.2. Acoustic Mechanics

As well as the magnetic and mechanical simulation, the acoustic simulation is a FEM based simulation, implemented in COMSOL. The acoustic simulation is implemented using the pressure acoustics physics module of COMSOL. In this module, the pressure variations are determined based on a linear elastic fluid model. Herein, the fluid is characterized by its density and the speed of sound within the fluid.

### Outer Surface of the Motor

In the acoustic simulation, the surface normal acceleration resulting from the mechanical simulation is applied to the outer surface of the motor. Both the results from the time domain and frequency domain mechanical simulation can be used, after they have been converted to the stationary reference frame, as discussed in 4.2.5.

To apply the results of the time domain mechanical study in the acoustic simulation, they need to be converted to the frequency domain. This is done by computing the FFT on the results of the mechanical study, which can directly be implemented in COMSOL. Once the results have been converted to the frequency domain, they are applied to the acoustic structure using a one to one mapping.

To apply the results of the frequency domain mechanical study, they first need to be converted from the rotor reference frame to the stator reference frame, as discussed in 4.2.5. Since for the frequency domain study, this is done in MATLAB, the results of this conversion have to be imported into COMSOL once the conversion is done. This is implemented in COMSOL by defining a 3D interpolation function node, which is defined using the data from MATLAB.

### 5.3. Meshing of the Acoustic Domain

Especially in the acoustic simulation, the size of the mesh elements is just as important as the size of the domain. To keep the error introduced by the mesh size reasonably low, it is recommended to have at least 5 node elements per wavelength [15]. However, a higher mesh resolution also results in an increased number of mesh elements and therefore an increase in the computational effort required to solve the model. Based on this tradeoff, a maximum mesh element size of 5 mm has been chosen. Since this is a compromise, it should be noted that the results of the acoustic simulation above 14 kHz may contain some error caused by less than 5 nodes per wavelength.

Just as mentioned for the domain size, it could be considered to implement a dynamic mesh size for different frequency bands. This way, the number of nodes per wavelength could be kept more constant, resulting in a better computational efficiency at the cost of having to remesh the domain for each frequency band. This has not been implemented in this thesis.

# 6

## Investigation and Results of the Numerical Model

This chapter describes how the previously developed simulation is executed and how the results of the simulation have to be interpreted. The results of the simulation are preprocessed and visualized in a way to obtain insight into how the acoustic noise is generated and propagates through the physical domains. Later on, this acts as a foundation for finding ways to reduce the total emitted noise. Sections 6.1 to 6.3 elaborate on how the results of the magnetic, mechanical and acoustic simulation are obtained, processed and visualized. Furthermore, it is discussed what can already be deduced from the results.

### 6.1. Magnetic Simulation

The magnetic simulation is performed under no load conditions at a fixed speed of 3000 rpm. To obtain the results for the time domain mechanical simulation, the simulation period is set to a full electrical cycle. For determining the force required for the frequency domain mechanical simulation, the duration of the simulation will be set to the duration determined in section 3.2.5. The time step is set to be at least 10 times lower than the period of the highest frequency of interest, which is 20 kHz, i.e., 5  $\mu$ s.

#### 6.1.1. Magnetic Flux Density

The base result of the FEM magnetic simulation is the magnetic flux. The flux density within the motor is plotted in 2D using a color scale and streamlines. In figure 6.1, the magnetic flux density is plotted at 8 different times within half of an electrical period, with a fixed interval. Since the magnetic flux density plot does not show the direction of the flux, but only the amplitude, the second half of the electrical period will be identical and is therefore not plotted.

The magnetic flux density plots are used to verify that the chosen material properties, make sense. This seems to be the case, since flux density is clearly higher in the silicon steel, but some leakage can be found within the air and the copper.

In figure 6.1, the effect of the fractional slot winding is very clear. A rotation in the magnetic field can be seen, and it is noted that this rotation rotates faster, but in the same direction, as the rotor. This rotation happens due to the fact that the magnets and slots are aligned in succession and not all at the same time. Furthermore, this verifies that the reasoning in section 3.2.5 is correct, and only  $1/84^{th}$  of

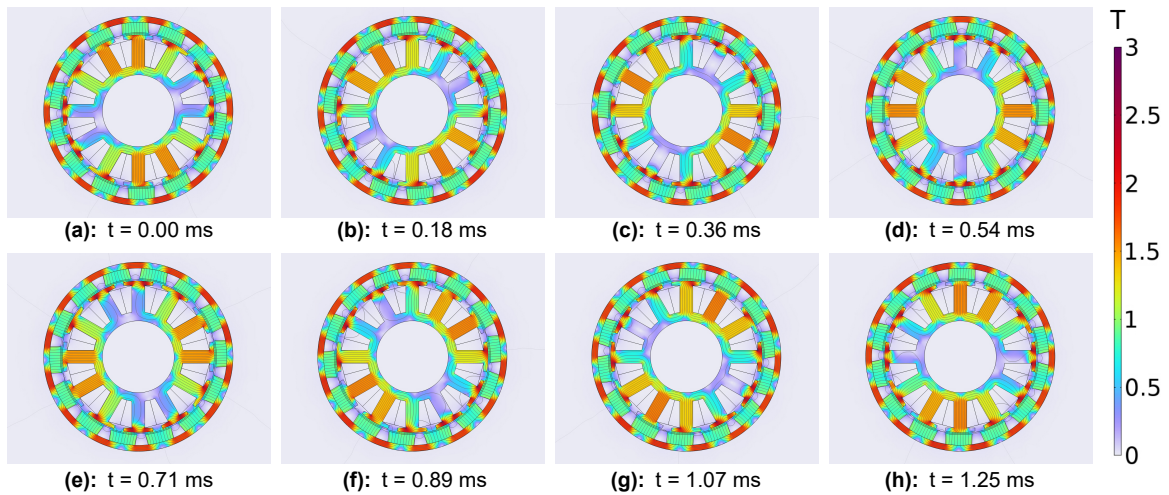


**Figure 6.1:** The magnetic flux density resulting from the magnetic simulation over half an electrical period.

a mechanical period needs to be simulated in the magnetic domain, to obtain all result necessary for the subsequent simulations, if rotating the result in space is possible.

### 6.1.2. Radial Air Gap Flux

The amplitude of the magnetic flux, in the radially outward direction, in the center of the air gap is also plotted. This is plotted over the curve where  $R = 14.25$  mm, at  $t = 0$ , and is shown in figure 6.2.

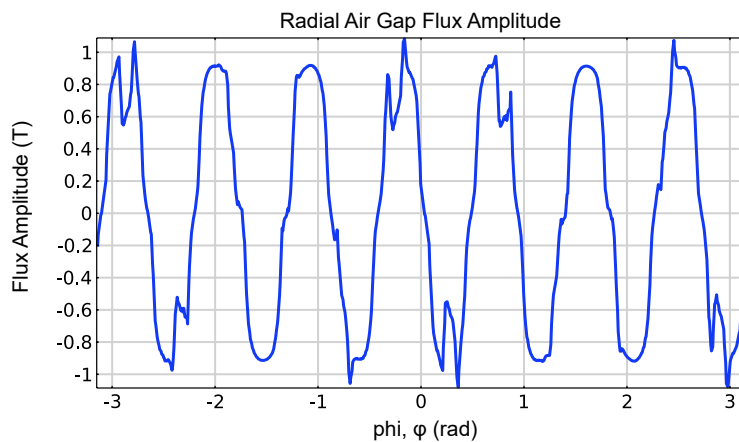


**Figure 6.2:** The amplitude of the magnetic flux in the center of the air gap in the radially outward direction. Plotted at  $t = 0$ ,  $R = 14.25$  mm and over  $\varphi$ , the spatial angular coordinate.

Using the data of the radial flux amplitude in the air gap, it is confirmed that this is a superposition of two spatially distributed sines with spatial order 7 and 12. These are a result of the permanent magnets and the stator saliency, respectively. This supports the assumption made in section 3.3.2, that the harmonics caused by the rotor magnets and stator saliency are the most prominent in the air gap flux.

### 6.1.3. Magnetic Force

As previously discussed, the magnetic forces acting on the rotor of the motor are calculated using Maxwell's stress tensor using the results of the magnetic simulation. To visualize the result of this calculation, the resulting force is plotted in a 2D arrow plot. This plot is shown in figure 6.3 for  $t = 0$ .

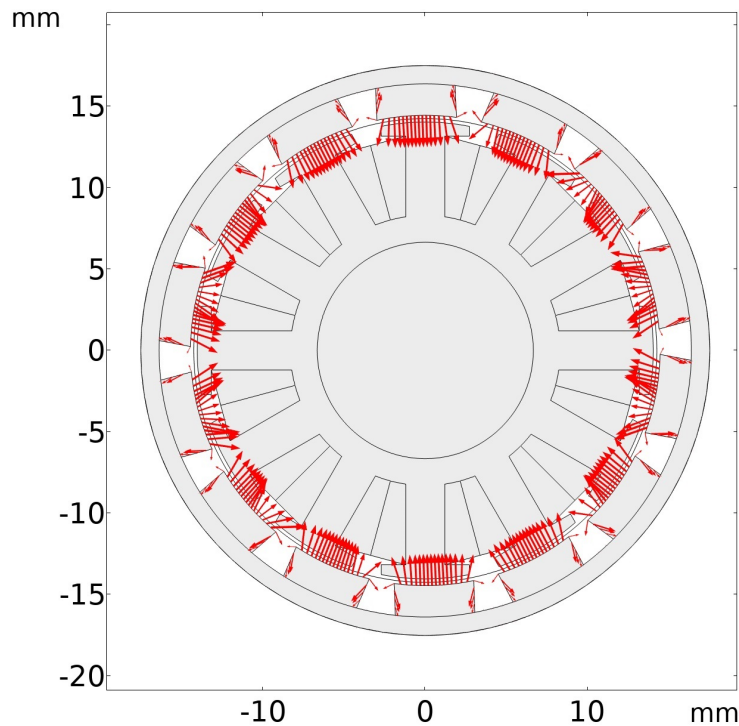


**Figure 6.3:** A 2D arrow plot of the electromagnetic force acting on the rotor of the motor at  $t = 0$ .

In figure 6.3 it can be seen that, as expected, the force acting on the rotor is largest when the permanent magnets are closest and most aligned to the stator slots. Furthermore, when the permanent magnets are not aligned to the stator slots, the forces acting on the permanent magnets are pulling them towards the stator slots. Due to the fact that the number of permanent magnets and stator slots are no multiple of each other, the total rotational force, i.e., the torque acting on the rotor is small, regardless of how the magnets are aligned.

#### 6.1.4. Spatial and Temporal Force Harmonics

Based on the plot of the radial air gap flux amplitude and electromagnetic force acting on the rotor, it is clear that the 7<sup>th</sup> and 12<sup>th</sup> spatial harmonic orders are significant. However, to gain a more detailed understanding of all the harmonics present and to identify the frequencies corresponding to each harmonic, the 2D FFT of electromagnetic rotor force is computed, according to section 3.3.1. This also allows verifying the results against the harmonics calculated in section 3.3.

To be able to calculate the 2D FFT of the rotor force resulting from the electromagnetic simulation, some preprocessing of the results is necessary. Since the actual force calculated in the simulation is located at the surface of the rotor, the distance between the location of each result and the origin is not the same. Therefore, the results are exported from COMSOL and imported into MATLAB, where the results are mapped from the 2-dimensional  $R$ - $\varphi$ -domain to a 1-dimensional domain with only  $\varphi$  as free variable. Since the force is given in  $N/m^2$ , the results are scaled to correct for the difference in radius from the original location of the result and the projected radius of the 1-dimensional  $\varphi$ -domain. Furthermore, the results are converted from the rotor's reference frame to the stator's reference frame. This is done by shifting the results in the  $\varphi$ -domain with a quantity equal to  $\omega_{mech}t$ . The result of this remapping can be seen in figure 6.4(a). The MATLAB code used to import the data from COMSOL and remap the data can be found in appendix B.2.1. The code used to compute the 2D FFT of the rotor force is added in appendix B.2.2.

In figure 6.4(b) the result of the first FFT over space can be seen, where the y-axis corresponds to

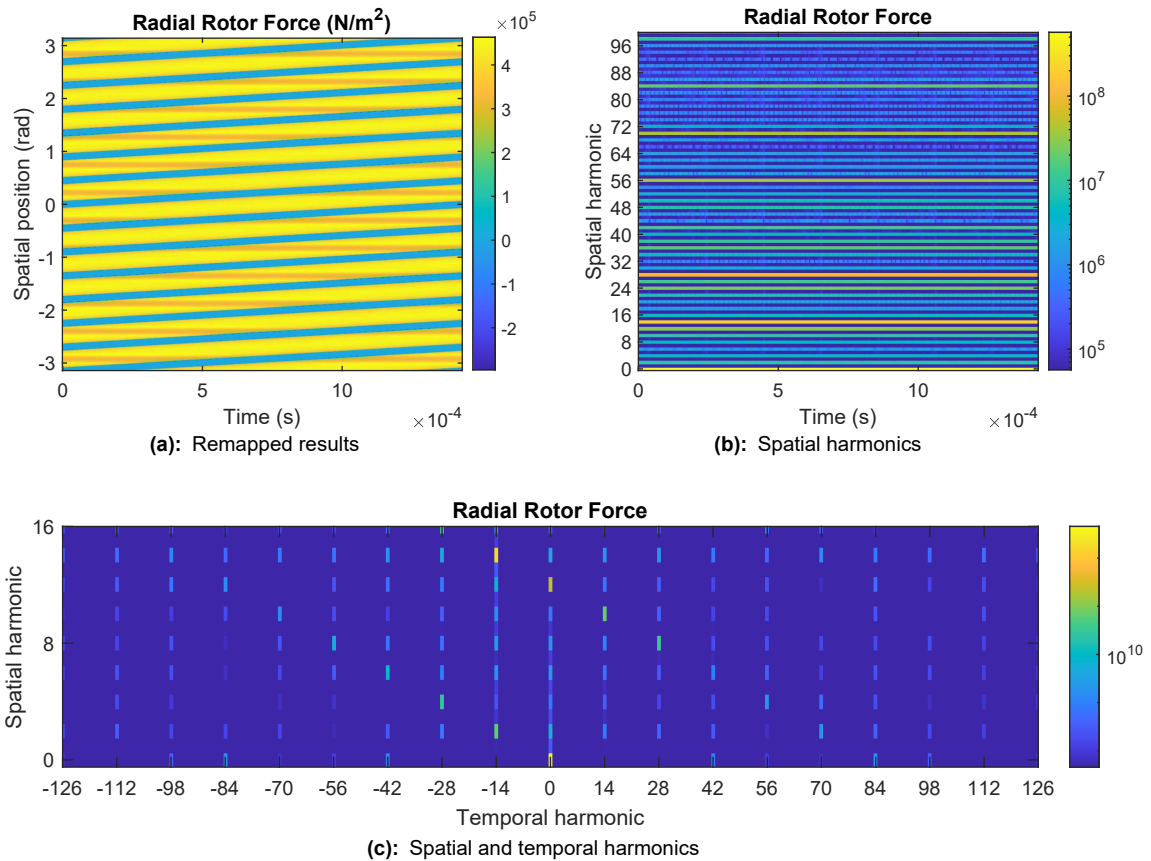


**Figure 6.4:** The remapped force harmonics in the 1-dimensional  $\varphi$ -domain over time on the left. In the middle, the result of the first FFT over space, showing the spatial harmonics over time. On the right, the result of the 2D FFT, showing the spatial and corresponding temporal harmonics.

the spatial position,  $\varphi$ . In this figure, it can already be noted that the 12<sup>th</sup> and 14<sup>th</sup> spatial orders are significantly present and that all other non-zero harmonics are multiples of 2. This is due to the effect that the rotor force is proportional to the flux density squared. Since the flux density is sinusoidally distributed over space with one period per  $2\pi$  radians, 2 is the fundamental harmonic order and only spatial harmonics that are multiples of 2 will be present in the force acting on the rotor.

The bottom figure, 6.4(c), shows the result of the 2D FFT. Herein, the frequencies at which the spatial harmonics occur can be seen. As expected, from the force in the stationary domain, the 12<sup>th</sup> harmonics, caused by the stator slots, occur at 0 Hz, whereas the 14<sup>th</sup> harmonics, caused by the rotors permanent magnets, occur at non-zero frequencies. Also, comparing figure 6.4(c) to the analytically predicted harmonics in figure 3.8, show that the most prominent harmonics resulting from the simulation do indeed match the predicted harmonics.

## 6.2. Mechanical Simulation

The mechanical simulation is performed using the results of the magnetic simulation and therefore also performed under the same conditions. For the time domain mechanical simulation, the modulo function is used inside COMSOL, to “repeat” the magnetic simulation results in time. For the frequency domain mechanical simulation, the result of the magnetic study is repeated and remapped according to the spatial and temporal symmetries determined in section 3.2.5. The MATLAB code used to do this can be found in appendix B.2.3.

The base result of the mechanical simulation is the deformation of the rotor, and the result that is of relevance for the acoustic simulation is the surface normal acceleration. In this section, the results of both the time and frequency domain simulations are shown. To interpret the frequencies present in the deformation and acceleration resulting from the mechanical simulation, a modal analysis is performed to find the eigenshapes corresponding to those frequencies.

### 6.2.1. Time Domain Results

To inspect the results of the mechanical simulation, the deformation is drawn with an amplification factor and animated over time. This allows to view the oscillations happening in the structure of the rotor. An animation, however, can not be added to a report, and drawing the deformation at various points in time would not give a complete view of how the structure is oscillating.

Therefore, the radial deformation of the outer shell of the rotor at a specific z-coordinate is plotted over time in a 2D surface plot. Since the deformation of the rotor is largely linear in the z-direction, this gives a good impression of the oscillation. The z-coordinate chosen for this result is  $z = 10.2$  mm, as this is the middle of the extruded 2D structure. Figure 6.5(a) shows the result of this, the radial outward deformation over time and the spatial angular coordinate  $\varphi$ .

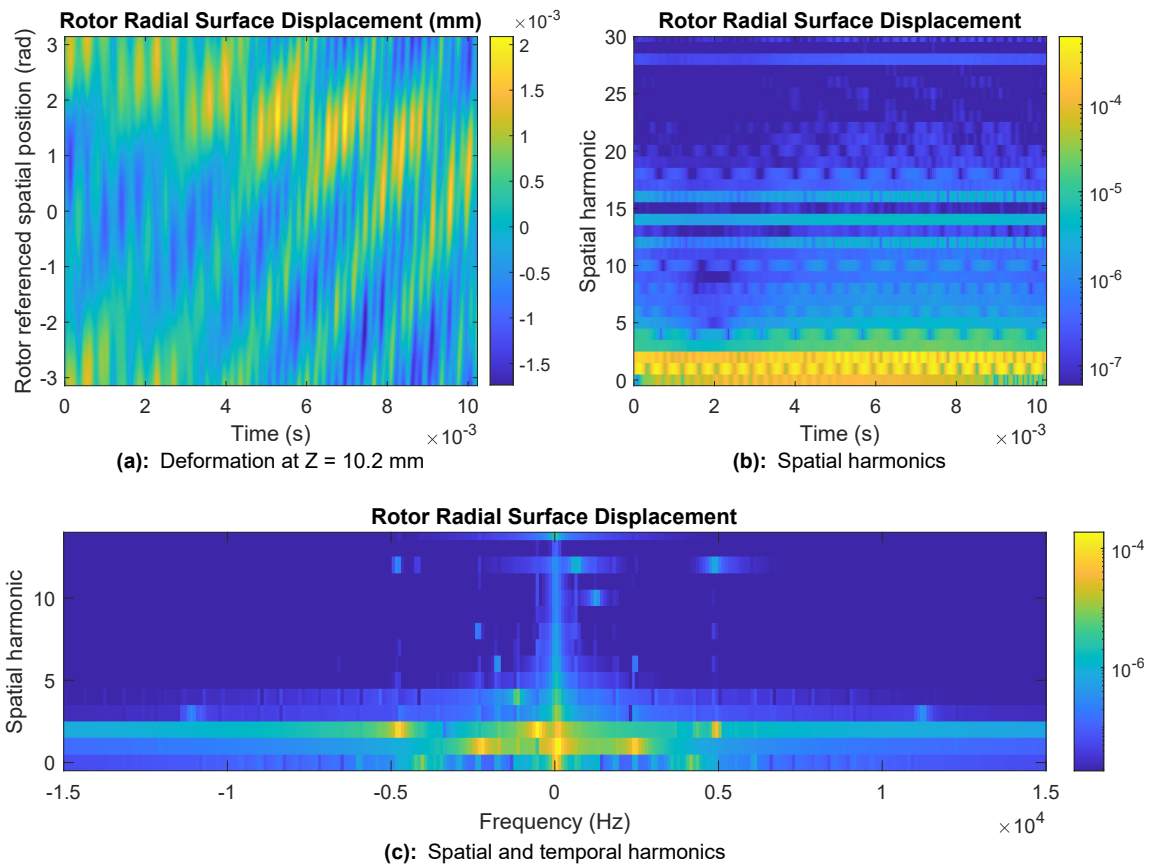


**Figure 6.5:** On the top left, the radial outward deformation over the spatial angular coordinate,  $\varphi$ , and time at  $z = 10.2$  mm. On the top right, the result of the first FFT over space, showing the spatial harmonics over time. At the bottom, the result of the 2D FFT, showing the spatial and corresponding temporal harmonics.

The first FFT is performed over space, which results in figure 6.5(b), the spatial harmonics present over time. From this plot, it can be concluded that the 1<sup>st</sup> and 2<sup>nd</sup> mode shapes are most present in the deformation. Furthermore, most mode shapes that are significantly present are multiples of 2, which is a logical consequence of the fact that this was also the case for the electromagnetic force which causes the deformation.

Next, the second FFT is performed over time, resulting in figure 6.5(c). From this figure, the frequencies corresponding to the harmonics can be seen. The code used to obtain the figures in 6.5 can be found in appendix B.3.1.

## 6.2.2. Frequency Domain Results

The mechanical simulation has also been performed in the frequency domain. As explained in section 4.2.4, magnetic excitation only occurs at harmonics of the electrical frequency, i.e. multiples of 14 times the mechanical rotational velocity. This has also been verified using the simulation results of the electromagnetic simulation in figure 6.3. Since there is no electromagnetic force acting on the rotor at other frequencies, there will be also no deformation at those frequencies. Therefore, the mechanical model is only simulated at multiples of the electrical frequency.

The input of the mechanical simulation in the frequency domain is the frequency domain magnetic force. The script used to construct this force, based on the results of the short time-domain magnetic simulation, can be found in appendix B.2.3.

Once the force has been processed and imported into COMSOL, the mechanical model is simulated and the resulting deformation at the center of the rotors outer surface is exported. This allows to compare the result of the frequency domain mechanical simulation to those of the time domain implementation. The deformation is processed the same as the results in section 6.2.1, however an important difference is that since the results are already in frequency domain, only the FFT over space has to be performed. This does however also mean that the FFTs are performed in reversed order, meaning that the resulting plot is not defined for positive and negative frequencies, but for positive and negative spatial harmonics. This means that to make the result comparable to the result of the time-domain mechanical simulation, the result is flipped up/down and left/right (or rotated 180 degrees) and append to the original result to obtain the full spectrum. The code in which this is performed can be found in appendix B.3.2. Figure 6.6 shows the result of the mechanical simulation and this preprocessing.

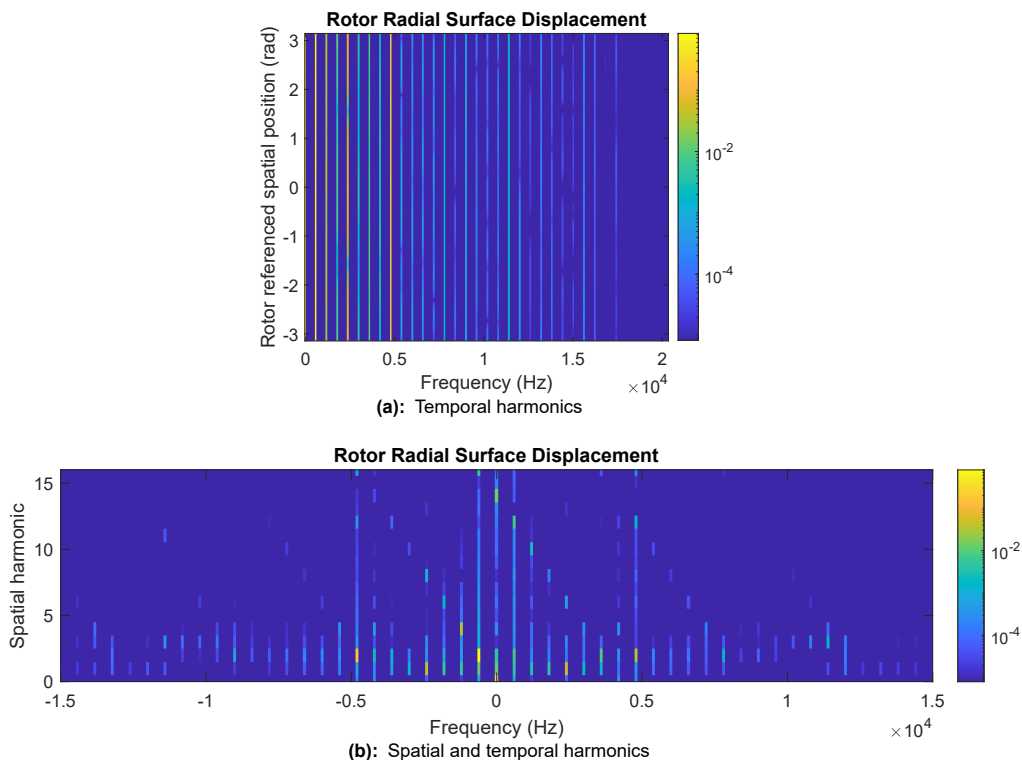


**Figure 6.6:** On the top, the radial outward deformation over the spatial angular coordinate,  $\varphi$ , and frequency at  $z = 10.2$  mm. At the bottom, the result of the FFT over space, showing the spatial and corresponding temporal harmonics.

From the results in figure 6.6(b), it can be seen that most of the peak frequencies are similar to the result of the time domain mechanical simulation results in figure 6.5(c). A big difference however is that in the results in 6.5(c), deformation is present at frequencies that are not a multiple of the fundamental electrical frequency, which is likely an effect of spectral leakage introduced with performing the FFT. This leakage does not occur when performing the mechanical simulation in the frequency domain.

### 6.2.3. Eigenfrequency Analysis

To reduce the noise emitted by the motor, the vibrations in the structure of the rotor have to be reduced. To find ways to reduce these vibrations, however, it is crucial to know the shape of the vibration. From the results in the previous sections, it is clear that the structure has frequencies at which it tends to vibrate the most. These are the eigenfrequencies, also called modal frequencies or resonance frequencies. Each eigenfrequency has a corresponding eigenshape. Using an eigenfrequency analysis, the eigenfrequencies and corresponding eigenshapes can be determined.

In the eigenfrequency analysis, the ARPACK code is used to find eigensolutions to the deformation analysis of the linear elastic solid model [16] [17]. The results of this analysis are the approximated eigenshapes and corresponding eigenfrequencies of the 3D structure of the rotor, within a certain frequency region. By matching the resulting eigenfrequencies to the frequencies present in the deformation spectrum resulting from the mechanical simulation, the eigenshapes corresponding to these deformations can be determined. This means that when finding methods to reduce the acoustic noise emitted by the motor, based on these results and the result of the acoustic study, the eigenshapes that cause most emitted noise are already known.

Figures 6.7(a) - 6.7(g) show the results of the eigenfrequency analysis, which is performed in the region of 0-20 kHz. For a cylindrical shape such as the rotor of the motor, each vibrational mode has two orthogonal shapes per vibrational mode. This means, for example, that there are two mode 2 eigenshapes, however the nodes of the first eigenshape correspond to the anti-nodes of the orthogonal eigenshape, and vice versa [9]. Since the structure of the rotor, however, is not completely cylindrical symmetric, the orthogonal eigenfrequencies are close to each other, but not completely equal and not each eigenshape has a corresponding orthogonal shape. The results shown are some of the most prominent eigenfrequencies and shapes. Eigenshapes that are not excited by the electromagnetic force are not included, since they are not of interest for the analysis in this thesis. Also, of each orthogonal eigenshape pair, only one has been included in figure 6.7, however the eigenfrequency of the corresponding orthogonal eigenshape has been provided in the subscript between brackets.

Since the 0<sup>th</sup> order spatial mode is commonly significant in electric motors with a high number of poles, but no such mode resulted from the eigenfrequency analysis, this mode has been separately analyzed. Figure 6.7(h) shows the result of this analysis. The eigenfrequency corresponding to the 0<sup>th</sup> order spatial mode turned out to be 38.456 kHz which explains why it was not present in the results of the initial eigenfrequency analysis.

The tangential vibrational mode in figure 6.7(a) is excited by variations in the torque delivered by the motor. Therefore, this mode will be present during operation of the motor, however since the normal deformation caused by it is relatively small, it will likely not be relevant for the acoustic noise emitted by the motor. The axial vibrational mode, in figure 6.7(d) will also not cause acoustic noise to be emitted from the rotor outer surface. This node will however cause noise to be emitted from the back of the motor (the end cap). Since this mode is however not excited by the electromagnetic field, it is not relevant for the acoustic noise that is emitted.

The eigenshapes in figure 6.7(a, c, e-h) do cause significant normal deformations. The mode 0 eigenshape in figure 6.7(h), has a very high corresponding eigenfrequency, which means the acoustic noise emitted by this mode is probably very small. Since the frequency at what this mode vibrates is far outside the frequency band of interest, the acoustic simulation results can however not be used to verify this.

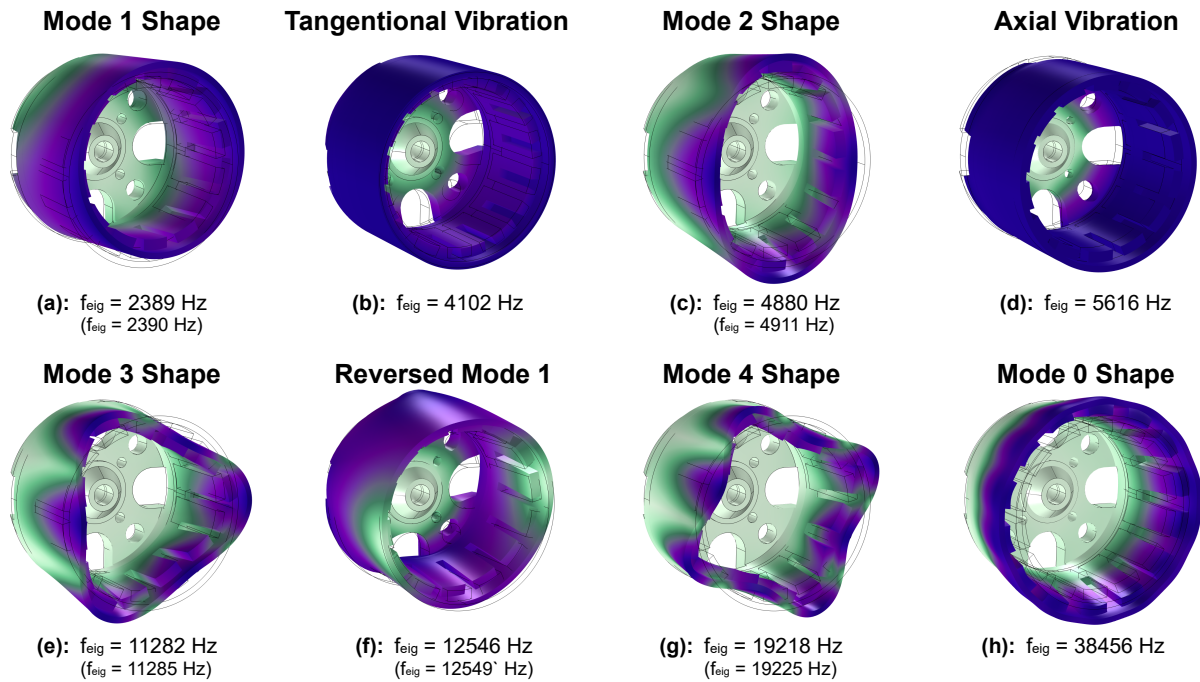


**Figure 6.7:** Some of the most prominent and relevant eigenshapes and corresponding eigenfrequencies resulting from the eigenfrequency analysis. White/green parts are close to their original position, while blue/purple parts are far from their original position. This means white/green parts indicate the nodes and the blue/purple parts indicate anti-nodes.

## 6.3. Acoustic Simulation

The final simulation step that is performed is the acoustic simulation. The acoustic simulation is a frequency domain simulation in the stationary reference frame. The input of the acoustic simulation is the normal acceleration of the rotor's outer surface. This means that the results of the time domain mechanical study, needs to be converted to the frequency domain and that the result of both the time and frequency domain mechanical study need to be converted from the rotor reference frame to the stator reference frame. The conversion from time domain to frequency domain is directly implemented in COMSOL using an FFT study node. The conversion from rotor domain to stationary domain is implemented according to section 4.2.5.

Once the acceleration from the mechanical simulation is converted to the stationary frequency domain, it is applied to the acoustic simulation. The results of the acoustic simulation is the acoustic pressure in the area surrounding the motor. First, the total acoustic power emitted by the motor for each frequency is determined. Based on this, the frequency spectrum of the total acoustically radiated power is plotted. Next, to visualize how the waves are propagating away from the motor, the acoustic pressure isosurfaces are plotted.

### 6.3.1. Total Acoustic Radiated Power

To determine the total acoustic radiated power, the sound intensity (in  $W/m^2$ ) is integrated over the boundary of the acoustic domain for each computed frequency. Based on this, the total power radiated by the motor at each frequency is plotted. The peaks in the resulting spectrum are analyzed and compared to the eigenshapes in figure 6.7 and the isosurfaces of the acoustic radiated waves in section 6.3.2. Based on this, the order of the mode shapes,  $m$ , that cause the peaks are determined and annotated. Figure 6.8 shows the result of this when the mechanical simulation is performed in the time domain, and figure 6.9 shows the results based on the frequency domain mechanical simulation.

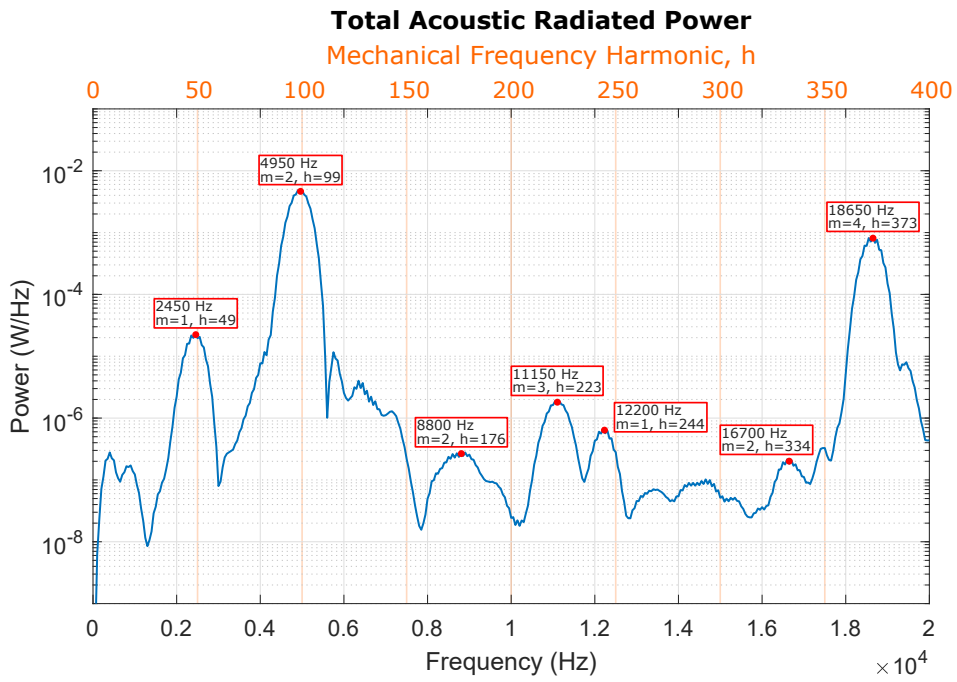


Figure 6.8: The total acoustically radiated power spectrum, based on the time domain mechanical study.

In figure 6.8, it can be seen that the two highest peaks in the acoustic noise spectrum are caused by mode 2 and mode 4 waves. This is as expected, since the fundamental spatial order of the force acting on the rotor is 2. Furthermore, no mode 0 acoustic waves are emitted by the rotor, which is in line with the observations in the modal analysis, which showed that the mode 0 eigenshape of the rotor’s structure has a corresponding eigenfrequency that is far out of the frequency region of interest.

A more unexpected result, is the occurrence of mode 1 and mode 3 acoustic waves, since these should theoretically not be excited by a symmetric electromagnetic field, such as the field in the air gap of the studied motor. Possible explanations for this will be discussed in section 7.4.1.

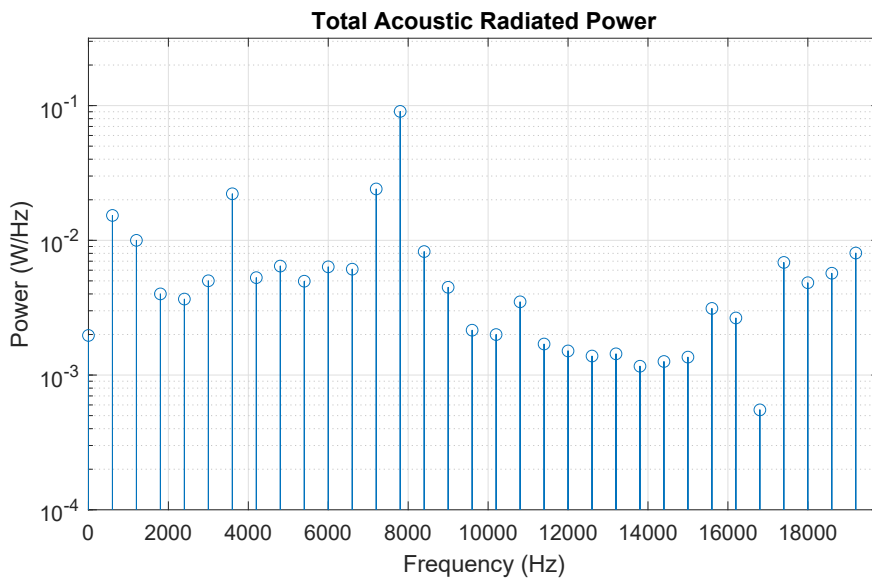


Figure 6.9: The total acoustically radiated power spectrum, based on the frequency domain mechanical study.

The acoustic radiated power based on the frequency domain mechanical simulation, shown in figure 6.9, clearly shows a huge mismatch compared to the result using the time domain mechanical study. Based on further investigation in chapter 7, it was found that the results based on the time domain mechanical study are most accurate and therefore these will be used. In section 7.4.3, the cause of this mismatch will be further investigated and explained.

### 6.3.2. Acoustic Pressure Isosurfaces

To visualize the 3D acoustic waves propagating through the air surrounding the motor, acoustic isosurfaces are plotted. These isosurfaces are surfaces at which the acoustic pressure is at a constant value. The surfaces are colored to indicate this pressure. A logarithmic scale is used for the coloring and values of the isosurfaces. Furthermore, to increase visibility of the wave shapes, a clipping plane is added. Since the results are in the frequency domain, they can be animated over the phase angle, however, in the report all isosurface plots are exported at a  $0^\circ$  phase angle.

The results of the simulation based on the time domain mechanical study are used. The frequencies at which the isosurfaces are plotted are the four peak frequencies in figure 6.8. The isosurfaces can be found in figure 6.10.

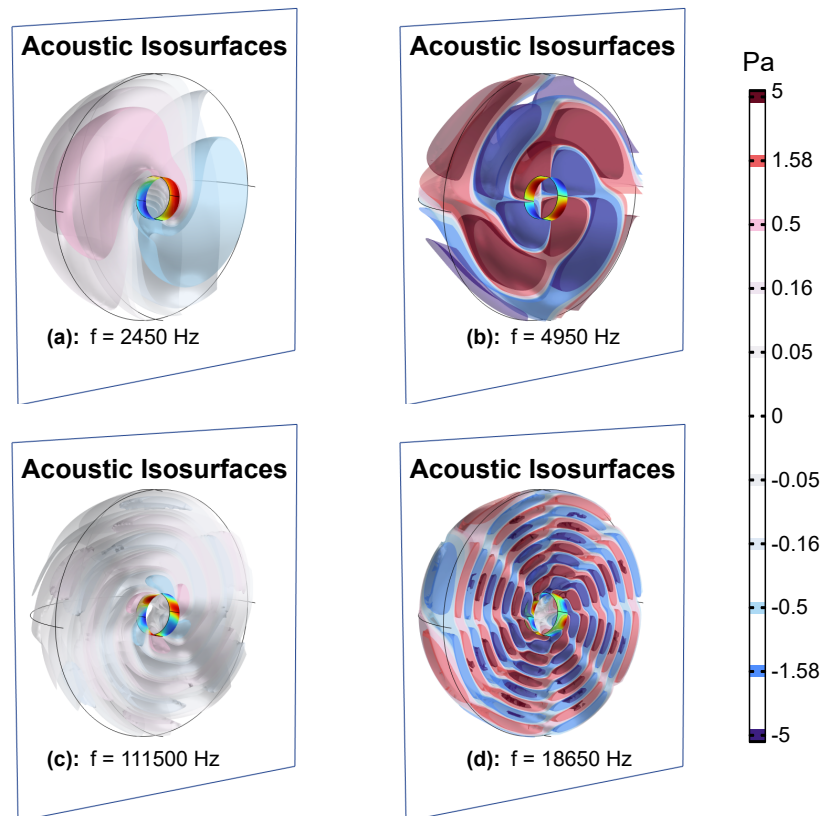


**Figure 6.10:** The acoustic isosurfaces of the acoustic waves radiated by the motor, at the 4 acoustic radiated power peak frequencies, based on the results of the time domain mechanical study.

Based on the shapes of the waves radiated by the motor, the subfigures of 6.10 can be coupled to the eigenshapes in 6.7. The relation between these are shown in table 6.1. At no frequency, mode 0 acoustic waves are emitted by the motor in the simulation results.

ISOSURFACE FIGURE	ACOUSTIC FREQUENCY	EIGENSHAPE FIGURE	EIGENFREQUENCY
6.10 (a)	2450 Hz	6.7 (a)	2389 Hz
6.10 (b)	4950 Hz	6.7 (c)	4880 Hz
-	8800 Hz	6.7 (c)	4880 Hz
6.10 (c)	11150 Hz	6.7 (e)	11282 Hz
-	12200 Hz	6.7 (a)	2389 Hz
-	16700 Hz	6.7 (c)	4880 Hz
6.10 (d)	18650 Hz	6.7 (g)	19218 Hz

**Table 6.1:** The relation between the eigenshapes in figure 6.7 and the acoustic radiated waves in figure 6.10. The eigenshapes corresponding to the peak frequencies, but not shown in figure 6.10, are also added.

# 7

## Comparison and Reflection of the Results

In this chapter, first in section 7.1, the computation duration for the implemented simulation steps are shown, since computational cost was an important consideration in developing the simulation. Next, the results of the numerical simulation are compared to real world measurements performed in the laboratory in section 7.2. Furthermore, in section 7.3, the results are compared to the results obtained in available literature. Finally, in section 7.4, based on the previous sections, a general reflection on the results is performed to further investigate and explain discrepancies that are observed in the results.

### 7.1. Computation Duration of Simulation Steps

An important part of implementing the simulation was to keep the computational costs of the simulation low. Therefore, the computational power required to perform the simulation is an important result of the performed analysis. There are various steps required to simulate the motor in the electromagnetic, mechanical and acoustic physics domains. Two main simulation paths are developed, tested and used in this thesis. To gain a structured overview of these paths and how long the individual steps take to compute, a flow chart is depicted in figure 7.1. The solid arrows indicate the paths used in this thesis, while the dotted arrows indicate paths that could be implemented without much effort, if desired to do so. The computation times indicated in this graph are indicative and should give a general idea of how long each step takes, however the actual time per step depends largely on the used hardware.

The main difference between the two implemented simulation paths is whether the mechanical simulation is performed in time domain or in frequency domain. But besides that there are other advantages and disadvantages for both implementations. The difference in results between the simulations can be seen in the previous chapter and will be discussed in section 7.4.3.

In the top path in figure 7.1, the mechanical simulation is performed in time domain which takes the most time. The actual time required for the time domain study does however depend largely on the duration for which the motor is simulated. Increasing the duration will increase the accuracy and resolution of the succeeding FFT, however this will also increase the required time. This does however make it a flexible implementation. Furthermore, since the mechanical study is implemented in the time domain it is relatively simple to animate the oscillation of the rotor, allowing for a better understanding of how the vibrations are propagated through the structure. Another advantage of the implementation based on the time domain mechanical simulation is that all simulation steps are implemented in one stand alone COMSOL, model. This means MATLAB or a COMSOL LiveLink module is not required.

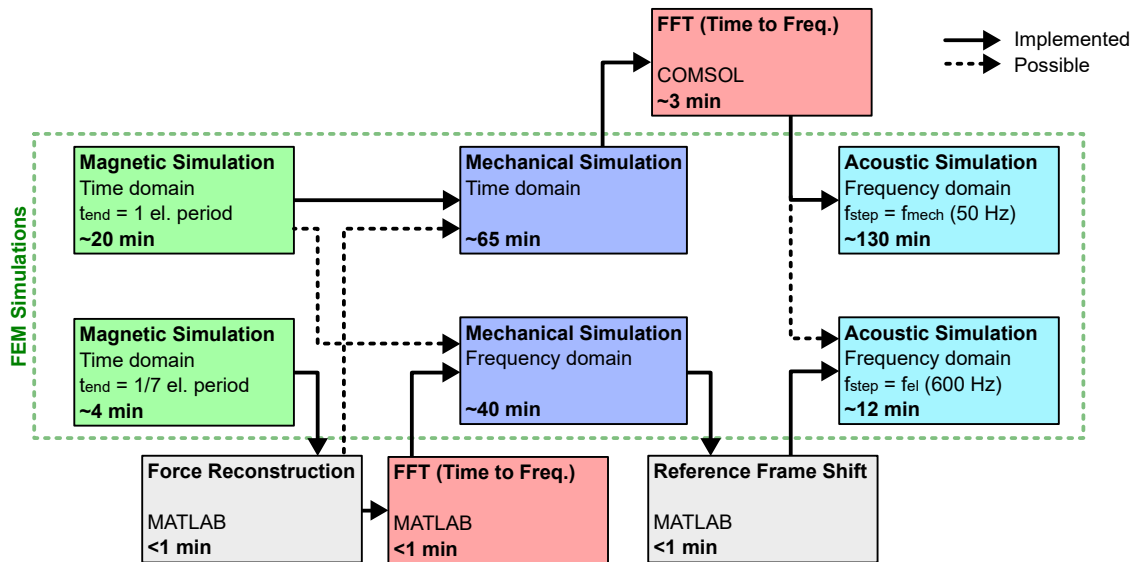


Figure 7.1: The steps of the two implemented simulation paths. The duration required to compute each step is indicated.

The bottom path, in figure 7.1, shows the implementation based on the frequency domain mechanical study. This implementation is relatively quicker, but also here the number of frequencies at which the model is analyzed determines the duration of the simulation. Since the results of the magnetic simulation in this implementation need to be exported to MATLAB to compute the FFT anyway, this implementation is more suitable to implement the transformation explained in section 3.2.5. This significantly reduces the duration of the magnetic time domain simulation, since the duration for which the motor has to be simulated is 7 times shorter. A disadvantage of the frequency domain mechanical study implementation is that the result of the mechanical simulation, which is in the frequency domain, needs to be converted from the rotor reference frame to the stator reference frame. This is relatively complicated and prone to numerical errors, as it comprises computing the IFFT, translating the results and computing the FFT successively. Furthermore, since the FFT of the magnetic simulation only results in excitation at the electrical frequency harmonics, the deformation and emitted noise at all other frequencies will be zero. This means that the mechanical and acoustic frequency domain simulation only have to be performed at harmonics of the electrical frequency. This reduces the computation time by a lot, but also simplifies the results.

## 7.2. Comparison of the Results with Measured Noise

To verify the developed simulation, the results of the simulation are compared to real world laboratory measurements. During the measurements, the motor is slowly accelerated to 3000 rpm. At 3000 rpm, the speed is briefly kept steady, before decelerating the motor again to a stop. The switching frequency of the motor controller is 20 kHz, and the control is performed without a sensor, using sliding mode control in the alpha-beta-reference frame.

To obtain the frequencies present in the noise emitted by the motor during the entire test, a waterfall plot is made. For this, the FFT is performed over a moving window with a fixed length. The code used to perform this analysis is included in B.6.1. The result can be seen in figure 7.2. In this plot, the black lines indicate the frequencies at which a relatively high amount of noise is emitted. Since these occur at a constant frequency, they are not dependent on the velocity of the motor. This means, they can be caused by the natural frequency of the rotor, harmonics in the motor control or other non-velocity dependent effects. The purple lines indicate harmonics of the fundamental electrical frequency (14 times the mechanical frequency). These are proportional to the rotational velocity of the motor. The black circles indicate locations where resonance occurs.

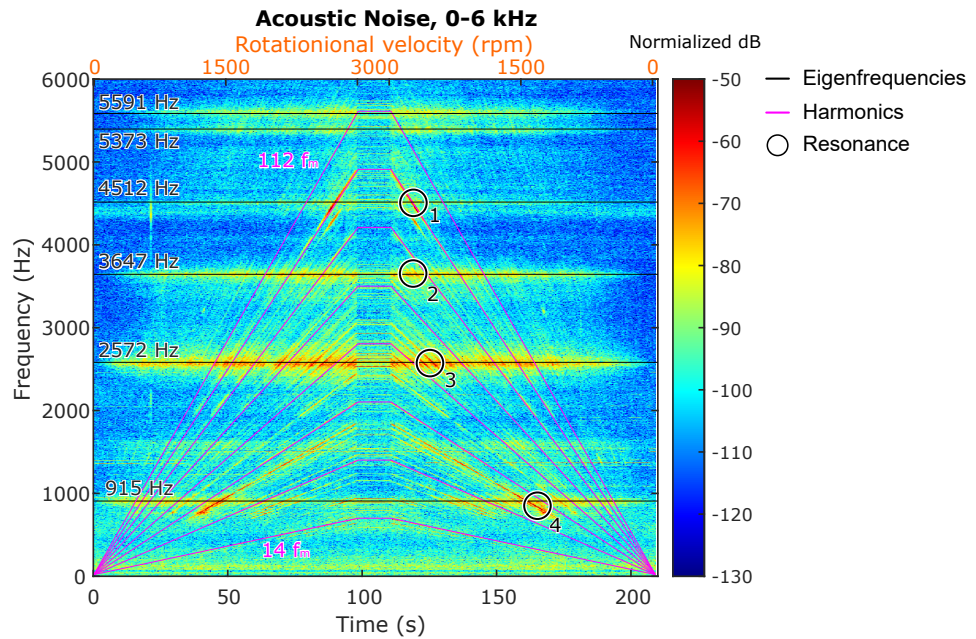


**Figure 7.2:** The waterfall plot of the acoustic noise emitted by the motor, measured during a complete cycle of accelerating, steady state and decelerating operation of the motor. The purple lines are the mechanical frequency harmonics. The black lines indicate noise emitted at constant frequencies, and the black circles indicate the locations where resonance occurs.

In the waterfall plot in figure 7.2, mainly the noise emitted at constant frequencies when the motor's velocity is constant are of interest, since these can be used to compare the measurements to the results of the simulation. However, also the non-constant frequencies are of interest. The noise with frequencies proportional to the rotational velocity of the motor are harmonics of the electrical or mechanical velocity. In section 3.3.2 the frequency harmonics and corresponding spatial harmonics were analytically determined. Based on the harmonics resulting from this analysis, the spatial harmonic corresponding to each purple line in figure 7.2 is known. When a resonance occurs, the force excitation is resonating with the eigenshape of the rotor structure. This indicates that the eigenshape at this frequency has the same spatial order as the harmonic causing the resonance.

Based on this logic, the resonance occurring at location 1 (black circle with a 1 next to it), which is caused by the 96<sup>th</sup> electrical harmonic, is resonating with the eigen-oscillation of the rotor's structure at 4512 Hz. Based on the results of the harmonic analysis (figure 6.4), it is known that the 96<sup>th</sup> harmonic corresponds to a mode 2 excitation. Since this excitation is causing resonance to happen, it is deduced that the vibrations in the rotor's structure at 4512 Hz are mode 2 vibrations. For the same reasons, the oscillations at 5373 Hz and 5591 Hz are expected to be caused by mode 2, probably orthogonal, oscillations.

The resonance that occurs at location 3 is not caused by any of the mechanical frequency harmonics. The oscillations at that frequency (2572 Hz) do however seem to resonate with a lot of other harmonics. Furthermore, this frequency is close to the mode 1 eigenfrequency of the rotor's structure determined in the modal analysis and the acoustic radiated power peak resulting from the acoustic simulation, which was also confirmed to be caused by mode 1 radiated waves. This all indicates that the oscillations occurring at 2572 Hz are mode 1 oscillations.

The resonance at location 2 and 4 are also not caused by any of the mechanical frequency harmonics. The frequencies at which they occur, 915 Hz and 3647 Hz respectively, are also not close to any of the frequencies resulting from the force analysis, modal analysis or the simulation. It should however be noted that these frequencies are almost exactly a factor of 4 apart, indicating that the oscillation at 3647 Hz is a harmonic of the oscillation at 915 Hz. Furthermore, the resonances that do occur are caused by the 36<sup>th</sup>, 72<sup>th</sup> and 108<sup>th</sup> electrical frequency harmonics, which are multiples of the number

of stator slots. This indicates that they may be due to the stator current used to drive the motor, which is not simulated in the no-load simulation, or due to tooth vibrations which are not considered in the simulation. To investigate this further, the phase currents will be analyzed in section 7.2.1.

Since humans are most sensitive to frequencies below 6 kHz, the waterfall plot added here is drawn up to this frequency, so that the details are clearly visible. In the full waterfall plot, up to 17 kHz, which is added in appendix A.2.1, some extra oscillations can be seen to occur around 10.65 kHz. The harmonics measured at these frequencies are very faint, making it hard to find what harmonics are resonating with the fixed frequency oscillation, and therefore determining the eigenshape at this frequency is complicated. However, since the oscillations occur at such a high frequency and is not very strong, it is not very relevant to reducing the noise emitted by the motor. In the simulation results, however, a peak can be found near the same frequency, at 11.15 kHz, that is caused by mode 3 vibrations.

Finally, the mode 4 oscillations that are present in the simulation results at 18.65 kHz, can not be verified using the measurement results that are up to 17 kHz. To verify whether a mode 4 oscillation is actually present at this frequency would require further investigation. Since this is far outside the frequency range that most humans can hear, this further investigation has not been performed.

### 7.2.1. Current Measurements

Since the oscillations at 915 Hz and 3645 Hz, could not be explained using the analytical force harmonics, modal analysis or simulation results and the current controller has a feedback loop close to 1 kHz, the current used to drive the motor during the measurements has been recorded, to look for a possible cause of these vibrations. Two phase currents are measured and stored. Based on the two measured phase currents, the alpha-beta current is determined. For the alpha-beta current, another waterfall plot has been made using a moving window FFT. Based on the waterfall plot, the harmonics and frequencies present in the current can be seen. Since the alpha-beta current consists of both a real and a complex part, the results of the short time FFTs will be non-symmetric, so both positive and negative frequencies are plotted. The resulting waterfall plot is shown in figure 7.3. The code used to generate the waterfall plot can be found in appendix B.6.2.

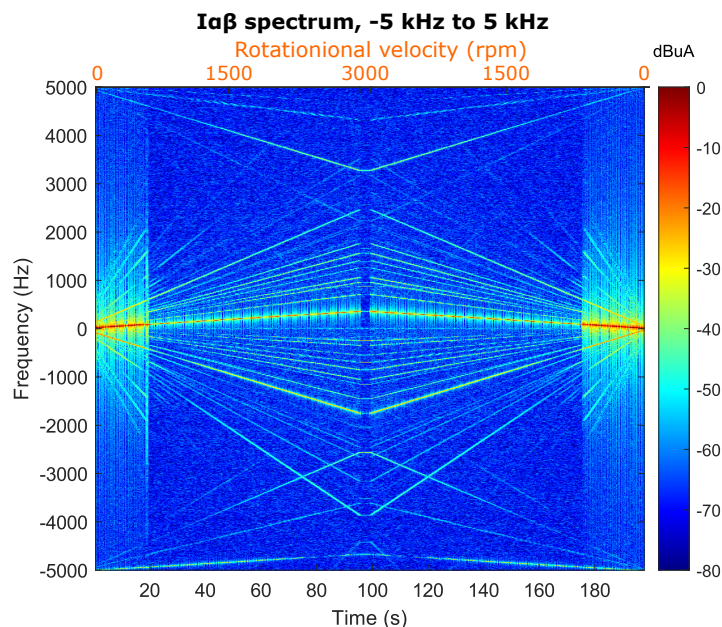


**Figure 7.3:** The waterfall plot of alpha-beta current, measured in the laboratory, during the complete cycle of accelerating, steady state and decelerating operation of the motor.

In the waterfall plot, the fundamental electrical frequency is very prominent and also the harmonics of the fundamental electrical frequency are clear. Furthermore, at 5 kHz, which is the switching frequency of the controller, the pattern is repeated. This is all as expected, and no significant fixed frequency components are visible. This means that the oscillations at 915 Hz and 3645 Hz are likely not directly caused by the controller but by another phenomena, such as tooth vibrations.

## 7.3. Comparison of the Results with Available Research

Next to comparing the results of simulation to laboratory measurements, it is useful to compare the results of the simulation to the results obtained in already available research. First, the implemented simulation is compared to implementations used in other literature. Next, the results of the simulation are compared to simulation results of electric motors in general and measurements performed on similar motors in available literature.

### 7.3.1. Implementation of the Simulation

An important difference that is found between available research about the simulation of electric motors, is that most of the research is focussed on large, automotive sized motors [18]–[20]. Furthermore, the available research that is tailored at small PMSMs, does commonly only consider inrunner motors and not outrunner motors [21]–[23], such as the ones commonly used in drones or other unmanned aerial vehicles, where the outside of the motor is spinning. Outrunner motor such as these are a popular choice for these applications as they provide a relatively high torque and power density [24].

Although the type or size of motor that is studied in other research focussed on simulating the acoustic noise emitted by electric motors is not the same, generally the same simulation procedure is used as in this thesis. First, the electromagnetic simulation is performed, then Maxwells stress tensor is used to determine the forces acting on the rotor, which is used to simulate the mechanical model to obtain the deformation/acceleration, which is used to perform an acoustic analysis [2], [19], [23].

### 7.3.2. Vibrational Modes of the Motor

Based on the result of the simulations and the measurements, it is found that the motor that is analyzed is very susceptible to mode 1 and mode 2 vibrations, while mode 0 and mode 4 vibrations occur at frequencies that are too high to be of relevance. This is a phenomenon that is generally not present in larger electric motors, since the eigenfrequencies of larger motors are lower and therefore mostly fall into the critical frequency range of 0-6 kHz [18], [20]. This is an inherent advantage of small electric motors, since higher eigenfrequencies reduces the overall vibration level that is transmitted [25].

The simulation results indicated a high susceptibility of the rotors structure to mode 1 oscillations. Theoretically, this mode should not be present, as it is not excited by the symmetrically distributed magnetic field [23]. The measurement result does also show a very significant peak in the measured radiated acoustic noise at the frequency where mode 1 oscillations are expected according to the modal analysis and simulation results. Measurements, performed by Henderson et al. in [26], on an almost identical motor using laser vibrometer probes to directly measure the deformation of the rotor, showed that, especially at a low rotational velocity, the mode 1 oscillation in the rotor of a small outrunner PMSM can be very significant and even the most significant mode of vibration. This supports the results obtained in this thesis, especially since the motor is analyzed at a relatively low rotational velocity, compared to the velocity for which it is designed based on the KV rating.

Furthermore, it was measured that the mounting of the motor to another structure can increase the amplitude of the mode 1 acoustic waves, while barely affecting the amplitude of the mode 2 acoustic waves that are emitted [26]. This makes sense, since a mode 1 oscillation causes the center of gravity

of the motor to oscillate, whereas a mode 2 oscillation does not affect the center of gravity. When the center of gravity is oscillating, this will cause the component to which the motor is mounted to oscillate as well and therefore increase the transmission from the structure borne oscillation to the airborne oscillations [9].

## 7.4. Reflection of the Simulation Results

In this section reflects on the results that were found. Unexpected results are explained, and an effort is made to find an explanation for these results.

### 7.4.1. Mode 1 Oscillations

Originally, it was not expected to encounter any mode 1 oscillations while analyzing the motor which is used as a test case in this thesis, as the symmetry in the electromagnetic field will prevent the magnetic field from exciting a mode 1 vibration. However, in contrast to the expectations, mode 1 vibrations were encountered in both the simulation results and the measurement results. Both these will be separately explained.

#### Mode 1 Oscillations in the Simulation

The mode 1 waves emitted by the motor in the result of the acoustic simulation are caused by mode 1 oscillations that result from the mechanical time domain simulation. That these mode 1 oscillations are already present in the result of the mechanical simulation can be seen in figure 6.5. Furthermore, when focussing on the 2D FFT results of the magnetic simulation in figure 6.4, it can be noted that also in those results, there is already a small mode 1 force component. To investigate the source of this mode 1 component, 2D FFT has also been computed over the electromagnetic force in the rotor reference frame. An interesting observation is that in this case, thus without converting the force from the rotor domain to the stator reference frame, the mode 1 force excitation is almost completely gone. The results of this rotor reference frame 2D FFT are added in appendix A.1.

Based on these observations, two possible causes of the mode 1 force acting on the rotor can be thought of. Either, the mode 1 force excitation can be a result of a combination of the original harmonics and the rotation of the rotor or the mode 1 force excitation is a numerical error introduced when interpolating the force that acts on the rotor. Further investigation is required to definitively determine the source of the mode 1 forces. Either way, the observation that a small mode 1 force excitation can cause a relatively large mode 1 deformation, shows that the structure is really susceptible to mode 1 oscillations.

#### Mode 1 oscillations in the Measurements

The noise measured in the acoustic measurements at the mode 1 eigenfrequency is more easily explainable. Although the motor is theoretically perfectly symmetric, each non-ideal motor will have some sort of imperfections causing imbalance in the rotation of the rotor [9]. Research has also shown that motors using a fractional slot winding are more likely to be subject to non-balanced magnetic forces [6]. Possible causes for imbalance could be, a nonuniform radial distribution of the mass of the rotor, a non-perfectly centered axis, play in the bearings or a difference in strength between the permanent magnets.

Combined with the susceptibility of the rotors structure to mode 1 oscillations that was observed in the simulation, these factors can cause mode 1 oscillations. That these oscillations can be very significant was also shown using laser vibrometric measurements of a similar motor [26]. These measurements also support that mode 1 oscillation can actually be the most significant form of oscillation when the motor is rotating relatively slow.

### 7.4.2. Comparison of the Results with the Measurements

There are two frequency bands in the measured acoustic noise, namely at 915 Hz and 3647 Hz, that could not be explained using the simulation results or another form of analysis. Since the higher frequency is almost exactly a multiple of the lower frequency, they likely share the same source. In an attempt to find the source of these oscillations, the phase current of the motor during operation was measured. The waterfall plot of the alpha-beta current derived from this did, however, not show any significant frequencies that were present. Since this confirms that the oscillations are not induced by the controller, they must be caused by another phenomenon. This means that there are two possibilities, either they are caused by the motor due to a phenomenon that was not considered in the simulation, or they are caused by an external component.

When the frequencies are caused by the motor due to a phenomenon that is not simulated, the first step into finding the source of the noise would be to determine the spatial order (mode) of the oscillations in the rotor that emit the waves at these frequencies. Since this could not be determined using the simulation results, the most effective way would be to measure the spatial order. This could be done by directly measuring the deformation of the rotor using laser vibrometers or by using array microphones to determine the spatial distribution of the waves emitted by the motor at these frequencies. Either way, more investigation is required to find the source of these oscillations.

The noise is not present when the motor is not rotating, so it can not be unrelated background noise, which means that if the frequencies are generated by an external component, it must be something that has to do with the measurement setup. A possible source could be the power supply. A switching power supply may start to make noise when current starts to be drawn, which would explain the measured results. However, to either verify or rule out that the noise is generated by an external component, further investigation of the measurement setup would be required.

### 7.4.3. Difference Between Time and Frequency Domain Mechanical Study

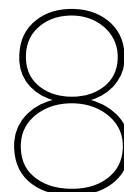
In section 6.3.1, it has been found that the results of the acoustic simulation using the frequency domain mechanical simulation are different to the results of the acoustic simulation when the results of the time domain mechanical simulation are used. Based on further investigation, it has been shown that the results based on the time domain mechanical simulation do match the measurements quite well, and therefore there probably is a problem with the results based on the frequency domain mechanical study.

Inherently, as predicted in section 4.2.4, there is a difference between both results, which was confirmed based on the results of both mechanical simulations in section 6.2.2. The difference between both results is due to the different locations in the simulation path when the results are converted to the frequency domain.

When the mechanical simulation is performed in the time domain, the FFT is performed after the mechanical simulation. Since the mechanical deformation at this point will consist of a combination between the frequencies excited by the electromagnetic force and eigenfrequencies of the structure. When performing the FFT on the results containing all these different frequencies, leakage will occur due to the non-infinite length for which the simulation has been performed. Therefore, the spectrum of the deformation resulting from this analysis will show spread out peak frequencies.

In contrast, when performing the mechanical simulation in the frequency domain, the FFT is performed before the mechanical simulation on the electromagnetic force resulting from the electromagnetic simulation. The electromagnetic force will only contain frequencies that are a multiple of the fundamental electrical frequency, as predicted in section 3.3.2 and verified in section 6.1.4. This means that when the FFT is performed over a time which is a multiple of the fundamental electrical period, no leakage will occur, meaning that only harmonics of the fundamental electrical frequency are excited in the mechanical simulation and therefore present in the deformation spectrum resulting from this simulation.

This difference in the deformation spectra of both implementations was shown in figure 6.5 and figure 6.6. Although there is a difference here in how “spread-out” the spectra are, they still show that the deformation consist of largely the same spatial and temporal harmonics. This means that the difference in the acoustic radiated power is likely caused by the conversion of the frequency domain results from the rotor reference frame to the stator reference frame. As mentioned in section 4.2.5, the process used for this transformation is very prone to numerical errors, which makes it even more likely that this is the source of the mismatch between the acoustic results. To verify whether this is indeed the source of the mismatch, further investigation would be required. The first step in this investigation would be to find an alternative way of converting the frequency domain deformation from the rotors reference frame to the stationary reference frame.



# Noise Reduction Recommendations

The underlying goal of simulating the acoustic noise emitted by the studied electric motor and for developing the simulation, is to be able to find general design optimizations that can be used to reduce the overall noise power that is emitted by the motor. In this chapter, three noise reduction methods that are based on the previously conducted research are proposed and explained in sections 8.1, 8.2 and 8.3. Where possible, the proposed noise reduction methods are verified using a modal analysis and the simulation that is developed in this thesis.

## 8.1. Rotor Balancing

Although theoretically, no mode 1 vibrations should be present, since they are ideally not excited by the electromagnetic force, they still showed up in the simulation and real world measurements. Both these indicate that rotor structures of small electric motors like this are very susceptible to mode 1 oscillations. This was also verified with other available literature in section 7.3, where measurements on similar motors also showed significant mode 1 oscillations. Since these modes are theoretically not excited by the electromagnetic forces acting on the rotor, they may be caused by imbalance of the rotor's structure or the bearings fixing the rotor in place. If this is the case, the source of these vibrations falls outside the scope of this thesis, which only includes acoustic noise with an electromagnetic source.

Nonetheless, since the mode 1 noise in the laboratory shows the highest emitted noise power, it can not be ignored that balancing the rotor might reduce the mode 1 vibrations and therefore the overall emitted noise. To balance the rotor, the same procedure as is used to propeller blades might be used. Using a sensitive measuring device, the imbalance could be determined and decreased by sanding off some of the rotor's material. This method does however only work if the vibrations are caused by imbalance, and not if the bearings induce the vibrations. In this case, the mode 1 vibrations could only be decreased by using higher grade bearings. Both these methods however will increase the cost of producing the motor, which means that using them or not is a tradeoff that has to be made. Furthermore, the effectiveness of these improvements can not be verified using the developed simulation, but would require a more detailed mechanical simulation or more laboratory testing.

As discussed in 7.4.1, another source of imbalance in the rotor that may cause mode 1 deviations is a variation of the magnetic strength between the rotor's permanent magnets. If this is the case, the imbalance may be reduced by measuring the strength of each of the permanent magnets, and mounting them in a configuration that minimizes the single-sided imbalance caused by the difference in magnetic strength.

## 8.2. Improving the End Cap Design

For small outrunner motors such as the one analyzed in this thesis, the rotor is almost always fixed at one side using an end cap with slots in it. The slots are required to prevent adequate cooling to the inside of the motor, and they reduce the overall weight of the motor. The places where a slot is located in the end cap are more susceptible to start oscillating and act as an anti-node in the oscillation of the motor. This means that using an even number of slots in the end cap makes it more susceptible to oscillations with an even spatial order.

The motor analyzed in this thesis has a fundamental electromagnetic order of 2 (since this is the least common divider between the number of stator slots and rotor permanent magnets), and at the same time uses an end cap with 4 slots. This means that the rotor's structure is by design extra susceptible to the oscillations that are expected to be excited by the electromagnetic field, which is really undesirable. This susceptibility can be reduced by altering the rotors structure to use a number of slots that is not a multiple of the fundamental magnetic frequency.

Verifying that the proposed change in the design can reduce the overall emitter acoustic noise power can be done using the developed simulation by altering the structure of the motor used in the mechanical simulation. Figure 8.1 shows the original rotor structure and the same structure using 5 slots. For a fair comparison, the width of the slots in the 5-slot design is decreased by 20%, such that approximately the same amount of material is used and the same air flow through the inside of the motor is achievable.

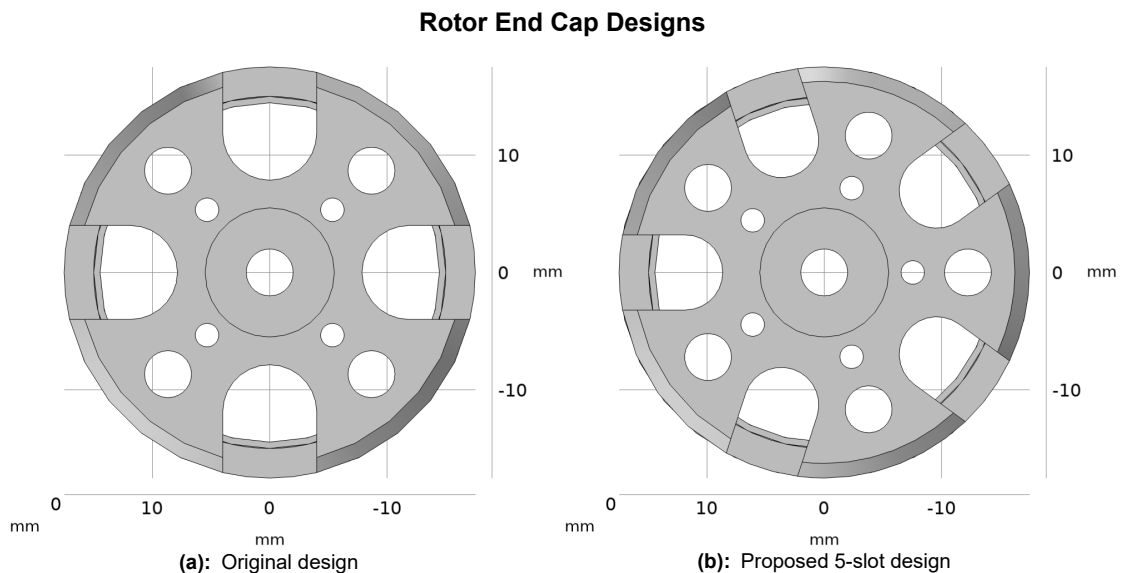


**Figure 8.1:** The original end cap design on the left and the proposed end cap design, which should reduce the emitted acoustic noise, on the right.

The mechanical and acoustic simulation are performed again using the updated structure, and the acoustic radiated power of both the original and the 5-slot design is plotted. Figure 8.2 shows both plots in the same graph, making it easy to compare the two.

The simulation results show that the two highest peaks at 4.9 kHz and 18.65 kHz, which corresponds to mode 2 and mode 4 oscillations, are lowered by 2.43 dB and 2.24 dB respectively. At the same time, especially at the peak at 4.9 kHz, it is interesting to note that although the peak value decreased, the value of the very close peak, at 4.25 kHz, which corresponds to the orthogonal vibration, did increase. This happens, because the change in number of slots decreases the susceptibility of one eigenshape, at the cost of increasing the susceptibility of its orthogonal eigenshape. Therefore, it makes sense that the reduction in vibrations are compensated by an increase in orthogonal vibrations. So, the actual overall emitted noise power does not change significantly, but its distribution over the frequency spectrum becomes more even, which is in general an improvement.

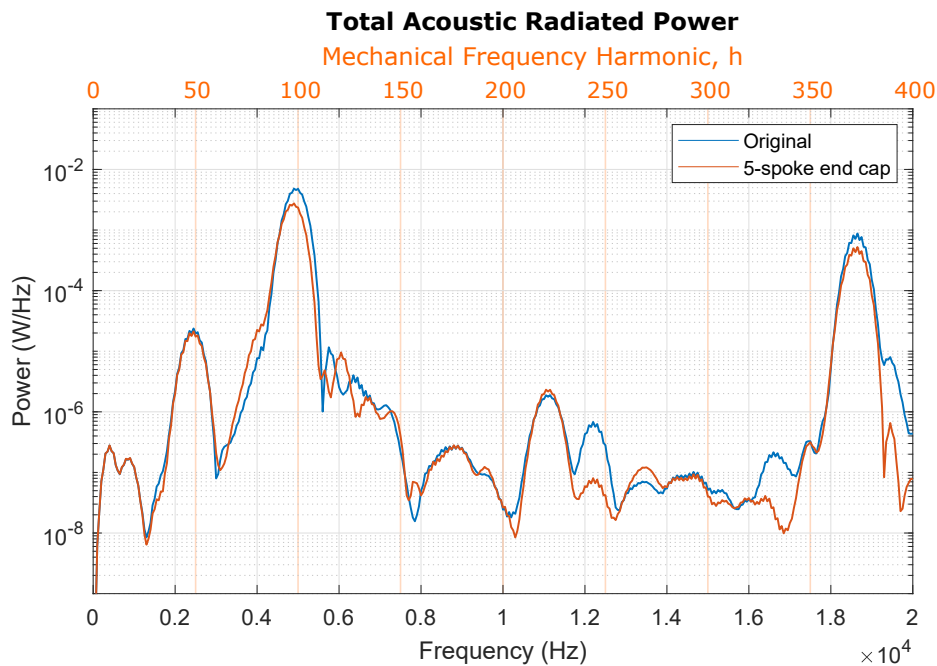


**Figure 8.2:** The original acoustic radiated power (same as in figure 6.8, and the acoustic radiated power using the proposed 5-slot end cap design.

At the same time, it is visible that the acoustic peak at 11.15 kHz, caused by mode 3 oscillations, is barely affected by the change. This supports the proposed theory that the noise reduction is a result of the fact that the number of slots is changed to a non-multiple of 2 and 4, since in this case mode 3 oscillations should not be altered, since 3 is not a multiple of 4 nor 5.

Another interesting observation, is that of the two mode 1 peaks that are present in the acoustic simulation result, the peak at 2450 Hz barely changed at all, while the peak at 12.2 kHz shows a large reduction in amplitude. By looking at the eigenshapes resulting from the modal analysis, this effect can be explained. In the mode 1 eigenshape oscillation with eigenfrequency 2389 Hz, the end cap is largely stationary and the front (positive Z side) of the motor is oscillating. In the “reversed” mode 1 eigenshape, with eigenfrequency 12546 Hz, the front of the motor is stationary and the back of the motor (negative Z side) is oscillating, which means that the end cap has to undergo large deformations for this mode to exist. This clarifies why oscillations of this mode are reduced by the end cap improvement, while the mode 1 oscillations at 2450 Hz are barely altered.

### 8.3. Two Side Rotor Support

The third optimization that is proposed to reduce the noise of the rotor is to fix the rotor at two sides. This would severely restrict susceptibility of the rotor’s structure to mode 1 oscillations and also largely that to other mode shapes. Furthermore, it will increase the eigenfrequencies of the motors structure, shifting the eigenfrequency corresponding to the mode 2 eigenshape out of the frequency region to which humans are most sensitive.

Although, supporting the rotor at two sides is likely the most effective improvement, it is also the most difficult and costly to implement. Outrunner motors, such as the one analyzed in this thesis, are almost always supported at one side, since the other side is used to provide access to the stator to mount the motor and connect the stator winding. However, using a large inner diameter bearing, might allow passing the winding connections through the bearing and provide enough space to mount the stator. An 3D printed outrunner motor that is constructed this way has already been made as a hobby project [27], showing that such an implementation is possible and might be a feasible optimization.

To verify the effectiveness of this improvement, the developed simulation can again be used. For this, a possible front cap that could be used for such an improvement has been designed and implemented in the mechanical model. The proposed front cap uses a similar structure as the end cap, however a larger diameter has been used for the bearing hole, allowing for a bearing through which the winding can be connected, and the stator can be mounted. This forced the slots to be shifted outwards, decreasing the usable cooling throughput, which means more slots have to be added. To make use of the improvement proposed in the previous section, it was chosen to use a total of 7 slots, which is not a multiple of all expected eigenshape orders. The material used for the front cap is the same aluminum as the end cap. The proposed structure can be seen in figure 8.3.

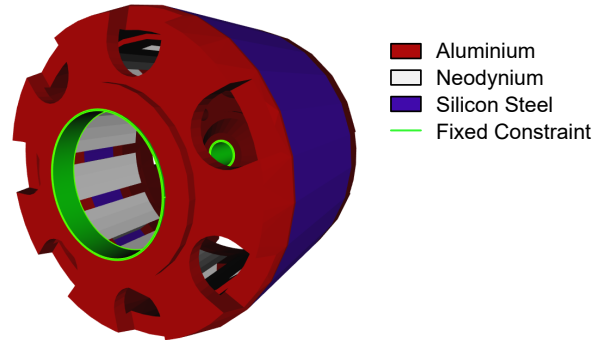


**Figure 8.3:** The mechanical structure with the added proposed front cap. The colors indicate the used materials, and the green boundaries indicated where the fixed constrained is applied.

First, the modal analysis is performed using the new structure, to verify the eigenshapes and corresponding eigenfrequencies of the new structure. Figure 8.4 shows the eigenshapes and corresponding eigenfrequencies that result from the modal analysis. The frequencies between brackets are the eigenfrequencies corresponding to the orthogonal eigenshape of the eigenshape in that subfigure.

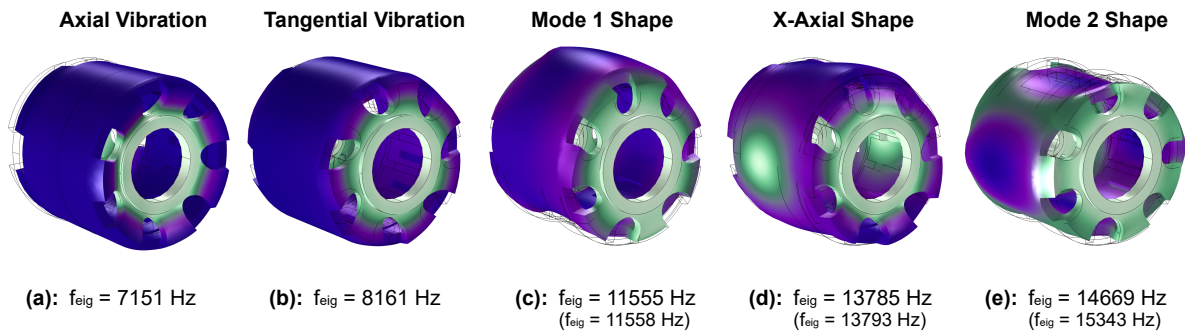


**Figure 8.4:** The eigenshapes and corresponding eigenfrequencies resulting from the modal analysis using the proposed front cap. The white/green parts indicate oscillation nodes (little deformation), whereas the purple/blue parts indicate antinodes (large deformation). The frequencies between brackets are the eigenfrequencies corresponding to the orthogonal eigenshape.

From the modal analysis results, it can already be seen that adding the front cap makes the rotor's structure less susceptible to mode 1 oscillations. Furthermore, it is confirmed that the eigenfrequencies of the mode shapes are shifted towards higher frequencies, out of the frequency range to which humans are most sensitive.

The next step is to run the simulation using the updated structure. The time domain mechanical simulation path has been chosen for this. All the simulation settings are kept the same as for the original mechanical design. Figure 8.5 shows the acoustic radiated power resulting from the simulation using the updated structure, together with the original acoustic radiated power. The peaks of the new results are annotated with the mode shape of the acoustic waves emitted by the motor at that frequency. This is determined using the acoustic isosurface plots, which are not discussed here further, but added in appendix A.3 for completeness.

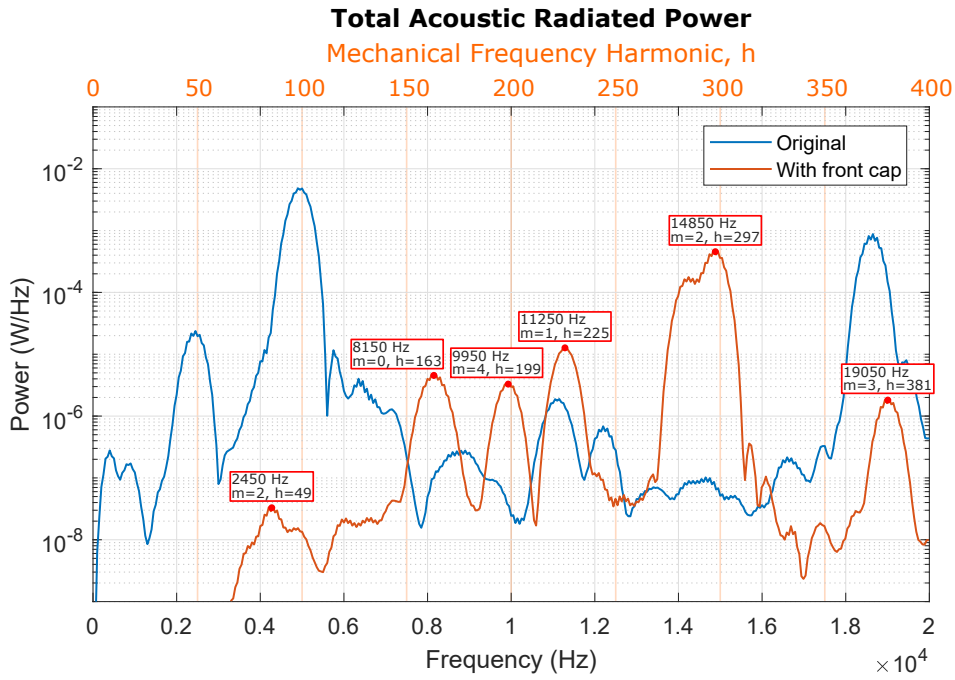


**Figure 8.5:** The acoustic radiated power of the original design, in blue, and the design with added front cap, in orange. The spatial orders (modes) of the acoustic waves emitted by the motor at the peak frequencies are added.

The results in figure 8.5 immediately show that, as predicted, the noise emitted by the motor in the spectrum to which humans are most sensitive (0 - 6 kHz) has been significantly reduced. The consequence is that the noise in the frequency range from 7 - 16 kHz has been increased. This is due to the shifting of the eigenfrequencies to higher values. An interesting observation is the change in spatial orders of the waves that are emitted by the rotor compared to the original spatial orders that were emitted. The acoustic noise power is more equally distributed over the different spatial orders, as a result of the reduced susceptibility to any specific eigenshape. The mode 2 oscillations are an exception to this, and are still higher than the other modes, which makes sense, since the fundamental spatial order of the magnetic field is 2 as well, so this spatial mode has a significantly higher excitation force. Even a mode 0 oscillation is now present, although this mode was not observed in the modal analysis.

In the end, the total acoustic noise power is lower, emitted at higher frequencies and more evenly distributed. This makes the acoustic emitted noise power of the design with added front cap, a significant improvement over the original design. It should however be noted that the improvement that is proposed will make the production of the motor more complicated, and the increased size of the second bearing may increase the vibrations induced by the bearings. Although these aspects fall outside the scope of this thesis, they need to be carefully considered and require further investigation to make sure that this would be an improvement over the original design. Of course, it also depends on the other requirements, besides the acoustic radiated noise power, whether such an optimization is viable.

# 9

## Conclusion

*In this thesis, acoustic noise with an electromagnetic source in electric motors has been analyzed. First, an analytical prediction was made, to determine the most prominent harmonics present in the air gap magnetic field. A simulation was then developed, covering the electromagnetic, mechanical and acoustic domain, to simulate the creation, propagation and emission of vibrations in a small permanent magnet synchronous outrunner motor. Two different simulation paths were implemented, based on the time domain and frequency domain mechanical simulation. The simulation based on the frequency domain mechanical simulation proved to require more investigation to obtain reliable results. The results of the simulation based on the time domain mechanical simulation was found to compare well to available literature and measurements performed in the laboratory, although two related frequency bands in the measurements could not be explained. Based on the results, it was found that small motors such as the one studied in this thesis are, in contrast to what was expected, very susceptible to mode 1 oscillations and that these vibrations account for a large part of the noise emitted by these motors. Furthermore, it was found that although these motors have a large number of poles, mode 0 vibrations are not significant as the mode 0 eigenfrequency of the motor's structure is above the frequency range of interest. Based on the results, general recommendations were proposed and explained to reduce the acoustic noise emitted by motors such as the one studied in this thesis. Two of these recommendations could be tested using the developed simulations, showing a small and a large reduction in the acoustic radiated noise power.*

### 9.1. The Simulation

To investigate the source of acoustic noise emitted by electric motors, a finite element method simulation has been developed. The simulation covers all domains from the magnetic field in the electromagnetic domain, the oscillations this causes in the mechanical domain, to the waves that are emitted in the acoustic domain. The electromagnetic, mechanical and acoustic FEM simulations were mostly implemented in COMSOL Multiphysics. Some of the processes that could not be performed in COMSOL directly were implemented in MATLAB. The electromagnetic simulation is performed in 2D, while the mechanical and acoustic simulations are performed in 3D. Two different simulation paths have been implemented, one based on the mechanical simulation in the time domain and the other based on the mechanical simulation in the frequency domain. In both versions, the electromagnetic simulation is performed in the time domain and the acoustic simulation in the frequency domain.

The first simulation path (based on the time domain mechanical study) is completely implemented in COMSOL, and does therefore not require MATLAB. The results of this simulation were validated using measurements and a comparison to other available research. An effort was made to keep the

computational cost of the simulation low. The duration of each of the simulation steps was therefore measured, to get an understanding of how computationally expensive each simulation step was. In this implementation, especially the acoustic simulation took a relatively long time to solve.

The implementation based on the frequency domain mechanical study was implemented using COM-SOL LiveLink, such that certain processes could be performed in MATLAB. This allowed for a shorter electromagnetic simulation, since the rotational symmetries in the motor could be exploited to only simulate part of the fundamental electrical period. Furthermore, performing the FFT in MATLAB was significantly faster, since the FFT only has to be performed of the results that are actually used in the next simulation step. The frequency domain conversion from the rotor reference frame to the stator reference frame was found to introduce a significant error in the model, so further investigation is required for this implementation to produce reliable results. If this problem is solved, however, the reduction in computational cost will be well worth the effort.

## 9.2. Results of the Simulation

The results of the simulations were used to analyze the mechanisms that cause the acoustic noise emitted by the small outrunner permanent magnet synchronous machine. An analysis of the air gap magnetic field and air gap force was performed, which was used to verify the results of the magnetic simulation. From this, it was found that the fundamental spatial order of the force acting on the rotor was 2. Based on this, the expectation was that mode 2 vibrations would be most significant in the rotor of the motor, and thus also in the acoustic waves transmitted into the surrounding air.

The simulation results did however also show that mode 1 vibrations and emitted acoustic waves were present. Further analysis showed that these are likely caused by very small mode 1 components, that were present in the force excitation as a result of the interpolation required to map the results of the magnetic simulation to the mechanical simulation. That these small mode 1 components caused such a relatively large mode 1 vibration in the rotor's structure, indicates a high susceptibility of the structure to mode 1 vibrations. That mode 1 vibrations are significant in the studied motor was also verified based on the acoustic measurements that were performed. Also, measurements performed in available literature with laser vibrometers on a similar motor, confirmed that mode 1 vibrations in such motors are high and can even be the most prominent vibrational mode.

Although there is a significant mode 0 force excitation, no mode 0 vibrations or emitted acoustic waves resulted from the simulation. This is due to the high eigenfrequency corresponding to the mode 0 eigenshape. With an eigenfrequency above 30 kHz, the mode 0 vibrations caused by motors as small as the one studied in this thesis are not relevant for the acoustically emitted noise.

## 9.3. Noise Reduction Methods

Based on the performed analysis of the source and propagation of the vibrations that cause acoustic noise, three noise reduction recommendations are proposed. The three proposed methods vary in implementation complexity and effectiveness, but whether they are feasible optimizations depends on the specific requirement and use of the motor.

Since mode 1 oscillations were found to be the most prominent source of the acoustically emitted noise, based on the simulation and measurement results, it is clear that balancing of the rotor is of crucial importance for silent operation of the motor. Sources of imbalance could be caused by an imbalance in the mass of the rotor, leniency in the bearings or a difference between magnetic field strength between the magnets. This imbalance could be reduced by balancing the rotor, using lower tolerance bearings or measuring the magnetic strength of each magnet before mounting them. How feasible and effective these optimizations are requires further (practical) investigation.

Another improvement that was proposed was to change the number of slots in the end cap to a value that is not a multiple of the fundamental spatial order of the force that excites the vibrations. The effect of this change was investigated using the developed simulation, which showed that the acoustic noise did decrease, although by a relatively small amount. An effect of this change is that the oscillations are more equally distributed between orthogonal eigenshapes, since one eigenshape is not preferred over the other anymore as a result of the shape of the end cap. Although the effect of this improvement is small, changing the shape of the end cap is a relatively easy improvement that could be used as a guideline when designing the motor.

The third, most complex improvement to implement, that is proposed, is to add a “front cap”. The proposal is to support the rotor on two sides, although to mount and connect the stator of the motor which is on the inside, a relatively large inner diameter bearing should be used. The theory is that supporting the rotor on two sides will restrict the mode 1 movement of the rotor and increase the eigenfrequencies so that they fall outside the frequency band to which humans are most sensitive. That this is indeed the case was verified using the simulation. Based on this, it was shown that the acoustic noise emitted by the motor would be drastically decreased. Whether this implementation is feasible, depends on the actual situation, since it makes the production of the motor more complicated and therefore more costly.

## 9.4. Future Work

Although all the research questions were answered, there are still a few things that could be investigated further, to improve the simulation and increase the understanding of how the noise is generated inside the motor.

### The Source of Mode 1 Oscillations

Since it has been found that, in contrast to the expectations, mode 1 oscillations account for a large part of the acoustically emitted noise, it would be interesting to further investigate what the source of these mode 1 oscillations actually is. Multiple possible causes of imbalance in the motor’s structure have been proposed, however, how significant these effects are in reality can only be determined using more experimentation. The simulation could be altered to incorporate an unbalanced mass distribution or add a difference in strength between the permanent magnets. The most effective way to find the source of the imbalance, however, would be to perform more real world measurements on the motor.

### Conversion From the Rotor to Stationary Reference Frame

It was found that the frequency domain conversion from the rotor’s reference frame to the stationary reference frame, required to couple the frequency domain mechanical simulation to the acoustic simulation, most likely caused the results of the second implementation of the simulation to be unreliable. Since it was found that this implementation does however significantly reduce the required computational effort required to simulate the motor, further investigation into this conversion could be a worthwhile investment.

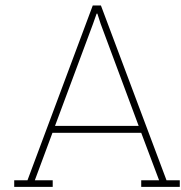
### Analysis of the Measurement Results

Two, likely related, frequencies that were present in the acoustic measurements could not be explained based on the simulation or another form of analysis. Also, measurements on the current did not elucidate the source of these frequencies. Since these frequencies may be caused by an important effect that is not considered in the simulation, it would be good for completeness to find the source of the noise at these frequencies. The first step in finding the source would be to determine whether the noise is caused by the motor or by any other components connected to the motor.

# References

- [1] P. L. Timär, A. Fazekas, J. Kiss, A. Miklos, and S. J. . Yang, "Noise and vibration of electrical machines," *Elsevier*, 1989.
- [2] M. Bösing, *Acoustic Modeling of Electrical Drives*. RWTH Aachen University: Shaker Verlag GmbH, 2014.
- [3] D. L. Huff and B. S. Henderson, "Electric motor noise from small quadcopters: Part i – acoustic measurements," *AIAA AVIATION Forum*, 2018.
- [4] M. Furlan and A. C. coupled electromagnetic-mechanical-acoustic model of a DC electric motor, *Compel*, 2003.
- [5] J. Gieras, C. Wang, and J. C. Lai, *Noise of Polyphase Electric Motors*. CRC Press, 2006.
- [6] J. A. Güemes, A. M. Iraolagoitia, P. Fernández, and M. P. Donsión, "Comparative study of pmsm with integer-slot and fractional-slot windings," *XIX International Conference on Electrical Machines*, 2010.
- [7] Dictionary.com. "Sound." (2023), [Online]. Available: <https://www.dictionary.com/browse/sound>.
- [8] P. Morse, *Vibration and Sound*, 2nd ed. New York: Mcgraw-hill Book Company, 1948.
- [9] T. Bertolini and T. Fuchs, *Vibrations and Noises in Small Electric Motors*. Munich, Germany: Süd-deutscher Verlag onpact GmbH, 2011.
- [10] COMSOL Multiphysics. "The rotating machinery, magnetic interface." (2021), [Online]. Available: [https://doc.comsol.com/6.0/doc/com.comsol.help.acdc/acdc\\_ug\\_magnetic\\_fields.08.105.html](https://doc.comsol.com/6.0/doc/com.comsol.help.acdc/acdc_ug_magnetic_fields.08.105.html).
- [11] Cogent. "Electrical steel, thin non oriented." (2006), [Online]. Available: <https://perso.uclouvain.be/ernest.matagne/ELEC2311/T2006/ThinNOFP.pdf>.
- [12] Skylar. "Common winding schemes." (2013), [Online]. Available: <https://www.bavaria-direct.co.za/scheme/common/>.
- [13] COMSOL Multiphysics. "The solid mechanics interface." (2021), [Online]. Available: [https://doc.comsol.com/6.0/doc/com.comsol.help.comsol/comsol\\_ref\\_structuralmechanics.27.02.html](https://doc.comsol.com/6.0/doc/com.comsol.help.comsol/comsol_ref_structuralmechanics.27.02.html).
- [14] F. Orban, "Damping of materials and members in structures," *Journal of Physics Conference Series*, 2011.
- [15] N. M. Papadakis and G. E. Stavroulakis, "Effect of mesh size for modeling impulse responses of acoustic spaces via finite element method in the time domain," *Euronoise*, 2018.
- [16] COMSOL Multiphysics. "The eigenvalue solver algorithms." (2021), [Online]. Available: [https://doc.comsol.com/6.0/doc/com.comsol.help.comsol/comsol\\_ref\\_solver.32.112.html](https://doc.comsol.com/6.0/doc/com.comsol.help.comsol/comsol_ref_solver.32.112.html).
- [17] R. Lehoucq, D. Sorensen, and C. Yang, *ARPACK Users Guide: Solution of Large Scale Eigenvalue Problems with Implicitly Restarted Arnoldi Methods*. MIT, 1997.
- [18] F. Lin, S. Zuo, W. Deng, and S. Wu, "Modeling and analysis of acoustic noise in external rotor in-wheel motor considering doppler effect," *IEEE TRANSACTIONS ON INDUSTRIAL ELECTRONICS*, vol. 65, no. 6, pp. 4524–4533, 2018.
- [19] R. Pindoriya, R. Thakur, B. Rajpurohit, and R. Kumar, "Numerical and experimental analysis of torsional vibration and acoustic noise of pmsm coupled with dc generator," *IEEE TRANSACTIONS ON INDUSTRIAL ELECTRONICS*, vol. 69, no. 4, pp. 3345–3356, 2022.

- [20] K. Qian, J. Wang, Y. Gao, Q. Sun, and J. Liang, "Interior noise and vibration prediction of permanent magnet synchronous motor," *JOURNAL OF VIBROENGINEERING*, vol. 20, no. 5, pp. 2225–2236, 2018.
- [21] J. L. Besnerais, Q. Souron, and E. Devillers, "Analysis of the electromagnetic acoustic noise and vibrations of a high-speed brushless dc motor," *IET International Conference on Power Electronics, Machines and Drives*, 2016.
- [22] A. Boglietti, A. Cavagnino, and A. Tenconi, "Low cost solutions to reduce cogging torque and acoustic noise of small brushed dc motors for automotive radiator cooling fan modules," *IECON 2012 - 38th Annual Conference on IEEE Industrial Electronics Society*, 2012.
- [23] J. Gieras, C. Wang, J. Lai, and N. Ertugrul, "Analytical prediction of noise of magnetic origin produced by permanent magnet brushless motors," *Electric Machines & Drives Conference, 2007*, 2007.
- [24] Zikodrive. "What are the different types of brushless dc (bldc) motor?" (2023), [Online]. Available: <https://zikodrive.com/support/zikouniversity-motor-control-theory-application/different-types-of-brushless-dc-bldc-motor/>.
- [25] G. Jang and D. Lieu, "The effect of magnet geometry on electric motor vibration," *5202 IEEE TRANSACTIONS ON MAGNETICS*, vol. 27, no. 6, pp. 5202–5204, 1991.
- [26] B. Henderson, D. Huff, J. Cluts, and C. Ruggeri, "Electric motor noise from small quadcopters: Part ii – source characteristics," *AIAA AVIATION Forum*, 2018.
- [27] C. Laimer. "600 watt, 3d-printed, halbach array, brushless dc electric motor." (2017), [Online]. Available: <https://www.instructables.com/600-Watt-3d-printed-Halbach-Array-Brushless-DC-Ele/>.



# More Simulation, Analysis and Measurement Results

In this appendix some results of the simulation or the analysis that are performed in this thesis, but too large or not relevant enough, are added. These results are not crucial to the understanding of the thesis, but are added for completeness.

## A.1. Rotor Reference Frame Force Harmonics

The following figure shows the result of performing a 2D FFT on the result of the magnetic study, when the results are not converted to the stationary reference frame.

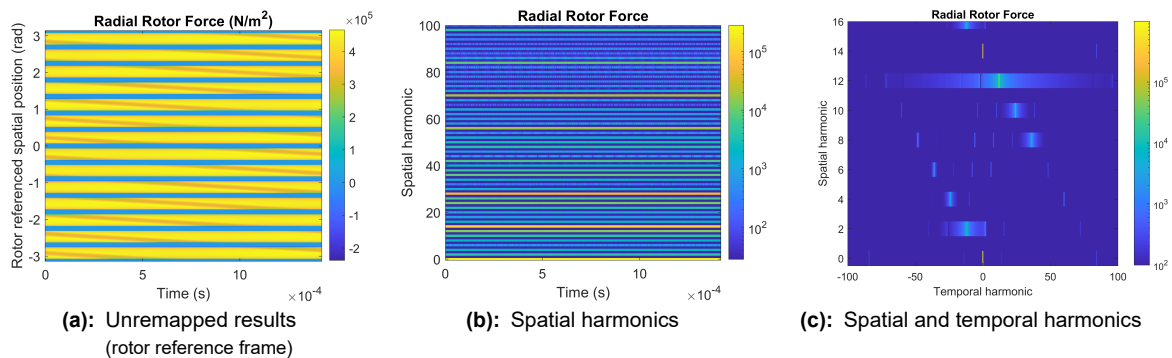


**Figure A.1:** The harmonics present in the force when the 2D FFT is performed on the results in the rotor reference frame

## A.2. Full Measurement Results

Since humans are most sensitive to noise below 6 kHz, it was chosen to only add waterfall plots up to this frequency in the report, so that the details in the range of 0 - 6 kHz are more clear. For completeness, the full range waterfall plots (up to 17 kHz) are added in this section.

### A.2.1. Acoustic Emitted Noise Waterfall Plot

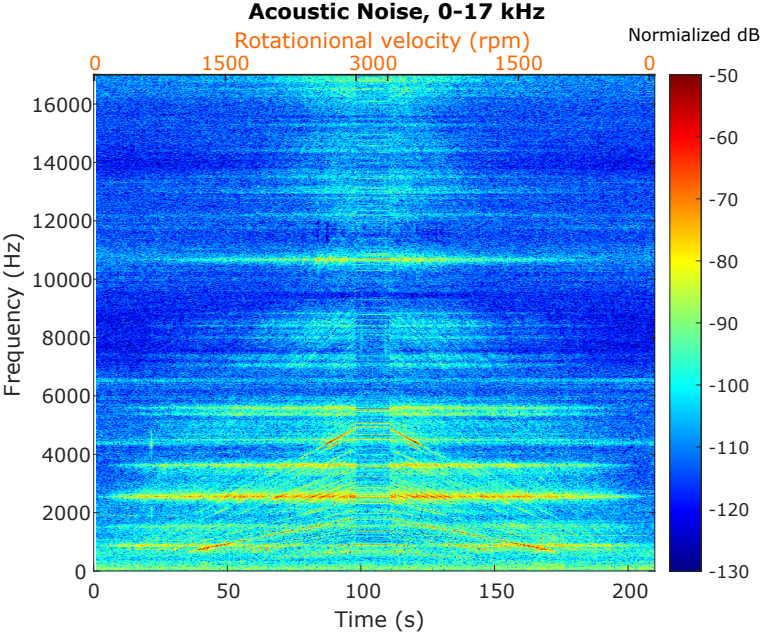


Figure A.2: The waterfall plot of the measured acoustic radiated power, for the full range of the microphone, up to 17 kHz.

### A.2.2. Measured Alpha-Beta Current Waterfall Plot

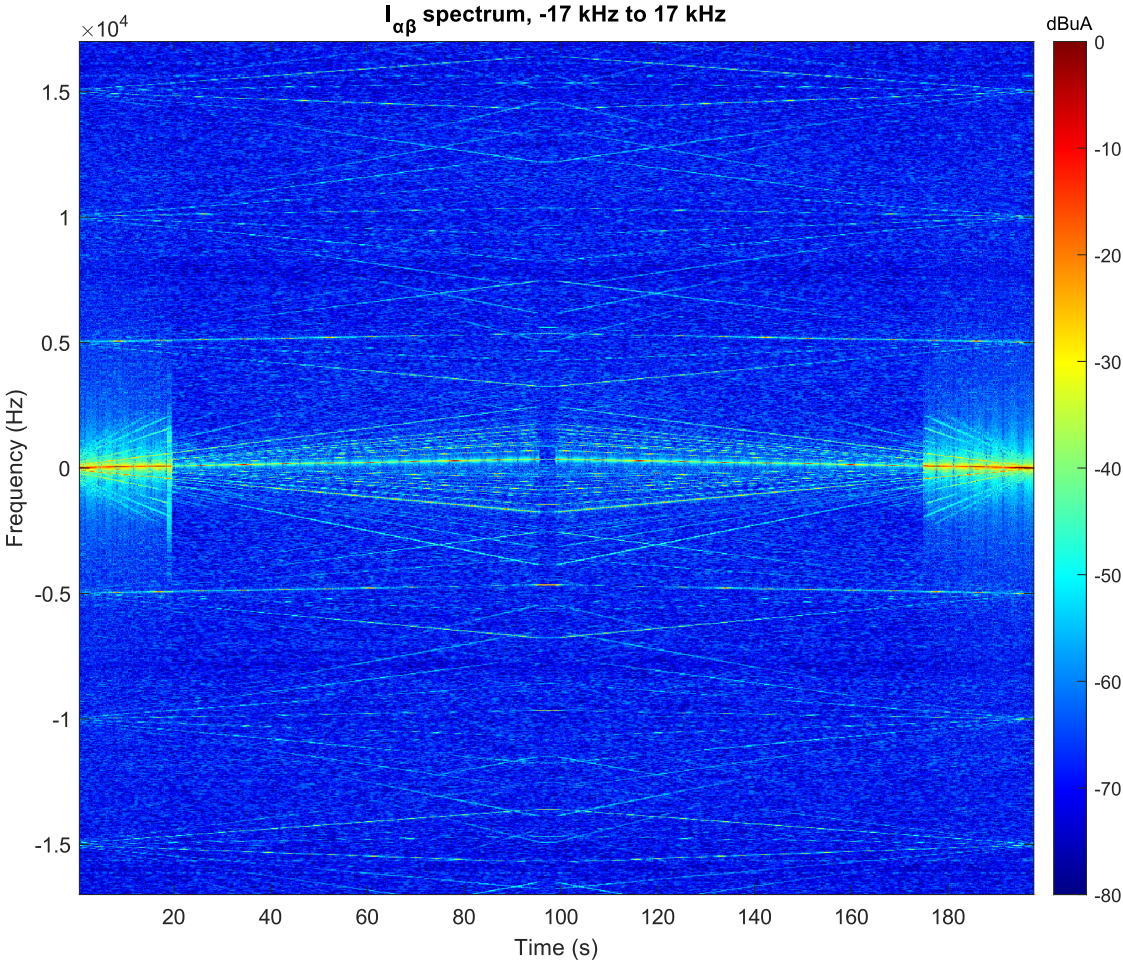


Figure A.3: The waterfall plot of the measured alpha-beta current from -17 kHz to 17 kHz.

### A.3. Acoustic Isosurfaces with Proposed Front Cap

This section shows the isosurfaces of the acoustic radiated waves resulting from the simulation, when the motor has been simulated with an added front cap as proposed in section 8.3. Based on these isosurfaces the spatial order of the waves emitted at the peak frequencies are determined. An interesting observation is that there are no high power mode 1 waves emitted anymore. However, interestingly enough, mode 0 waves are emitted by the newly proposed design.

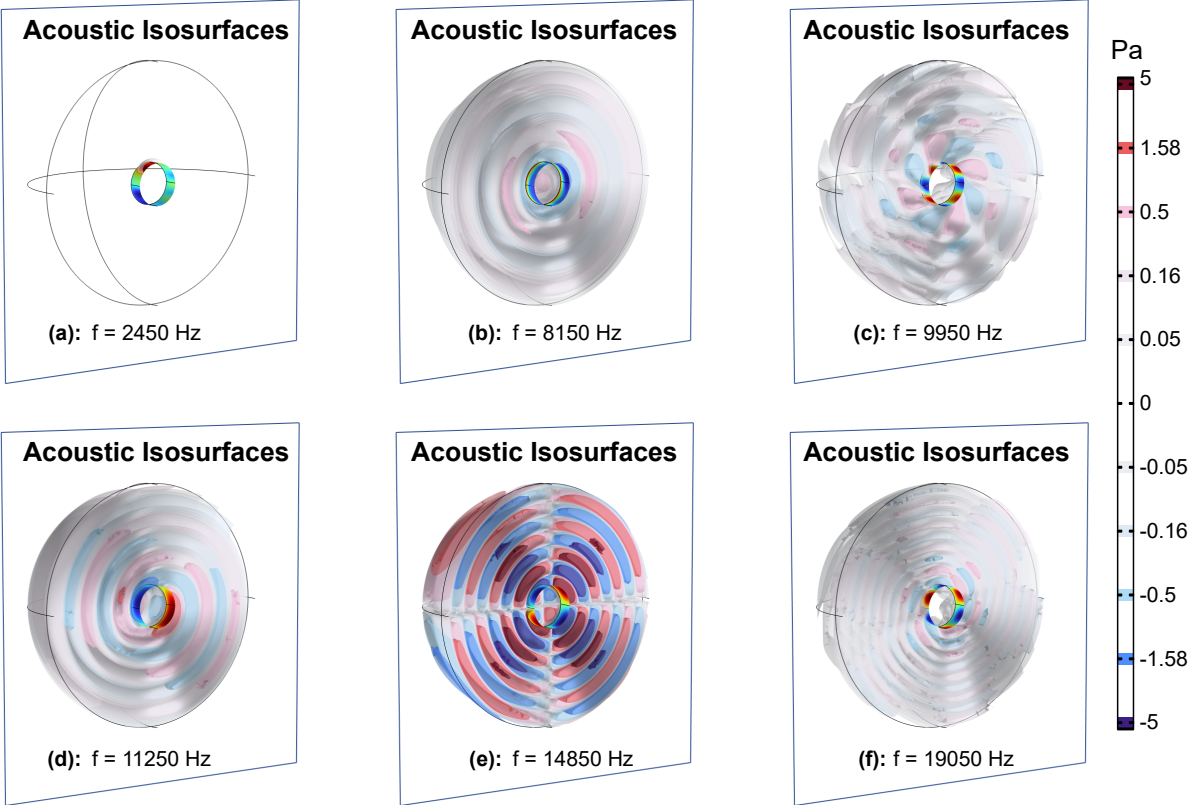


Figure A.4: The acoustic isosurfaces of the acoustic waves emitted at the peak frequencies, determined using the implemented simulation based on the design including the proposed front cap.

# B

## MATLAB Code Used for Analysis and Processing of the Data

*In this appendix, the MATLAB code that is written and used for the simulation is added. Although far from all code written for this project is added here, this should be all the code necessary for running the simulation and repeating the performed analysis.*

### B.1. Plotting of Analytical Force Harmonics

The following short script is used to plot the image depicting the harmonics that should be present in the force acting on the rotor, due to the interaction between the stator slots and permanent magnets on the rotor. The equations for these harmonics are based on the analytical analysis performed in section 3.3.2.

```
1 % F.C.B.Pacilly - 23/01/2023 - R2022b
2 % This simple script is used to plot the harmonics that should be present
3 % in the air-gap force based on the analytical interaction between the
4 % stator slots and rotor permanent magnets.
5
6 %% Define the range of harmonics to calculate/plot:
7 harm = -100:100; % normalized to base mode
8 freq = -200:200; % nomalized to f_m
9
10 %% Machine parameters:
11 p = 7;
12 Ns = 12;
13
14 %% Stator slots and Rotor PM Induced harmonics:
15 grid = ones(length(harm), length(freq), 3);
16
17 % for each value for k1 and k2, determine the spatial and temporal
18 % harmonics resulting from the derived equations. Then in the defined grid,
19 % set the pixel corresponding to this harmonic to red:
20 for k1 = -20:2:20
21     for k2 = -20:20
22         a = (length(harm)+1)/2 + (k1*p + k2*Ns);
23         b = (length(freq)+1)/2 - k1*p;
24         if a > 0 && a <= length(harm) && b > 0 && b <= length(freq)
25             grid(a, b, :) = [1, 0, 0];
26         end
27     end
28 end
29
```

```

30 image(freq, harm, grid);
31 xlim([-126 126]); ylim([-0.5 16]);
32 set(gcf,'Position',[100 100 1000 250]);
33 xticks(-140:14:140);
34 yticks(-200:4:200);
35 set(gca,'YDir','normal');
36 title('Estimated Radial Rotor Force Harmonics');
37 xlabel('Temporal harmonic'); ylabel('Spatial harmonic');

```

## B.2. Processing of the Rotor Force

This section includes the code used to obtain the rotor force from COMSOL and process the force for harmonic analysis or for further use in the mechanical frequency domain simulation.

### B.2.1. Exporting the Rotor Force from COMSOL

The following function is used to export the force acting on the rotor from COMSOL. Although the function exports the force acting on the rotor, it is called *getStatorForce()*, since it obtains the force in the stator reference frame. The inputs of the function are a handle to the COMSOL LiveLink model, the times for which the force should be exported, the angular velocity of the motor (necessary for converting the force to the stator domain) and the resolution used for the 1-dimensional phi-domain to which the force is mapped. This function is only used for the harmonic analysis and not for preprocessing the results for the mechanical simulation.

```

1 function [rotorForce, phi] = getStatorForce(model, times, angularVelocity, resolution)
2 % F.C.B.Pacilly - 27/03/2023
3 % Exports force from MultiComponentModel.mph in the stator reference frame
4     projectedRadius = 16.38; % [mm] radius to which the force is projected
5
6     boundaries = model.result("pg15").selection.entities;
7     boundaries = flip(boundaries);
8     numberOfTimes = length(times);
9     model.result('pg36').set('interp', sprintf("range(%.99g, %.99g, %.99g)", ...
10         times(1), times(2)-times(1), times(end)));
11
12     numberOfBoundaries = length(boundaries);
13     phi = 1/resolution-pi:2*pi/resolution:pi;
14     rotorForce = zeros(numberOfTimes, resolution);
15     fprintf('\t\tImported boundary (%3d/%3d)\n', 0, length(boundaries));
16     %% Export force data from COMSOL to MATLAB
17     for j = 1:numberOfBoundaries
18         % Import boundary force data into MATLAB:
19         model.result('pg36').feature('lngr1').selection.set(boundaries(j));
20         model.result.export('plot2').set('plot', 'lngr1');
21         model.result.export('plot2').run;
22         fileID = fopen('tmp.txt', 'r');
23         data = fscanf(fileID, '%f\t%f', [1 Inf]);
24         fclose(fileID);
25         data = reshape(data, 2, []);
26         th = reshape(data(1,:), [], length(times));
27         F = reshape(data(2,:), [], length(times));
28
29         % Import boundary 'r' data into MATLAB:
30         model.result('pg36').feature('lngr2').selection.set(boundaries(j));
31         model.result.export('plot2').set('plot', 'lngr2');
32         model.result.export('plot2').run;
33         fileID = fopen('tmp.txt', 'r');
34         data = fscanf(fileID, '%f\t%f', [2 Inf]);
35         fclose(fileID);
36         thr = reshape(data(1,:), [], length(times));
37         r = reshape(data(2,:), [], length(times));
38
39         % Shift to stator frame
40         mechanicalAngle = times*angularVelocity;

```



```

16 ttime = 2*pi/angularVelocity/p/2;
17 ntimes = 2*p*ceil(ttime*20*maxFrequency/p/2);
18 times = linspace(0, ttime, ntimes);
19
20 if(exist('StatorRotorForce.mat', 'file'))
21     load('StatorRotorForce.mat');
22 else
23     rotorForce = getStatorForce(model, times, angularVelocity, 2016);
24     save('StatorRotorForce.mat', 'rotorForce');
25 end
26 resolution = size(rotorForce, 2);
27 phi = 1/resolution-pi:2*pi/resolution:pi;
28
29 %% plot image:
30 image(times, phi, -rotorForce.', 'CDataMapping','scaled');
31 title('Radial Rotor Force (N/m^2)');
32 xlabel('Time (s)'); ylabel('Spatial position (rad)');
33 colorbar;
34 set(gca,'YDir','normal');
35 storePlot('RadialRotorForce');
36
37 %% Repeat result to increase resolution to 1 temporal harmonic
38 segmentLength = size(rotorForce, 1);
39 shiftAmount = 0;
40 numberOfRepeats = 14;
41
42 rotorForce = rotorForce(1:segmentLength, :);
43 for i = 1:numberOfRepeats-1
44     rotorForce(end+1:end+segmentLength, :) = circshift(rotorForce(1:segmentLength, :), i*
45         shiftAmount, 2);
46 end
47
48 %% plot image:
49 image(phi, times, -rotorForce, 'CDataMapping','scaled');
50 title('Radial Rotor Force (N/m^2)');
51 xlabel('Spatial position (rad)'); ylabel('Time (s)');
52 colorbar;
53
54 %% perform fft over space:
55 spaceFFT = fftshift(fft(rotorForce, size(rotorForce,2), 2), 2);
56 sHarm = -size(rotorForce, 2)/2:1:size(rotorForce, 2)/2-1;
57
58 %% plot image:
59 image(times, sHarm, abs(spaceFFT).', 'CDataMapping','scaled');
60 title('Radial Rotor Force');
61 xlabel('Time (s)'); ylabel('Spatial harmonic');
62 yticks(-200:8:200);
63 ylim([-0.5 100]);
64 colorbar;
65 set(gca,'YDir','normal');
66 set(gca,'ColorScale','log');
67
68 %% perform fft over time:
69 %window = repmat(hann(size(spaceFFT,2)).', size(spaceFFT,1), 1);
70 %windowedSpaceFFT = spaceFFT .* window;
71 FFT = fftshift(fft(spaceFFT, size(spaceFFT,1), 1), 1); % Original
72 %FFT = fftshift(fft(spaceFFT, 2^14, 1), 1); % Zero padded
73 freq = (-0.5:1/size(FFT,1):0.5-1/size(FFT,1))/(times(2)-times(1));
74 tHarm = 2*pi*freq./angularVelocity;
75
76 %% plot image:
77 image(tHarm, sHarm, abs(FFT).', 'CDataMapping','scaled');
78 title('Radial Rotor Force');
79 xlabel('Temporal harmonic'); ylabel('Spatial harmonic');
80 xlim([-50 50]); ylim([-0.5 40]);
81 xticks(-140:14:140);
82 yticks(-200:4:200);
83 colorbar;
84 set(gca,'YDir','normal');
85 set(gca,'ColorScale','log');

```

### B.2.3. Conversion from Time Domain to Frequency Domain

This is the code used to preprocess the results of the magnetic simulation before they can be used in the frequency domain mechanical simulation. The results of the magnetic study are imported from a file saved by COMSOL. Next, the result is remapped and repeated according to section 3.2.5, to obtain the result of a full electrical cycle. Next, the result is repeated, and the FFT is performed to obtain the frequency domain force acting on the rotor. This result is then stored in a format that can directly be imported into COMSOL.

```

1 % F.C.B.Pacilly - 05/04/2023
2 % Imports the rotor force from a COMSOL export by "ModalComponent3D.mph",
3 % converts the force from time to frequency domain and stores the force in
4 % a COMSOL compatible format. (grid text format)
5
6 %% Import the data exported by COMSOL:
7 clear all;
8 data = readmatrix('RotorForce-Time.txt');
9
10 % read the x and y data from the first two columns
11 xy = [data(:, 1), data(:, 2)].';
12
13 % From the succeeding columns, take the time and force data. The last three
14 % columns are skipped, since they will overlap with the first 3 (in time):
15 t = data(1, 3:3:end-3);
16 Fr = data(:, 4:3:end-3).'; % radial component of the force
17 Fp = data(:, 5:3:end-3).'; % phi component of the force
18 clear data;
19
20 % Get the time steps and check that the time steps are equal:
21 t = t-t(1);
22 dt = t(2:end) - t(1:end-1);
23 if max(dt) - min(dt) > 1e-9
24     error('The timesteps from the magnetic simulation are not equally distributed!')
25 end
26 dt = dt(1);
27
28 %% Construct repeated force from one 7th of an electrical period:
29 a = -360/14; % degrees to rotate section
30 R = [cosd(a), -sind(a); % rotation matrix
31     sind(a), cosd(a)];
32
33 close all;
34 %plot(xy(1, :), xy(2, :), 'o');
35 % hold on
36 Tm = 1/(3000/60);
37
38 timepoints = size(Fr, 1);
39 spacepoints = size(Fr, 2);
40
41 xyn = xy;
42 Frn = zeros(7*timepoints, spacepoints);
43 Fpn = zeros(7*timepoints, spacepoints);
44 for p = 1:7
45     % Find the points corresponding to each other and plot the data
46     for k = 100%:spacepoints
47         index = find(sum(abs(xy-xyn(:, k)))<1e-3); % where the new coordinates are placed in
48             the original array
49         if length(index) == 2
50             index = index(1); % If there is found a duplicate point,
51                 use the first one
52         end
53         Frn((p-1)*timepoints+1:p*timepoints, k) = Fr(:, index);
54         Fpn((p-1)*timepoints+1:p*timepoints, k) = Fp(:, index);
55         plot((t+dt*length(t)*(p-1))./Tm, Fr(:, index));
56         hold on;
57         %plot(xy(1, index), xy(2, index), 'ro');
58         %hold on
59     end
60 end
61 % Rotate the coordinates and the xy force data around the z axis using

```

```

59     % the defined rotation matrix:
60     xyn = R*xyn;
61 end
62
63 title("Radial force at node 100");
64 ylabel("Force (N/m^2)")
65 xlabel("Time / Mechanical period")
66 ylim([2.5e5 3.7e5]);
67 %%
68 Fr = repmat(Frn, [20, 1]);
69 Fp = repmat(Fpn, [20, 1]);
70 time = 0 : dt : dt*(size(Fr, 1)-1);
71
72 %plot(time, Fp(:, 102))
73
74 %% Perform FFT of the force data:
75
76 FR = fft(Fr);
77 FP = fft(Fp);
78 freq = 0:1/dt/size(FR,1):1/dt-1/dt/size(FR,1);
79
80 %% Shorten the FFT result, since we're not interested in the super high frequencies:
81 freqpoints = spacepoints;
82 FR = FR(1:freqpoints, :);
83 FP = FP(1:freqpoints, :);
84 freq = freq(1:freqpoints);
85
86 %% store the result for COMSOL import (spreadsheet):
87 data = zeros(7, spacepoints*freqpoints);
88 data(1:2, :) = repmat(xy, [1, freqpoints]);
89 data(3, :) = kron(freq, ones(1, spacepoints));
90 data(4, :) = reshape(real(FR).', 1, []);
91 data(5, :) = reshape(imag(FR).', 1, []);
92 data(6, :) = reshape(real(FP).', 1, []);
93 data(7, :) = reshape(imag(FP).', 1, []);
94 writematrix(data.', "RotorForce-Frequency.txt")

```

## B.3. Processing the Mechanical Simulation Results

In this section, the code used to analyze and preprocess the results of the mechanical simulation is added.

### B.3.1. Rotor Deformation Harmonic Analysis (2D FFT) - Time Domain Study

This is the code used for the harmonic analysis of the rotor's deformation resulting from the time domain mechanical study. The data is imported from a file stored by COMSOL.

```

1 % F.C.B.Pacilly - 21/02/2023
2 % Calculates FFT over space and time of the radial rotor deformation.
3
4 %% open/read the radial displacement:
5 % the times corresponding to each column:
6 angularVelocity = 2*pi*3000/60;
7 maxFrequency = 20e3;
8 t = 0.1/maxFrequency*(0:1:2^11-1);
9
10 fileID = fopen('radial_displacement_time.txt', 'r');
11 data = fscanf(fileID, '%f\t%f', [length(t)+1 Inf]);
12 fclose(fileID);
13
14 phi = data(1, :);
15 displacement = data(2:end, :);
16
17 %% plot image:
18 image(t, phi, displacement.', 'CDataMapping','scaled');

```

```

19 title('Rotor Radial Surface Displacement (mm)');
20 xlabel('Time (s)');
21 ylabel('Rotor referenced spatial position (rad)');
22 colorbar;
23 set(gca,'YDir','normal');
24
25 %% perform fft over space:
26 spaceFFT = fftshift(fft(displacement, size(displacement,2), 2), 2)./size(displacement, 2);
27 %spaceFFT = spaceFFT(:, 1:end/2); %% remove second half
28 sHarm = -size(displacement, 2)/2:1:size(displacement, 2)/2-1;
29
30 %% plot image:
31 image(t, sHarm, abs(spaceFFT).', 'CDataMapping','scaled');
32 title('Rotor Radial Surface Displacement');
33 xlabel('Time (s)');
34 ylabel('Spatial harmonic');
35 ylim([-0.5 30]);
36 colorbar;
37 set(gca,'YDir','normal');
38 set(gca,'ColorScale','log');
39
40 %% perform fft over time:
41 %window = repmat(hann(size(spaceFFT,2)).', size(spaceFFT,1), 1);
42 %windowedSpaceFFT = spaceFFT .* window;
43 FFT = fftshift(fft(spaceFFT, size(spaceFFT,1), 1), 1)./size(spaceFFT, 1); % Original
44 %FFT = fftshift(fft(spaceFFT, 2^14, 1), 1); % Zero padded
45 freq = linspace(-1/(t(2)-t(1))/2, 1/(t(2)-t(1))/2, size(FFT, 1));
46 tHarm = 2*pi*freq./angularVelocity;
47
48 %% plot image:
49 image(freq, sHarm, abs(FFT).', 'CDataMapping','scaled');
50 title('Rotor Radial Surface Displacement');
51 xlabel('Frequency (Hz)');
52 ylabel('Spatial harmonic');
53 xlim([-maxFrequency maxFrequency]); ylim([-0.5 30]);
54 colorbar;
55 set(gca,'YDir','normal');
56 set(gca,'ColorScale','log');

```

### B.3.2. Rotor Deformation Harmonic Analysis (2D FFT) - Frequency Domain Study

In this section the code is included which is used to perform the same analysis as in the previous section, however for the result of the frequency domain mechanical study. The process of obtaining the 2D FFT in the desired form is significantly different, since the results are already provided in the frequency domain. This also means that both the real and imaginary part of the frequency domain deformation have to be separately imported from COMSOL to MATLAB.

```

1 % F.C.B.Pacilly - 04/06/2023 - R2022b
2 % Calculates FFT over space of the frequency domain radial rotor deformation.
3
4 %% open/read the radial displacement:
5 angularVelocity = 2*pi*3000/60;
6 freqStep = 600;
7 maxFrequency = 20e3;
8 f = 0:freqStep:maxFrequency; % The frequencies corresponding to each column.
9
10 % import real part:
11 fileID = fopen('radial_displacement_frequency-real.txt', 'r');
12 data = fscanf(fileID, '%f\t%f', [length(f)+1 Inf]);
13 fclose(fileID);
14
15 phi = data(1, :);
16 displacement_real = data(2:end, :);
17
18 % import imaginary part, and check that phi-coordinates are equal:
19 fileID = fopen('radial_displacement_frequency-imag.txt', 'r');
20 data = fscanf(fileID, '%f\t%f', [length(f)+1 Inf]);

```

```

21 fclose(fileID);
22
23 if sum(abs(data(1,:) - phi)) > 1e-10
24     error("Phi-coordinates not equal!");
25 end
26 displacement_imag = data(2:end, :);
27
28 %combine:
29 displacement = displacement_real + 1i*displacement_imag;
30
31 %% Add zeros (run only once!):
32 % The frequency domain results are only defined at harmonics of the
33 % electrical frequency, since the deformation at all other frequencies will
34 % be 0. For plotting the data, the 0 do need to be added, otherwise the
35 % resulting plots will give a distorted view of the simulation results.
36 grow = 6;
37
38 freqStep = freqStep/grow;
39 maxFrequency = grow*freqStep*size(displacement, 1) - freqStep;
40 f = 0:freqStep:maxFrequency;
41
42 grewed_displacement = zeros(grow*size(displacement, 1), size(displacement, 2));
43 grewed_displacement(1:grow:end, :) = displacement;
44 displacement = grewed_displacement;
45
46 %% plot image:
47 image(f, phi, abs(displacement).', 'CDataMapping','scaled');
48 title('Rotor Radial Surface Displacement');
49 xlabel('Frequency (Hz)');
50 ylabel('Rotor referenced spatial position (rad)');
51 colorbar;
52 set(gca,'YDir','normal');
53 set(gca,'ColorScale','log');
54
55 %% perform fft over space:
56 FFT = fftshift(fft(displacement, size(displacement,2), 2), 2)./size(displacement, 2);
57 harm = -size(displacement, 2)/2:1:size(displacement, 2)/2-1;
58
59
60 %% plot image:
61 image(f, harm, abs(FFT).', 'CDataMapping','scaled');
62 title('Rotor Radial Surface Displacement');
63 xlabel('Frequency (Hz)');
64 ylabel('Spatial harmonic');
65 xlim([0 15e3]); ylim([-16 16]);
66 colorbar;
67 set(gca,'YDir','normal');
68 set(gca,'ColorScale','log');
69 %storePlot('RadialSurfaceDisplacement-ModalFrequency');
70
71 %% For comparability, get the full plot and flip the image bounds:
72 fullFFT = zeros(2*size(displacement,1)-1, size(displacement, 2));
73 fullFFT(1:end/2+1, :) = circshift(rot90(FFT, 2), 1, 2);
74 fullFFT(end/2:end, :) = FFT;
75 fFreq = [-fliplr(f) f(2:end)];
76
77 %% plot image:
78 image(fFreq, harm, abs(fullFFT).', 'CDataMapping','scaled');
79 title('Rotor Radial Surface Displacement');
80 xlabel('Frequency (Hz)');
81 ylabel('Spatial harmonic');
82 xlim([-15e3 15e3]); ylim([0 16]);
83 colorbar;
84 set(gca,'YDir','normal');
85 set(gca,'ColorScale','log');

```

### B.3.3. Rotor to Stator Reference Frame Conversion

This is the code used to convert the acceleration resulting from the frequency domain mechanical simulation from the rotor reference frame to the stator reference frame.

```

1 % F.C.B.Pacilly - 07/05/2023
2 % Imports the rotor surface acceleration and converts the acceleration from
3 % the rotor reference frame to the stationary reference frame. This is done
4 % by performing the IFFT over time, then shifting rotatating the result and
5 % then performing the FFT to obtain the shifted result.
6 clear all;
7
8 %% Determine points to where to evaluate the acceleration:
9 PhiLength = 240;
10 ZLength = 100;
11
12 R = 35.02/2; % Lengths specified in mm
13 Z = linspace(0, 17.43, ZLength);
14 Phi = -pi:2*pi/PhiLength:pi-2*pi/PhiLength;
15
16 X = R.*cos(Phi);
17 Y = R.*sin(Phi);
18
19 points = zeros(3, length(X)*length(Z));
20 points(1:2, :) = repmat([X; Y], [1 length(Z)]);
21 points(3, :) = kron(Z, ones(1, length(X)));
22
23 plot3(points(1, :), points(2, :), points(3, :), "o");
24 writematrix(points.', "SurfacePoints.txt")
25
26 %% EXPORT DATA IN COMSOL (HAS TO BE DONE MANUALLY)
27
28 %% Import the data exported by COMSOL:
29 data = readmatrix('RotorAcceleration-RotorFrame.txt');
30
31 %% Read the data and convert to R-phi domain:
32 Xs = data(:, 1);
33 Ys = data(:, 2);
34 Phi_s = atan2(Ys, Xs);
35 Zs = data(:, 3);
36 A_s = data(:, 4:end);
37
38 %plot3(Xs, Ys, Zs, 'o');
39 plot3(Phi_s, Zs, real(A_s(:, 2)), 'o');
40 title(sprintf("Normal Outward Acceleration (f=600Hz)"))
41 xlabel("Phi (rad)")
42 ylabel("Z (mm)")
43 zlabel("Acceleration (mm/s)")
44
45 Phi = Phi_s(1:PhiLength);
46 Z = Zs(1:PhiLength:length(Zs));
47 image(Phi_s, Zs, real(reshape(A_s(:, 2), [PhiLength, ZLength]).'), 'CDataMapping','scaled');
48 title(sprintf("Normal Outward Acceleration (f=600Hz)"))
49 xlabel("Phi (rad)")
50 ylabel("Z (mm)")
51
52 %% Perform inverse FFT
53 freqStep = 600;
54 maxFreq = 20e3;
55
56 f = 0:freqStep:maxFreq;
57 a_s = ifft(A_s, [], 2, 'nonsymmetric');
58 t = 0:1/freqStep:(floor(maxFreq/freqStep))/freqStep;
59
60 %% Rotate the acceleration in time:
61 omega = 2*pi*3000/60;
62 alpha = omega.*t;
63 shift = -round(PhiLength/2/pi .* alpha); % the round should only remove
64 % numerical errors if PhiLength
65 % is correctly chosen

```

```

66 a_n = zeros(PhiLength* ZLength, length(t));
67 for i = 1:length(t)
68     a_n(:, i) = reshape(circshift(reshape(a_s(:, i), [PhiLength, ZLength]), shift(i)), [1,
69         PhiLength*ZLength]);
70 end
71
72 %% Perform the FFT on the rotated data:
73 A_n = fft(a_n, [], 2);
74
75 plot3(Phi_s, Zs, real(A_n(:, 2)), 'o');
76 title(sprintf("Normal Outward Acceleration (Stator frame)(f=600Hz)")
77 xlabel("Phi (rad)")
78 ylabel("Z (mm)")
79 zlabel("Acceleration (mm/s)")
80
81 image(Phi_s, Zs, real(reshape(A_n(:, 2), [PhiLength, ZLength].')), 'CDataMapping','scaled');
82 title(sprintf("Normal Outward Acceleration (f=600Hz)")
83 xlabel("Phi (rad)")
84 ylabel("Z (mm)")
85
86 %% Store the data to read into COMSOL:
87 odata(:, 1) = repmat(Phi_s, [length(f), 1]);
88 odata(:, 2) = repmat(Zs, [length(f), 1]);
89 odata(:, 3) = kron(f, ones(1, length(Phi_s)));
90 odata(:, 4) = real(reshape(A_n, [size(A_n, 1)*size(A_n, 2), 1]));
91 odata(:, 5) = imag(reshape(A_n, [size(A_n, 1)*size(A_n, 2), 1]));
92
93 writematrix(odata, "RotorAcceleration-StatorFrame.txt")

```

## B.4. Eigenshape Oscillation Animation Export

This code is used to automatically export and convert the oscillation animations resulting from the eigenfrequency simulation. The script uses FFMPEG to convert the simulation to GIF files, so make sure ffmpeg.exe is downloaded and added in the folder, or comment line 36 and 37.

```

1 % F.C.B.Pacilly - 05/04/2023
2 % Automatically exports the eigenshape oscillation animation for multiple
3 % frequencies. The animation is also converted to low and high resolution
4 % GIF files using FFMPEG.
5
6 % The COMSOL model has been computed and the results should have been
7 % stored.
8
9 %% Open model and get the eigenfrequencies:
10 import com.comsol.model.*
11 import com.comsol.model.util.*
12
13 ModelUtil.showProgress(true);
14 if ~exist('model', 'var')
15     mphopen('FinalModalAnalysis_v2.3.mph');
16 end
17 model.result().evaluationGroup("std1EvgFrq").run;
18 eigenFrequencies = model.result().evaluationGroup("std1EvgFrq").getReal;
19 eigenFrequencies = eigenFrequencies(:, 1);
20
21 %% Export animations for the eigenfrequencies closest to the target frequencies:
22 %targetFrequencies = [3886 4380 9200 9268 9750 13745 14312 19270 2160 2164 3177 3845];
23 targetFrequencies = eigenFrequencies;
24
25 if ~exist('ModeShapes', 'dir')
26     mkdir('ModeShapes');
27 end
28
29 fprintf('\t\tExported Animation (%2d/%2d)\n', 0, length(targetFrequencies));
30 for f = 1:length(targetFrequencies)
31     % get looplevel and filename

```

```

32     [~, i] = min(abs(eigenFrequencies - targetFrequencies(f)));
33     filename = sprintf("./ModeShapes/ModeShape-%uHz", round(eigenFrequencies(i)));
34
35     % export animation from COMSOL
36     model.result("pg16").set('looplevel', sprintf('%d', i));
37     model.result().export("anim1").set("avifilename", filename+'.avi');
38     model.result().export("anim1").run();
39
40     % convert to small and original sized GIF animations
41     [~,~] = system(sprintf('ffmpeg.exe -i "%s.avi" -loop 0 "%s.gif" -y', filename, filename)
42     );
43     [~,~] = system(sprintf('ffmpeg.exe -i "%s.avi" -vf scale=480:-1 -loop 0 "%s-small.gif" -y
44     ', filename, filename));
45     fprintf('\b\b\b\b\b\b\b\b\b\b(%2d/%2d)\n', f, length(targetFrequencies));
46 end

```

## B.5. Acoustic Isosurfaces Animation Export

The following code can be used to automatically export multiple acoustic isosurface animation. Since the exporting of these animations, especially at higher frequencies, can take a lot of time, this code can be useful to make this process run automatically overnight. Keep in mind that the frequencies have to be defined such that they match the frequencies at which the acoustic simulation is performed.

```

1 % F.C.B.Pacilly - 06/03/2023 - R2022b
2 % Automatically exports the acoustic isospheric animation from
3 % "FinalTimeDomainModel_v4.x.mph" for multiple frequencies. Make sure the
4 % frequencies array is correct, otherwise the wrong frequencies will be
5 % exported (and their name will be incorrect).
6
7 % The COMSOL model has been computed and the results should have been
8 % stored. Then run "mphopen('FinalTimeDomainModel_v4.x.mph');", before
9 % executing this script. The command "mphlaunch('Model')" can be used to
10 % open the GUI for the model.
11
12 import com.comsol.model.*
13 import com.comsol.model.util.*
14
15 ModelUtil.showProgress(true);
16
17 maxFrequency = 20e3;
18 angularVelocity = 2*pi*3000/60;
19 frequencies = angularVelocity/2/pi:angularVelocity/2/pi:maxFrequency; %HAS TO BE CORRECT
20
21 %targets = [400, 850, 1650, 2450, 3150, 3500, 4150, 4950, 5700, 6050, 6650, 7250, 7900, 8800,
22           9550, 11150, 12200, 13500, 14650, 15350, 16700, 17850, 18650, 19350];
23 targets = [400, 2450, 4950, 8800, 11150, 12200, 16700, 18650];
24 fprintf('\t\tExported Animation (%2d/%2d)\n', 0, length(targets));
25 for f = 1:length(targets)
26     [~, i] = min(abs(frequencies - targets(f)));
27     model.result("pg3").set('looplevel', sprintf('%d', i));
28     model.result().export("anim3").set("avifilename", sprintf("AcousticIsosurfaceLogarithmic-
29     %uHz.avi", round(frequencies(i))));
30     model.result().export("anim3").run();
31     fprintf('\b\b\b\b\b\b\b\b\b\b(%2d/%2d)\n', f, length(targets));
32 end

```

## B.6. Processing of Laboratory Measurements

In this section, the code used to preprocess the measurements performed in the laboratory is included. Thanks to Dr. Jianning Dong, my supervisor, for providing most of the code in this section.

### B.6.1. Acoustic Noise Analysis

The code in this section is used to plot the waterfall plot of the measured acoustic noise. This is done by computing the FFT over a moving window.

```

1 % Dr. Jianning Dong - 06/06/2023
2 % Changed by:
3 % - F.C.B. Pacilly
4 %
5 % In this script the acoustic laboratory measurements are used to compute
6 % the FFT over a moving window to obtain a waterfall plot of the acoustic
7 % noise emitted by the motor while slowly accelerating and decelerating.
8 % Furthermore the FFT is performed over the acoustic measurements during
9 % the steady state rotation of the motor at 3000 rpm.
10
11
12 %% Read recorded data:
13 noise_temp_data = audioread('motor_noise_20230609_slow.m4a');
14 %noise = noise_temp_data(:,1); % left
15 noise = noise_temp_data(:,2); % right
16 noise_info = audioinfo('motor_noise_20230609_slow.m4a');
17
18 f_samp = noise_info.SampleRate; % sampling time
19 t_samp = 1/f_samp.*(0:(length(noise)-1));
20
21 plot(t_samp, noise)
22 xlabel('Time (s)')
23 ylabel('Normalized noise')
24
25 %% Short time fourier transform:
26 fft_len = 2nextpow2(floor(f_samp));
27 noise_len = floor(length(noise)/fft_len)*fft_len;
28
29 overlap = 1-1/4;
30
31 mid_ind = fft_len/2:(1-overlap)*fft_len:(noise_len-fft_len/2);
32 mid_tim = mid_ind/f_samp; % index of the mid time of each segment
33
34 base_freq = 1/(fft_len/f_samp);
35 max_freq = fft_len/2*base_freq; % shannon freq, f_samp/2
36 freq_ind = 0:base_freq:max_freq;
37
38 spec_mat = zeros(fft_len/2+1,length(mid_ind));
39
40 for ind = mid_ind
41     noise_seg = noise(ind-fft_len/2+1:ind+fft_len/2);
42     noise_wind = hann(fft_len, "periodic");
43     noise_seg = noise_wind.*noise_seg;
44     noise_fft = fft(noise_seg);
45     fft_res = abs(noise_fft(1:fft_len/2+1))/fft_len;
46     fft_res(2:end-1) = 2*fft_res(2:end-1);
47     spec_mat(:,ind==mid_ind) = fft_res;
48 end
49
50 close all;
51 im = image(mid_tim, freq_ind(freq_ind <=20e3), 20.*log10(spec_mat(freq_ind <=20e3,:)), '
52     CDataMapping','scaled');
53 set(gca,'YDir','normal');
54 clim([-130 -50])
55 colormap(jet);
56 hcb = colorbar;
57 hcb.Title.String = 'Normalialized dB';

```

```

57 xlim([0, 210])
58 xlabel('Time (s)')
59 title('Acoustic Noise, 0-6 kHz')
60 ylim([0 6e3])
61 ylabel('Frequency (Hz)')
62
63 %% Get spectrum for 3000 rpm:
64 mid_tim(289)
65
66 noise_3000_seg = noise(mid_ind(289)-fft_len/2+1:mid_ind(289)+fft_len/2);
67 %noise_wind = hann(fft_len, "periodic");
68 %noise_3000_seg = noise_wind.*noise_3000_seg;
69 %noise_3000_seg = noise_3000_seg;
70 noise_fft = fft(noise_3000_seg);
71 fft_3000_res = abs(noise_fft(1:fft_len/2+1))/fft_len;
72 fft_3000_res(2:end-1) = 2*fft_3000_res(2:end-1);
73
74 close all;
75 plot(20*log10(fft_3000_res))
76 xlabel('Frequency (Hz)')
77 title('Measured Acoustic Noise Spectrum, 3000 rpm')
78 ylabel('Normalized noise (dB)')
79 xlim([0 10e3])

```

## B.6.2. Measured Current Analysis

This following code is used to analyze the motor current during the acoustic measurements. Two phase currents are measured and used to calculate the alpha-beta-current. Next, the FFT is performed over a moving window to obtain the waterfall plot.

```

1 % Dr. Jianning Dong - 23/06/2023
2 % Changed by:
3 % - F.C.B. Pacilly
4 %
5 % In this script the current measurements are used to determine the
6 % alpha-beta current and compute compute the moving window FFT over it to
7 % plot a waterfall plot, showing the frequencies present in the current.
8
9 % To run the model the WDFAcces MATLAB App should be downloaded from
10 % Yokogawa, and the MATLAB support for MinGW Compiler AddOn should be
11 % installed.
12
13 matlab.apputil.run('WDFAccess')
14
15 %% Read measurement data
16 Ia = ytmWdfGetData('DATA001.wdf', 2, 1);
17 Ib = ytmWdfGetData('DATA001.wdf', 1, 1);
18 Ia = Ia(189552:end) '-mean(Ia(189552:end));
19 Ib = Ib(189552:end) '-mean(Ib(189552:end));
20 h_samp = ytmWdfGetHResolution('DATA001.wdf', 1, 1);
21 f_samp = 1/h_samp;
22 t_samp = h_samp.*(0:(length(Ia)-1));
23
24 %% Plot current over time
25 plot(t_samp, Ia)
26 hold on
27 plot(t_samp, Ib)
28 xlabel('Time (s)')
29 ylabel('Current (A)')
30
31 %% Calculate and plot alpha-beta-current
32 Ic = 0 - Ia - Ib;
33 I_albe = 2/3*(Ia + Ib*exp(1j*2*pi/3)+Ic*exp(-1j*2*pi/3));
34 plot(real(I_albe), imag(I_albe))
35 xlabel('$I_{\alpha}$', 'interpreter', 'latex')
36 ylabel('$I_{\beta}$', 'interpreter', 'latex')
37
38 %% Perform moving window FFT

```

```

39 fft_len = 2nextpow2(floor(f_samp));
40 ialbe_len = floor(length(I_albe)/fft_len)*fft_len;
41
42 overlap = 1-1/8;
43
44 mid_ind = fft_len/2:(1-overlap)*fft_len:(ialbe_len-fft_len/2);
45 mid_tim = mid_ind/f_samp; % index of the mid time of each segment
46
47 base_freq = 1/(fft_len/f_samp);
48 % max_freq = fft_len/2*base_freq; % shannon freq, f_samp/2
49 % freq_ind = 0:base_freq:max_freq;
50 freq_ind = (-fft_len/2:fft_len/2-1)*(f_samp/fft_len);
51
52 spec_mat = zeros(fft_len,length(mid_ind));
53
54 for ind = mid_ind
55     ialbe_seg = I_albe(ind-fft_len/2+1:ind+fft_len/2);
56     %ialbe_wind = hann(fft_len, "periodic"); %% uncomment if you would like to apply the
        window
57     %ialbe_seg = ialbe_wind.*ialbe_seg; %% uncomment if you would like to apply the
        window
58     ialbe_fft = fft(ialbe_seg);
59     fft_res = abs(fftshift(ialbe_fft))./fft_len;
60     spec_mat(:,ind==mid_ind) = fft_res;
61 end
62
63 %% Plot alpha-beta-current spectrum
64 close all;
65 max_freq = 5e3;
66 im = image(mid_tim, freq_ind, 20.*log10(spec_mat), 'CDataMapping','scaled');
67 set(gca,'YDir','normal');
68 clim([-80 -0])
69 colormap(jet);
70 hcb = colorbar;
71 hcb.Title.String = 'dBuA';
72 xlabel('Time (s)')
73 title(' I_ spectrum, -5 kHz to 5 kHz')
74 ylim([-max_freq max_freq])
75 ylabel('Frequency (Hz)')

```